

# **Interplays and feedback loops of oncogenic signaling pathways in B cell non-Hodgkin lymphoma**



## **Dissertation**

for the award of the degree

"Doctor rerum naturalium (Dr. rer. nat.)"

at the Georg-August-University Goettingen

within the doctoral degree program Molecular Medicine  
of the Georg-August-University School of Science (GAUSS)

submitted by

**Isabel Rausch**

born in Bremen

Goettingen, 2019



## Thesis Advisory Committee

<b>Prof. Dr. Dieter Kube</b> (Supervisor)	Clinic of Hematology and medical Oncology University Medical Centre Goettingen
<b>Prof. Dr. Heidi Hahn</b>	Institute of Human Genetics University Medical Centre Goettingen
<b>Prof. Dr. mult. Thomas Meyer</b>	Clinic of Psychosomatic Medicine and Psychotherapy University Medical Centre Goettingen

## Members of the examination board

<b>Prof. Dr. Dieter Kube</b> (Referee)	Clinic of Hematology and medical Oncology University Medical Centre Goettingen
<b>Prof. Dr. Heidi Hahn</b> (Co-referee)	Institute of Human Genetics University Medical Centre Goettingen
<b>Prof. Dr. mult. Thomas Meyer</b>	Clinic of Psychosomatic Medicine and Psychotherapy University Medical Centre Goettingen
<b>Prof. Dr. Ralf Dressel</b>	Institute for Cellular and Molecular Immunology University Medical Centre Goettingen
<b>Prof. Dr. Peter Burfeind</b>	Institute of Human Genetics University Medical Centre Goettingen
<b>Prof. Dr. Jörg Großhans</b>	Institute for Developmental Biochemistry University Medical Centre Goettingen

Date of the oral examination:

## Affidavit

By this, I declare that I independently authored the presented thesis:

"Interplays and feedback loops of oncogenic signaling pathways in B cell non-Hodgkin lymphoma"

and that I did not use other auxiliary means than indicated. Paragraphs that are taken from other publications, by wording or by sense, are marked in every case with a specification of the literary source.

Furthermore, I declare that I carried out the scientific experiments following the principles of Good Scientific Practice according to the valid "Richtlinien der Georg-August-Universität Göttingen zur Sicherung guter wissenschaftlicher Praxis".

---

Isabel Rausch

Goettingen, January 2019

## List of Publications

### Articles in preparation:

Rausch I., Klinger B., Witzel F., Sieber A., Kutz H., Kieser A., Blüthgen N., Kube D. (2018): Quantitative modelling of B cell signaling unveils global feedback loops and crosstalk from p38 MAPK to ERK signaling.

Rausch I., Feist M., von Bonin F., Kube D. (2018): NF-κB activation reduces migration capacity despite STAT3 activation in non-Hodgkin lymphoma.

### Abstracts:

Rausch I., Hand E., Kutz H., Klinger B., Witzel F., Sieber A., Kieser A., Beissbarth T., Spang R., Blüthgen N., Kube D. (2017): Interaction of signalling pathways in Burkitt lymphoma. Poster presentation at the EKFS Cancer Symposium, Goettingen, Germany, 15-17 Nov 2017.

Rausch I., Klinger B., Witzel F., Sieber A., Kutz H., Kieser A., Blüthgen N., Kube D. (2018): Quantitative modelling of B cell signalling unveils global feedback loops and crosstalk from p38 MAPK to ERK signalling. Poster presentation at the STS – 22<sup>nd</sup> Joint Meeting “Signal Transduction – Receptors, Mediators and Genes”, Weimar, Germany, 05-07 Nov 2018.

## Table of Contents

Acknowledgment .....	I
Abstract.....	II
List of Tables.....	III
List of Figures.....	IV
Abbreviations .....	V
1. Introduction .....	1
1.1 Non-Hodgkin Lymphoma.....	1
1.1.1 Burkitt Lymphoma.....	2
1.1.2 Diffuse Large B cell Lymphoma.....	3
1.2 BCR signaling.....	4
1.2.1 PI3K-AKT-mTOR pathway .....	5
1.2.2 MEK-ERK pathway .....	5
1.2.3 p38 MAPK pathway .....	6
1.2.4 NF- $\kappa$ B pathway .....	7
1.3 JAK-STAT signaling.....	8
1.4 Oncogenic signaling .....	9
1.4.1 Burkitt lymphoma .....	9
1.4.2 Diffuse large B cell lymphoma .....	11
1.5 Important pathway interactions and crosstalks.....	13
Aims.....	15
2. Material and Methods .....	16
2.1 Material, recipes and equipment .....	16
2.1.1 Biological material.....	16
2.1.2 Chemicals, solutions and consumable supplies .....	16
2.1.3 Buffers and media.....	19
2.1.4 Cell culture supplements, inhibitors and siRNA .....	21
2.1.5 Antibodies .....	22
2.1.6 Oligonucleotides .....	24
2.1.7 Ready to use reaction systems .....	24
2.1.8 Equipment.....	25
2.1.9 Software.....	26
2.2 Cell Biology .....	26
2.2.1 Cell Culture .....	26
2.2.2 Stable isotope labeling by amino acids in cell culture .....	27
2.2.3 Inhibitor treatment and stimulation of the BCR signaling .....	27

---

2.2.4	IL10 and CpG stimulation .....	27
2.2.5	RNA-interference-mediated gene knockdown.....	28
2.2.6	Cell viability assay .....	28
2.2.7	Migration assay.....	29
<b>2.3</b>	<b>Protein biochemistry.....</b>	<b>29</b>
2.3.1	Preparation of cell lysates and cell fractionation for Western Blot analysis .....	29
2.3.2	SDS Page, Western Blot and Immunodetection .....	30
2.3.3	Bio-Plex® Multiplex Immunoassay.....	31
2.3.4	Mass spectrometry based phosphoproteomics.....	32
<b>2.4</b>	<b>Molecular Biology .....</b>	<b>32</b>
2.4.1	RNA isolation .....	32
2.4.2	Reverse transcription.....	33
2.4.3	Quantitative real-time polymerase chain reaction .....	33
2.4.4	RNA sequencing.....	34
<b>2.5</b>	<b>Statistics and bioinformatical analyses.....</b>	<b>35</b>
3.	Results .....	36
<b>3.1</b>	<b>Tonic and active BCR signaling contains several feedback loops.....</b>	<b>36</b>
3.1.1	Determination of a suitable time point for pathway interaction analyses .....	37
3.1.2	Tonic BCR signaling is enhanced by positive feedback loop .....	38
3.1.3	Active BCR signaling is influenced by positive and negative interplays.....	40
3.1.4	Schematic model represents interactions of signaling pathways .....	43
<b>3.2</b>	<b>p38 MAPK attenuates the MEK-ERK pathway.....</b>	<b>45</b>
3.2.1	p38 $\alpha$ (MAPK14) limits the MEK-ERK pathway .....	45
3.2.2	RAF-1 phosphorylations are affected by ERK1/2 but not by p38 MAPK .....	47
3.2.3	p38 MAPK reduces activation and duration of the MEK-ERK pathway .....	48
3.2.4	Early target gene expression of ERK1/2 is not influenced by p38 MAPK .....	50
3.2.5	p38 MAPK attenuates ERK1/2-regulated gene expression of the kinase MKK6 .....	52
<b>3.3</b>	<b>DLBCLs with chronic active BCR contain divers feedback loops .....</b>	<b>56</b>
3.3.1	Positive and negative feedbacks influence chronic active BCR signaling .....	56
3.3.2	Negative feedbacks of the chronic active BCR signaling have no impacts on proliferation .....	59
<b>3.4</b>	<b>IL10R and TLR9 activation modify cell response and behavior.....</b>	<b>60</b>
3.4.1	IL10R and TLR9 activation change 239 protein phosphorylations .....	60
3.4.2	Phosphoproteome reveals influence on cell cycle, metabolism and migration .....	63
3.4.3	Phosphoproteome analysis indicates MAP kinase involvement .....	65
3.4.4	IL10R and TLR9 activation reduce migration capacity of P493-6 cells.....	67

---

## Table of Contents

---

4.	Discussion.....	69
4.1	Positive feedback loop enhances tonic BCR signaling.....	69
4.2	BCR signaling contains crosstalk from AKT and ERK1/2 to GSK3 $\beta$ .....	71
4.3	MEK-ERK pathway is diminished by several negative feedbacks.....	73
4.4	p38 MAPK attenuates the MEK-ERK pathway.....	75
4.5	Feedback loops differ in ABC DLBCLs with chronic active BCR signaling.....	77
4.6	Interplay of TLR9 and IL10R activation induces CDK2 and JNK.....	79
5.	Summary and Conclusion .....	81
6.	References.....	82
	Appendix .....	97
	Curriculum Vitae.....	116

## Acknowledgment

I would first like to thank my advisor Prof. Dieter Kube for his continuous support and supervision during the last years. I am grateful for his advice, helpful discussions and the opportunity to develop my own ideas.

I would sincerely like to thank Prof. Lorenz Trümper for the possibility to accomplish this thesis in his department.

In addition, I would like to express my gratitude to Prof. Heidi Hahn and Prof. Thomas Meyer for their guidance and encouragement during the thesis committee meetings.

I would also like to thank Bertram Klinger, Prof. Nils Blüthgen and Prof. Arnd Kieser for the great collaboration, the nice discussions and the lovely meetings. Furthermore, special thanks to Anja Sieber for the kind support with the multiplex immunoassay. I would like to thank Prof. Tim Beissbarth and Maren Sitte for the new calculation of the gene expression data. Moreover, I would like to acknowledge Prof. Henning Urlaub and Jasmin Corso for their support and the opportunity to perform the phosphoproteom analysis.

For always offering a helpful hand and their positive attitudes, a big thank you to Annekatrin Arlt and Franziska Linke. I would also like to thank Vanessa Kruse for her critical proofreading of this thesis, Frederike von Bonin and all former and present lab members for the great time.

Most importantly, I want to thank my family, my partner and my friends for their love, encouragement and unconditional support. I cannot thank my mum enough for being there for me and for all she has done for me. In addition, I would like to thank Matze for inspiring and supporting me.

## Abstract

The B cell receptor (BCR) signaling, required for the survival and maturation of B cells, is one major deregulated pathway in B cell lymphomas. Several mutations are known to enhance the tonic BCR signal in Burkitt lymphomas (BL) or to mimic an activated receptor in some diffuse large B cell lymphomas (DLBCL). While the proximal events and kinases of the BCR signaling are well studied, less is known about the interactions of downstream effector pathways. As the signaling interplays and feedback loops can influence the therapeutic success, this thesis aims for a better understanding of signaling interplays and for an improvement of oncogenic network models of B cell lymphomas.

For this purpose, BCR-related pathway interplays were examined by analyzing several protein phosphorylations with a multiplex immunoassay. Our investigations of pathway activations after thirteen defined perturbations revealed positive as well as negative interplays of pathways downstream of the BCR in BLs. During the tonic and active BCR signaling, the PI3K-AKT pathway, essential for many B cell lymphomas, enhanced its own activation probably through a positive feedback to kinases in close proximity of the BCR. We proposed that the positive feedback loop is one explanation for the potent effects of PI3K, AKT and mTOR inhibitors on BL proliferation. Furthermore, two negative feedbacks on the MEK-ERK pathway were detected after BCR activation. Beside ERK1/2 itself, p38 MAPK negatively influenced upstream kinases of ERK1/2. Interestingly, further fine-tuning of the p38 MAPK and ERK1/2 activation was assumed due to the ERK-mediated upregulation of MKK6 which could contribute to p38 MAPK activation. The mentioned feedbacks were generally identified downstream of the BCR signaling in all examined BL and DLBCL cell lines except for the p38 MAPK-dependent attenuation of the MEK-ERK pathway which was not observed in the DLBCL cell line OCI-LY3. In a second approach, the NF-κB and JAK-STAT-dependent proliferation of B cell lymphomas was investigated. Therefore, the signaling network following TLR9 and IL10R stimulation was analyzed by a phosphoproteom analysis. Our results revealed that the simultaneous activation of TLR9 and IL10R changed over 200 protein phosphorylations influencing cell cycle, metabolism and migration. The direct phosphorylation of CDK2 and JNK was suggested to contribute to the proliferative effect after TLR9 and IL10R activation.

The signaling interplays and feedbacks identified in this study provide a deeper insight and refinement of the signaling network structure in lymphomas. Additional improvements of computational network models are advantageous to predict signaling alterations by external influences as well as therapeutic responses.

## List of Tables

Table 1: Cell lines .....	16
Table 2: Chemicals .....	16
Table 3: Solutions .....	18
Table 4: Consumables.....	18
Table 5: Recipes of buffers.....	19
Table 6: Media .....	21
Table 7: Stimulants used in cell culture .....	21
Table 8: Inhibitors used in cell culture .....	22
Table 9: siRNA.....	22
Table 10: Antibodies .....	22
Table 11: Oligonucleotides .....	24
Table 12: Reaction systems .....	24
Table 13: Equipment .....	25
Table 14: Software .....	26
Table 15: Reverse transcriptase master mix.....	33
Table 16: Thermocycler program .....	33
Table 17: qRT-PCR program.....	34
Table A-1: The changed phosphosites after IL10+CpG stimulation .....	103
Table A-2: GO annotation of phosphoproteins changed by IL10+CpG stimulation .....	109

## List of Figures

Figure 1: Schematic representation of some known deregulated signaling pathways in BLs.	10
Figure 2: Schematic overview of some known deregulated signaling pathways in DLBCLs.	12
Figure 3: Time dependent activation of specific signaling pathways after BCR activation.	37
Figure 4: Signaling changes by pathway perturbations during the tonic BCR signaling.	39
Figure 5: Cell viability of BLs after pathway inhibition during the tonic BCR signaling.	40
Figure 6: Signaling changes by pathway perturbations during the active BCR signaling.	42
Figure 7: Network model of BCR signaling interactions and feedbacks.	44
Figure 8: Verification of TAK-1 and p38 MAPK influence on the MEK-ERK pathway	46
Figure 9: p38 MAPK and ERK1/2 impact on RAF-1 phosphorylations	48
Figure 10: Alteration of ERK1/2 activity after p38 MAPK inhibition	50
Figure 11: Impact on early target gene expressions by ERK1/2 and p38 MAPK	51
Figure 12: Impact of ERK1/2 and p38 MAPK on early target gene expression	52
Figure 13: p38 MAPK influence on ERK1/2 target gene expression	54
Figure 14: p38 MAPK influence on ERK1/2 target gene expression	55
Figure 15: Signaling changes by pathway perturbations during the chronic active BCR signaling.	57
Figure 16: Comparison of BL-2, HBL-1 and OCI-LY3 cells on protein and RNA level	59
Figure 17: Cell viability of HBL-1 and OCI-LY3 cells after MEK1/2 or p38 MAPK inhibition	60
Figure 18: Workflow and global phosphosites identification of mass spectrometry analysis	61
Figure 19: Global phosphoproteomics results of Ctrl and IL10+CpG stimulated Myc <sup>low</sup> cells	62
Figure 20: Network of affected phosphoproteins after IL10+CpG stimulation	63
Figure 21: GO annotation of biological process changed by IL10+CpG stimulation	65
Figure 22: IL10+CpG stimulation caused phosphorylation and expression of CDKs and MAPKs	66
Figure 23: IL10+CpG impact on movement associated proteins and the migration potential	68
Figure 24: Proposed network scheme of pathway interplays for the tonic BCR signaling	71
Figure 25: Proposed network scheme of pathway interplays for the activated BCR signaling	74
Figure A-1: Multiplex immunoassay values and standard deviation of the BL-2 cell analysis	98
Figure A-2: Multiplex immunoassay values and standard deviation of the BL-41 cell analysis	99
Figure A-3: Literature-derived network model with the experimental setup	100
Figure A-4: Network model of BCR signaling interactions and feedbacks of BL-41 cells	101
Figure A-5: Multiplex immunoassay values and standard deviation of ABC DLBCLs analyses	102
Figure A-6: GO annotation of phosphoproteins changed by IL10+CpG stimulation	115

## Abbreviations

4E-BP1	eIF4E binding protein
α	Anti
α-IgM	Anti-human IgM F(ab')2
ABC	Activated B cell
AKT	v-akt murine thymoma viral oncogene homolog
APS	Adenosine phosphosulfate
ASK	Apoptosis signal regulating kinase
B2M	Beta 2 microglobulin
BAD	Bcl2-associated agonist of cell death
BAFF	B cell activating factor
BCAP	B cell adaptor for phosphatidylinositol 3 kinase
BCL6	B cell lymphoma 6 protein
BCR	B cell receptor
BL	Burkitt lymphoma
BLNK	B cell linker
BSA	Albumin Fraction V
BTK	Bruton's tyrosine kinase
CARD11	Caspase recruitment domain-containing protein 11
CD	Cluster of differentiation
CDK	Cyclin dependent kinase
CDKN2A	Cyclin dependent kinase inhibitor 2A
cDNA	Complementary DNA
Ctrl	Control
DAG	Diacyl glycerol
ddH <sub>2</sub> O	Double-distilled water
DEPC	Diethylpyrocarbonate
DLBCL	Diffuse large B cell lymphoma
DLK1	Protein delta homolog 1
DMSO	Dimethyl sulfoxide
DNA	Deoxyribonucleic acid
dNTP	Desoxyribonucleosid triphosphate
DPBS	Dulbecco's Phosphate Buffered Saline
DTT	Dithiothreitol
DUSP	Dual-specificity MAPK phosphatases
E2A	Transcription factor E2-alpha
EDTA	Ethylenediaminetetraacetic acid
EGR	Early growth response
EGTA	Ethylene glycol bis(2-aminoethyl ether) tetraacetic acid
ERK	Extracellular regulated kinase

---

EZH2	Enhancer of zeste homolog 2
FBS	Fetal Bovine Serum
FOXO	Forkhead/winged helix box class O
g	gravitational force
GAPDH	Glyceraldehyde-3-phosphate dehydrogenase
GCB	Germinal center B cell
GNA13	G protein subunit alpha 13
GO	Gene Ontology
GRB2	Growth factor receptor-bound protein 2
GRB10	Glycine-rich RNA-binding protein 10
GSK3 $\beta$	Glycogen synthase kinase 3 beta
GTP	Guanosine triphosphate
HDAC1	Histone Deacetylase 1
HEPES	4-(2-hydroxyethyl)-1-piperazineethanesulfonic acid
HIV	Immunodeficiency virus
HLA	Human leukocyte antigen
Hsp27	Small heat shock 27 kDa protein
ID3	Inhibitor of DNA binding 3
Ig	Immunoglobulin
IKK	I $\kappa$ B kinase
IL	Interleukins
IPBA	Iodophenylboronic acid
IRS-1	Insulin receptor substrate 1
ITAM	Immunoreceptor tyrosine-based activation motifs
JAK	Janus kinase
JNK	c-JUN N-terminal kinase
KCl	Potassium chloride
kDa	Kilodalton
KEA2	Kinase Enrichment Analysis 2
LCK	Lymphocyte cell-specific protein tyrosine kinase
MALT1	Mucosa-associated lymphoid tissue lymphoma translocation protein 1
MAP	Mitogen-activated protein
MAPK	Mitogen-activated protein kinase
MAPKAPK	Serine/threonine protein kinase MAPK-activated protein kinase
MEK	Mitogen-activated protein kinase kinase
MEKK	Mitogen-activated protein kinase kinase kinase
MgCl <sub>2</sub>	Magnesium chloride
MKK	Mitogen-activated protein kinase kinase
MKP	MAP kinase phosphatases
MLK3	Mixed lineage kinase 3
MTMR4	Myotubularin-related protein 4

---

mTOR	Mammalian target of rapamycin
mTORC	mTOR complex
MYC	Myelocytomatosis oncogene cellular homolog
Myc <sup>high</sup>	P493-6 cells with <i>MYC</i> expression
Myc <sup>low</sup>	P493-6 cells with reduced <i>MYC</i> expression
MyD88	Myeloid differentiation primary response 88
NaCl	Sodium chloride
NFAT	Nuclear factor of activated T cells
NF-κB	Nuclear factor kappa B
NLRP11	NACHT, LRR and PYD domains-containing protein 11
NOP2	Nucleolar protein 2 homolog
NOTCH2	Neurogenic locus notch homolog protein 2
NP-40	Nonylphenyl-polyethylene glycol
P	Phospho
p90RSK	90 kDa ribosomal protein S6 kinase
PAGE	Polyacrylamide gel electrophoresis
PAK	p21-activated kinase
PALD1	Paladin
PARN	Poly(A)-specific ribonuclease
PDP1	Pyruvate dehydrogenase phosphatase 1
PDK1	Phosphoinositide-dependent kinase 1
PI3K	Phosphatidylinositol 3 kinase
PIAS	Protein inhibitors of STATs
PLC $\gamma$ 2	Phospholipase C $\gamma$ 2
PLD6	Phospholipase D6
PMSF	Phenylmethanesulfonyl fluoride
PRDM1	PR/SET domain 1
PTEN	Phosphatase and tensin homolog
PTGS1	Prostaglandin-endoperoxide synthase 1
PTPN	Tyrosine protein phosphatase non-receptor type
qRT-PCR	Quantitative real-time polymerase chain reaction
RAS	Rat sarcoma
RASGRP1	RAS guanyl-releasing protein 1
RCSD1	CapZ-interacting protein 1
RNA	Ribonucleic acid
RPS6	40S ribosomal protein S6
RT	Room temperature
S	Serine
S6K	Ribosomal S6 kinase
SATB1	Special AT-rich sequence-binding protein 1
scrb	Negative control

---

SDS	Sodium dodecyl sulfate
SFK	SRC family tyrosine kinases
SH2	Src Homology 2
SHP	SH2 domain containing protein tyrosine phosphatase
SILAC	Stable isotope labeling by amino acids in cell culture
siRNA	Small interfering RNA
SOS	Son of sevenless homolog
SOCS	Suppressors of cytokine signaling
STAT	Signal transducer and activator of transcription
SYK	Spleen tyrosine kinase
T	Threonine
TAK1	TGF-beta activated kinase 1
TBS	Tris buffered saline
TEMED	Tetramethylethylenediamine
TLR	Toll like receptors
TRAF6	TNF receptor-associated factor 6
Tris HCl	Tris(hydroxymethyl)-aminomethanhydrochlorid
v/v	volume/volume
w/v	weight/volume
Y	Tyrosine
ZAP70	70 kDa zeta-chain associated protein
ZFP36L1	Zinc finger protein 36 C3H1 type-like 1
ZNF800	Zinc finger protein 800

### Deoxyribonucleotides

G	deoxyguanosine monophosphate
A	deoxyadenosine monophosphate
T	deoxythymidine monophosphate
C	deoxycytidine monophosphate

Units and Prefixes are in conformity with the International system of Units.

## 1. Introduction

The immune system consists of various cell types to counteract pathogens through recognition, destruction and disposal. B cells including antibody secreting plasma cells and memory B cells are involved in the detection and labeling of foreign molecules. To cover the diversity and to increase the affinity of antibodies, B cells have the opportunity to modify their immunoglobulins. The adaptation and selection of B cells secreting high-affinity antibodies occur in germinal centers (Klein and Dalla-Favera, 2008; Natkunam, 2007). Germinal centers are histological structures in lymphoid tissues with a dark and a light zone (MacLennan, 1994). In the dark zone, B cells proliferate extensively and undergo somatic hypermutations to alter their antigen specificity. To further adjust the effector functions, B cells perform class switch recombination in the light zone. Depending on the suitability of the antibody affinity, B cells are selected in the light zone to exit the germinal center. All other B cells with unsuitable antibody affinity die by apoptosis or re-enter the dark zone for further somatic hypermutations (Victora and Nussenzweig, 2012; Victora *et al.*, 2010).

The adaptation and selection of antibody secreting B cells follow a distinct program of signals and transcriptional alterations. Beside the activation of B cells, cell-cell interactions and costimulatory signals are essential to induce a specific set of intracellular signaling cascades and transcriptional modulators. These pathway activations regulate B cell proliferation, somatic hypermutations or class switch recombination during the germinal center reaction (Kuppers, 2005; Pone *et al.*, 2010). Although different check points serve as a strong control to avoid and eliminate mistakes, the gene remodeling process provides an opportunity for B cells to transform into malignancies like B cell lymphomas (Basso and Dalla-Favera, 2015; Victora *et al.*, 2012).

### 1.1 Non-Hodgkin Lymphoma

B cell lymphomas comprise a wide spectrum of malignancies and thus are further categorized in Hodgkin and non-Hodgkin lymphoma due to different genetically, phenotypically and clinically aspects (Vardiman *et al.*, 2009). B cell lymphomas derive from mature B cells during the germinal center reaction (Kuppers, 2005). The heterogeneity of lymphomas reflects the origin from distinct phases of the germinal center reaction. Therefore, lymphomas can be classified by the B cell state of origin and on the basis of genetic alterations causing abnormal signal transductions (Victora *et al.*, 2012). The aggressive non-Hodgkin lymphomas include Burkitt lymphoma (BL) and diffuse large

B cell lymphoma (DLBCL). While BLs derive from germinal center B cells of the dark zone, the DLBCLs are closer related to B cells from the light zone (germinal center B cell like) or to early stages of post germinal center plasma cell differentiation (activated B cell like) (Basso and Dalla-Favera, 2015).

### 1.1.1 Burkitt Lymphoma

BL was first described by Denis Burkitt as a highly aggressive B cell lymphoma in African children (Burkitt, 1958). The characteristics of BLs are uniform, highly proliferating cells and a starry-sky appearance due to tingible body macrophages phagocytosing the apoptotic debris (Blum *et al.*, 2004). Nowadays, BLs are subdivided in three different types with some distinct pathological features (Molyneux *et al.*, 2012). The endemic variant occurs predominantly in 4 to 7 years old children of equatorial Africa. A variant affecting children and young adults worldwide is classified as sporadic BL. The third, the immunodeficiency-related type is associated with immunodeficiency virus (HIV) infected individuals or with posttransplant complications. In addition, an infection with the Epstein-Barr virus is related to all endemic, 15 % of sporadic and 40 – 50 % of immunodeficiency-associated BLs although its impacts are still discussed (Molyneux *et al.*, 2012; Spender and Inman, 2014). BLs account for 40 - 50 % of lymphomas in children and only 1 - 2 % of lymphoma cases in adults (Aldoss *et al.*, 2008).

The typical immune-phenotype of BLs comprises high Ki67 indices, the expression of surface immuno-globulin M (IgM) and B cell markers such as cluster of differentiation (CD) 10, CD19, CD20, CD22 (Kelemen *et al.*, 2010). Furthermore, BLs are characterized by a chromosomal translocation affecting the proto-oncogene *myelocytomatosis oncogene cellular homolog (MYC)*. The translocation places MYC under the control of the regulatory elements of Ig and thus causes an aberrant expression. The transcription factor c-MYC is involved in regulation of proliferation, cell growth, differentiation, metabolism and apoptosis (Basso and Dalla-Favera, 2015). In addition, the transcription factor E2-alpha (E2A) or its negative regulator inhibitor of DNA binding 3 (ID3) are frequently mutated in 70 % of BL patients and 38 % of BL patients have cyclin D3 aberrations (Richter *et al.*, 2012; Schmitz *et al.*, 2012). E2A is known to enhance phosphatidylinositol 3-kinase (PI3K) activation and constitutive PI3K and c-MYC activation is sufficient to provoke BL-like lymphomas in transgenic mice. However, due to a clonality of the tumor, further mutations are suggested to be necessary for lymphomagenesis (Klaproth and Wirth, 2010; Sander *et al.*, 2012; Schmitz *et al.*, 2012).

### 1.1.2 Diffuse Large B cell Lymphoma

DLBCLs are the most frequent type of non-Hodgkin lymphomas in adults accounting for 40 % of cases. The medium to large-sized lymphoid cells are arranged in a diffuse pattern and displacing the normal tissue architecture (Boyd *et al.*, 2013). Due to the molecular diversity and different clinical outcomes, DLBCLs can be distinguished by different criteria. In Germany, DLBCLs are subdivided by their centroblastic or immunoblastic morphology (Stein and Hummel, 2006). Furthermore, a molecular classification was introduced by Alizadeh and coworkers. The germinal center B cell (GCB) like and activated B cell (ABC) like DLBCLs are characterized by subtype specific mutations although some genetic alterations are found in both subtypes (Alizadeh *et al.*, 2000). A common feature of all DLBCLs is the influence on chromatin modifiers and the immune escape (Basso and Dalla-Favera, 2015).

The typical immune-phenotype of DLBCLs comprises the expression of the surface immunoglobulin M (IgM) or G (IgG) and B cell markers such as CD19, CD20, CD22 and CD79a (Boyd *et al.*, 2013). Common genetic alterations of DLBCLs increase the activity of B cell lymphoma 6 protein (BCL6) in order to enhance proliferation, to suppress DNA damage response and to block terminal differentiation (Basso and Dalla-Favera, 2015). Additionally, defects of cell surface markers promote the immune escape. Mutations of human leukocyte antigen class I (HLA-I), beta 2 microglobulin (B2M) and CD58 cause invisibility to cytotoxic T cells and nature killer cells (Challa-Malladi *et al.*, 2011). Apart from these common features, the pathogenesis of GCB DLBCLs is poorly understood and only in a fraction of cases mutations of phosphatase and tensin homolog (PTEN), BCL2, c-MYC, enhancer of zeste homolog 2 (EZH2) or G protein subunit alpha 13 (Gα13) are found (Basso and Dalla-Favera, 2015; Rickert, 2013). Aberrations of EZH2 enhance proliferation, impair differentiation and promote germinal center formation. However, mutations of EZH2 are insufficient to induce DLBCL development and additional alterations of for example BCL2 are required to accelerate lymphomagenesis in mice (Beguelin *et al.*, 2013). On the contrary, ABC DLBCLs depend on constitutive active nuclear factor kappa B (NF-κB) which is induced for instance by oncogenic mutations of BCR components, myeloid differentiation primary response 88 (MyD88) or caspase recruitment domain-containing protein 11 (CARD11) (Davis *et al.*, 2001; Young and Staudt, 2013). The blockage of terminal differentiation in ABC DLBCLs can occur through inactivation of *PR/SET domain 1* (*PRDM1*) (Pasqualucci *et al.*, 2006). Interestingly, *PRDM1* inactivation promotes lymphoma development in mice with critical features of ABC DLBCLs (Mandelbaum *et al.*, 2010).

## 1.2 BCR signaling

The PI3K and NF-κB pathways, aberrantly regulated in BLs and DLBCLs, are major components of the BCR signaling. Many non-Hodgkin lymphomas show a strong dependency on the BCR signaling implicating a pivotal role of the BCR in lymphomagenesis (Young and Staudt, 2013). The BCR is essential for normal B cell development and maturation. The strength of BCR signaling and the additional activation of cofactors like CD40, toll-like receptors (TLR) and the survival factor B cell activating factor (BAFF) are necessary for the adaptation and survival of the B cells during the germinal center reaction (Pone *et al.*, 2010). While the survival of resting mature B cells depends on a basic so called “tonic” BCR signal, the activation of the BCR by antigens induces B cell proliferation, maturation and antibody production (Avalos and Ploegh, 2014; Lam *et al.*, 1997).

A functional BCR consists of a membrane bound immunoglobulin and the two co-receptors Ig alpha (CD79a) and Ig beta (CD79b) (Kurosaki, 1999). In normal and malignant B cells, the BCR can transmit a tonic signal through the PI3K pathway or induces further pathway activations after recognition of an antigen (Rickert, 2013). Ligation of an antigen to the BCR induces conformational changes and crosslinking of several receptors (Avalos and Ploegh, 2014). Hence, tyrosine phosphorylations within the immunoreceptor tyrosine-based activation motifs (ITAMs) of CD79a and CD79b are triggered by SRC family tyrosine kinases (SFKs) such as Lyn. These phosphorylations promote the binding of spleen tyrosine kinase (SYK) and initiate the formation of a signalosome complex (Jin *et al.*, 2013; Kurosaki, 1999; Pao *et al.*, 1998). The complex is assembled by adaptor proteins and multiple tyrosine kinases. While adaptor proteins as B cell linker (BLNK) and B cell adaptor for phosphatidylinositol 3-kinase (BCAP) manage the signal distribution, tyrosine kinases like Bruton's tyrosine kinase (BTK) and phospholipase Cy2 (PLCy2) forward the signal (Jin *et al.*, 2013; Takata and Kurosaki, 1996; Wienands *et al.*, 1998). Besides, phosphatases are also implicated in the BCR signaling regulation. The SH2 domain-containing protein tyrosine phosphatase 1 (SHP-1) counteracts the activity of SRC and SYK whereas the SH2 domain-containing protein tyrosine phosphatase 2 (SHP2) enhances the signaling especially of the extracellular regulated kinase (ERK) pathway (Jiang *et al.*, 2014; Pao *et al.*, 2007; Tartaglia *et al.*, 2004).

Although even further signaling events occur, the outcome of proximal BCR signaling leads to activation of the NF-κB, PI3K, mitogen-activated protein kinase (MAPK) and nuclear factor of activated T cells (NFAT) pathway (Kurosaki, 2011; Niilo and Clark, 2002). The signal transmission through the MAPK pathways includes ERK, p38 MAPK

and JUN N-terminal kinase (JNK) activation (Jiang *et al.*, 1998). All BCR-induced pathway activations contribute to proliferation and survival of B cells with the exception of the NFAT pathway. The NFAT pathway is suggested to modulate B cell responses in plasma cell differentiation (Niiro and Clark, 2002; Winslow *et al.*, 2006). In the following sections, the pathways relevant for this study are described in more detail.

### **1.2.1 PI3K-AKT-mTOR pathway**

Activation of the PI3K pathway is sufficient to maintain resting mature B cell survival after depletion of the BCR. Therefore, the PI3K signal transduction is suggested to be the main component of the tonic BCR signaling (Srinivasan *et al.*, 2009). Besides, the tonic signal is essential for many B cell malignancies although the PI3K itself is infrequently mutated (Blachly and Baiocchi, 2014).

The BCR signal is transmitted by the adapter protein BCAP to a PI3K heterodimer consisting of a catalytic and a regulatory subunit (Blachly and Baiocchi, 2014; Okada *et al.*, 2000). A variety of effectors are further involved. On the one hand, PI3K together with BTK activates NF- $\kappa$ B. On the other hand, v-akt murine thymoma viral oncogene homolog (AKT) acts as an immediate effector between PI3K and mammalian target of rapamycin (mTOR). For this purpose, PI3K induces phosphoinositide-dependent kinase-1 (PDK1) and along with the mTOR complex 2 (mTORC2) the serine-threonine protein kinase AKT is recruited and phosphorylated. Following, AKT phosphorylates the mTOR complex 1 (mTORC1) and additionally inactivates Forkhead/winged helix box class O (FOXO) to induce cell cycle progression and survival (Baracho *et al.*, 2011; Brunet *et al.*, 1999; Rickert, 2013). Two of the best characterized downstream targets of mTORC1 are the ribosomal S6 kinase (S6K) and the eIF4E binding protein (4E-BP1) (Laplante and Sabatini, 2012). The signaling affects protein synthesis, nutrient response and many additional functions required for a rapid growth (Limon and Fruman, 2012). Furthermore, a S6K-dependent inactivation of insulin receptor substrate 1 (IRS-1), S6K-dependent suppression of mTORC2 and a mTORC1-dependent phosphorylation of the adaptor protein glycine-rich RNA-binding protein 10 (GRB10) serve as negative feedback mechanisms to reduce the upstream PI3K-AKT signaling (Logue and Morrison, 2012; Tremblay *et al.*, 2007; Yea and Fruman, 2011).

### **1.2.2 MEK-ERK pathway**

Several MAPK pathways like ERK are activated following BCR activation and transmit the signal through a distinct core cascade of kinases (Dhillon *et al.*, 2007). ERK plays an important role in B cell development and is required for the proliferative expansion of

immature and the differentiation of mature B cells (Yasuda *et al.*, 2011; Yasuda *et al.*, 2008). Similar to other cancer identities, constitutive ERK activation is also described for B cell malignancies (Ogasawara *et al.*, 2003).

For initiation, receptor tyrosine kinases trigger the loading of guanosine triphosphate (GTP) to the small GTPase rat sarcoma (Ras). After BCR activation this is mediated rather by the guanine nucleotide exchange factor RAS guanyl-releasing protein 1 (RASGRP1) then by the growth factor receptor-bound protein 2 (GRB2)- son of sevenless homolog (SOS) complex (Oh-hora *et al.*, 2003). Once activated the GTP-bound Ras recruits RAF family members like RAF-1 and B-RAF to the plasma membrane for activation. The effector protein mitogen-activated protein kinase kinase 1 and 2 (MEK1/2) is activated by RAF and phosphorylates ERK1 and ERK2 (ERK1/2) on a threonine-X-tyrosine motif (Alessi *et al.*, 1994; Dhillon *et al.*, 2007; Wellbrock *et al.*, 2004).

Phosphorylated ERKs can function in the cytosol or dimerize and translocate to the nucleus (Chen *et al.*, 1992). In the nucleus, ERK1/2 contributes to several tasks which are determined by the signal strength and duration. Early target gene expressions and activations of the proto-oncogene *FOS*, *early growth response 1* (*EGR-1*), *MYC* or proto-oncogene *JUN* point to a sustained signaling of ERK1/2 (Dhillon *et al.*, 2007; Murphy and Blenis, 2006). Furthermore, about hundred other targets are modulated in an ERK-dependent manner (Roskoski, 2012). Interestingly, upstream pathway components are affected by ERK1/2 target genes indicating the existence of autoregulatory feedback loops (Corbalan-Garcia *et al.*, 1996; Dougherty *et al.*, 2005). For instance, ERK1/2 induces the expression of *Sprouty* to prevent the GRB2-SOS complex and *MAP kinase phosphatases* (*MKPs*) to reduce its own activation (Hanafusa *et al.*, 2002; Ozaki *et al.*, 2001; Sun *et al.*, 1993). Additionally, the ERK-dependent phosphorylations of SOS, RAF and MEK1 lead to inactive conformations, reduced binding capacities and finally to a decreased pathway activation (Brunet *et al.*, 1994; Dhillon *et al.*, 2007).

### 1.2.3 p38 MAPK pathway

The p38 MAPK pathway is also activated by a distinct kinase cascade and is induced by inflammatory cytokines and environmental stress factors. However, the role and impacts of p38 MAPK are versatile and still controversially discussed (Ding *et al.*, 2009; Trempolec *et al.*, 2013a). Nevertheless, p38 MAPK activation is found in numerous B cell malignancies and predicts the failure of response in CHOP-treated DLBCL patients (Vega *et al.*, 2015).

The first kinases of the p38 MAPK activating cascade are mitogen-activated protein kinase kinase kinase 3 and 4 (MEKK3/4), apoptosis signal regulating kinase (ASK), protein delta homolog 1 (DLK1), mixed lineage kinase 3 (MLK3) and TGF-beta activated kinase 1 (TAK1). After activation of one of the first kinases, mitogen-activated protein kinase kinase 3 (MKK3), 4 (MKK4) and 6 (MKK6) are induced to further activate one out of five p38 MAPK subunits. Thereby, a threonine-X-tyrosine motif existing in all subunits is phosphorylated (Feng *et al.*, 2009; Zarubin and Han, 2005).

In the cytosol, p38 MAPK regulates protein activations, for instance, the activation of the serine/threonine protein kinase MAPK-activated protein kinase 2 (MAPKAP-K2) with subsequent small heat shock 27 kDa protein (Hsp27) activation. Furthermore, p38 MAPK initiates protein degradation through phosphorylation-mediated destabilization or ligase activation (Cuenda and Rousseau, 2007; Trempolec *et al.*, 2013a). After activation p38 MAPK can also translocate into the nucleus to enhance transcription factor activity for a rapid induction of immediate-early genes. The p38 MAPKs are emerging as important modulators of gene expression by regulation of chromatin modifiers and remodelers (Ashwell, 2006; Trempolec *et al.*, 2013b; Zarubin and Han, 2005). Several targets and anti-apoptotic as well as pro-apoptotic functions are described and so far not elucidated in detail (Feng *et al.*, 2009).

#### 1.2.4 NF-κB pathway

The NF-κB pathway is important for the proliferation and survival of B cells as it counteracts apoptotic signals (Jost and Ruland, 2007). An aberrant NF-κB activation is a hallmark of several B cell malignancies to induce cell cycling and to block apoptosis (Staudt, 2010).

Through PLC $\gamma$ 2, BTK and the adapter protein BLNK the canonical NF-κB pathway activation is initiated (Niilo and Clark, 2002). In addition to diacyl glycerol (DAG) and increased intracellular calcium flux, PLC $\gamma$ 2 activity induces the classical isoform PKC $\beta$  to phosphorylate CARD11 (Young and Staudt, 2013). Furthermore, the mucosa-associated lymphoid tissue lymphoma translocation protein 1 (MALT1) associates with BCL-10 and becomes activated. After multimerization with CARD11, TNF receptor-associated factor 6 (TRAF6) and TAK1 are recruited to the complex. TRAF6 further activates IκB-kinase (IKK) in an ubiquitin-dependent manner while TAK1 leads to phosphorylation of the activation loop of IKK. IKK-mediated phosphorylations of the inhibitory protein IκB triggers IκB polyubiquitylation with subsequent proteolytic degradation thus releasing the transcription factor NF-κB (Ruland and Mak, 2003; Shinohara *et al.*, 2005; Staudt, 2010; Thome *et al.*, 2010). Besides, the alternative NF-κB pathway also activates IKKs to induce

a direct phosphorylation and partial proteolysis of specific subunits of NF-κB (Jost and Ruland, 2007).

As result heterodimers are formed consisting the subunits RelA (p65), RelB, c-Rel, NF-κB1 (p50) and NF-κB2 (p52). The heterodimeric NF-κB transcription factors accumulate in the nucleus and activate the transcription of target genes (Jost and Ruland, 2007). NF-κB target genes include positive cell cycle regulators, anti-apoptotic proteins, inflammatory and immunoregulatory factors as well as negative feedback regulators to decrease the activation of upstream pathway components. For instance, cell cycle regulators like *MYC* and *cyclin D1* are upregulated and anti-apoptotic proteins of the BCL-2 family are enhanced by NF-κB. The expression of immunoregulatory cytokines includes interleukins (IL) like IL2, IL6 and IL10 to activate growth receptors in an autocrine or paracrine fashion (Jost and Ruland, 2007; Lam *et al.*, 2008).

### 1.3 JAK-STAT signaling

Autocrine as well as paracrine secreted interleukins are the main activators of the Janus kinase (JAK) and signal transducer and activator of transcription (STAT) pathway (Leonard and Lin, 2000). The JAK-STAT pathway is a pivotal signaling to regulate cell proliferation, survival, differentiation and immune response (Levy and Darnell, 2002). In addition to BCR signaling, several interleukin serum levels are elevated in non-Hodgkin lymphomas (Fabre-Guillevin *et al.*, 2006). Especially in ABC DLBCLs the aberrant regulated NF-κB pathway leads to the expression of IL6 or IL10 and thereby to a subsequent growth factor stimulation (Gupta *et al.*, 2012; Jost and Ruland, 2007).

The binding of a cytokine to a basally inactivated cognate receptor initiates to conformational changes or dimerization of the receptor. Intracellular bound JAKs become activated and trigger cross phosphorylations with the receptor. The phosphorylation sites serve as anchor points for STAT proteins to receive phosphorylations through JAKs (Ihle, 1995). For instance, in non-Hodgkin lymphoma the receptor activation by IL6 or IL10 causes a signal transmission over JAKs to STAT3 (Gupta *et al.*, 2012; Lam *et al.*, 2008). Besides, JAKs can activate the MAPK, PI3K and mTOR pathway while receptor internalization or phosphatase recruitment terminates the JAK activity (Vainchenker and Constantinescu, 2013).

Phosphorylated STATs can dimerize and translocate into the nucleus where they perform their task as transcription factors. Apart from proliferation and survival associated genes, STATs regulate the transcription of *suppressors of cytokine signaling* (SOCS) (Rawlings

*et al.*, 2004). SOCS 1 to 7 belong to negative feedback loops of this pathways and deactivate STAT signaling by direct binding to JAK and hence preventing further STAT phosphorylation. In addition, protein inhibitors of STATs (PIAS) interact directly with STATs to repress the transcriptional activity (Vainchenker and Constantinescu, 2013).

## 1.4 Oncogenic signaling

The complexity of the germinal center reaction provides many vulnerabilities for B cells to transform into malignancies. Mutations, leading to aberrant signaling through modulation of cascades and feedbacks, play an important role in tumor progression and survival (Basso and Dalla-Favera, 2015; Young and Staudt, 2013). Due to the heterogeneity of lymphomas and their causing mutations, the understanding of molecular pathways that drive and maintain tumorigenesis is necessary in order to improve therapies and to avoid resistances or relapses (Schmitz *et al.*, 2012; Victora *et al.*, 2012). Despite subtype specific mutations and different clinical outcomes, many B cell malignancies are highly sensitive to kinase inhibitors disrupting the BCR signaling. Thus, targeted therapy aiming at the BCR signaling emerges as a new treatment opportunity for several B cell malignancies (Smith, 2015).

### 1.4.1 Burkitt lymphoma

BLs in young patients are often cured by high dose chemotherapy whereas the outcome for elderly patients is worse due to therapeutic intolerance. The common chemotherapy of BLs includes DNA and cell cycle damaging reagents beside glucocorticoids to target cells with high proliferation rates. The treatment-associated immune suppression is a major hurdle in less developed regions emphasizing the need for new targetable candidates (Aldoss *et al.*, 2008; Schmitz *et al.*, 2012).

In BLs the genetic aberrations apart from c-MYC are often associated with an enhanced PI3K pathway comprising the tonic BCR signal (Figure 1) (Spender and Inman, 2014). E2A and its negative regulator ID3 are normally expressed in germinal center B cells of the dark zone to modulate the BCR signaling (Ott *et al.*, 2013). In BLs ID3 is often mutated as well as the ID3 binding site in E2A. As a result, E2A activation is enhanced and appears to promote the PI3K signaling by inhibiting the BCR-related phosphatase SHP-1 (Love *et al.*, 2012; Schmitz *et al.*, 2014). Another mechanism to induce the PI3K-AKT pathway is the modulation of the negative regulator PTEN. While direct PTEN mutations are infrequent, the upregulation of the miR-17-92 cluster occurs more often in order to inhibit *PTEN* expression in BLs (Lenz *et al.*, 2008c; Schmitz *et al.*, 2012). In

addition to the tonic signal promotion, E2A could also induce the cell cycle through its downstream target *cyclin D3* (*CCND3*). Cyclin D3 induces cell cycle progression along with cyclin dependent kinase 6 (CDK6). Furthermore, repression of the CDK6 inhibitor *cyclin dependent kinase inhibitor 2A* (*CDKN2A*) is a common lesion in BLs to promote proliferation (Schmitz *et al.*, 2012; Spender and Inman, 2014).

As many mutations in BL enhance the tonic BCR signaling, the PI3K pathway is suggested as a new druggable pathway for the treatment of BL. The inhibition of PI3K is so far approved for chronic lymphocytic leukemia and indolent lymphoma (Smith, 2015). *In vitro* studies using BL cell lines clearly demonstrated that proliferation is reduced after inhibition of PI3K, AKT, mTOR and cyclin D3/CDK6 (Spender and Inman, 2014). Therefore, the number of small pharmaceutical molecules targeting BCR-specific kinases increases steadily but their benefits still remains to be examined in clinical trials (Smith, 2015).

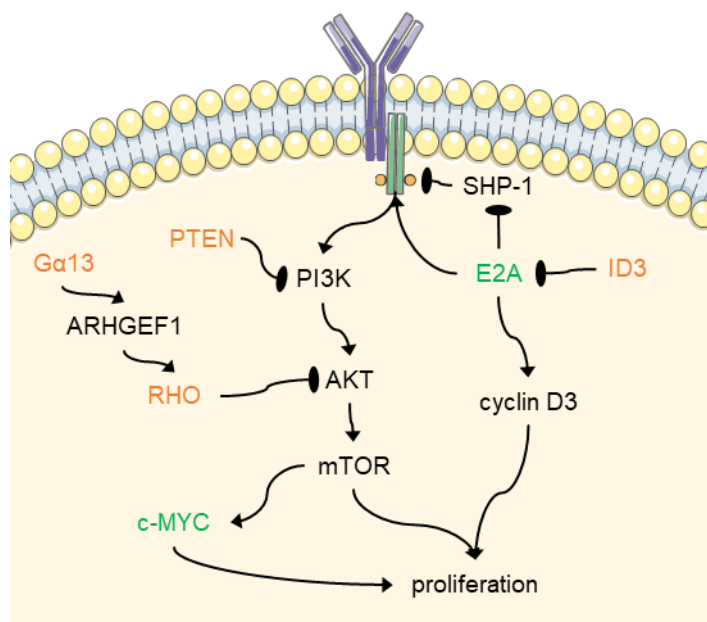


**Figure 1: Schematic representation of some known deregulated signaling pathways in BLs.**

Activation of c-MYC and the PI3K pathway are the main oncogenic alterations in BLs. An enhanced activation of E2A or a missing suppression of PI3K by PTEN contributes to the tonic BCR signaling in BLs. Black lines represent the interaction. Upregulated and downregulated proteins are displayed in green and red, respectively. Adapted from Spender and Basso (Basso and Dalla-Favera, 2015; Spender and Inman, 2014).

#### 1.4.2 Diffuse large B cell lymphoma

Due to their divergent genetic mutations and the different developmental states they derive from, DLBCL subtypes have various pathway dependencies. GCB DLBCLs mainly comprise a tonic BCR signaling and occur more often in younger patients. Mutations in ABC DLBCLs mimic a chronic active BCR with constitutive activation of the NF- $\kappa$ B pathway and are associated with worse outcomes than GCB DLBCLs. However, GCB and ABC DLBCLs cannot be clearly distinguished and both subtypes are treated with the same standard therapy (Deeb *et al.*, 2015; Lenz *et al.*, 2008b; Pfeifer and Lenz, 2013). As 40 % of all DLBCL cases are still incurable, a better understanding of deregulated pathways in each subtype is needed to reveal similarities as well as differences (Ott *et al.*, 2010).

The pathogenesis of GCB DLBCLs is poorly understood, however some aberrations are quite similar to BLs (Figure 2 A). In a fraction of cases mutations of PTEN, c-MYC, BCL-2, EZH2 or Ga13 are found (Basso and Dalla-Favera, 2015; Rickert, 2013). Similar to BLs, c-MYC enhances cell cycle progression but this is rather mediated by gain of low gene copy numbers or mutations of c-MYC regulators than by genetic translocations as seen in BLs (Ott *et al.*, 2013). Furthermore, like in BLs the PI3K-AKT pathway is induced through loss of the negative regulator PTEN in 55 % of cases (Lenz *et al.*, 2008c; Pfeifer *et al.*, 2013). The aberrations of Ga13 modulate the germinal center formation and cell movements but can also contribute to an enhanced PI3K-AKT pathway (Basso and Dalla-Favera, 2015; Muppidi *et al.*, 2015; Muppidi *et al.*, 2014).

While in ABC DLBCLs no deregulations of PTEN are found, the PI3K pathway activation is still increased due to receptor mutations of CD79a/b (Figure 2 B) (Kloo *et al.*, 2011). These mutations in addition to receptor activation by self-antigens contribute to a constitutive activation of NF- $\kappa$ B, ERK and NFAT (Davis *et al.*, 2010; Young *et al.*, 2015). Beside the receptor activation, NF- $\kappa$ B can also be activated by modulation of CARD11 or MyD88. MyD88 induces NF- $\kappa$ B activation independent of upstream signals through IL1 receptor-associated kinase (IRAK) (Lenz *et al.*, 2008a; Ngo *et al.*, 2011). A further enhanced NF- $\kappa$ B signaling is caused by inactivation of the repressor A20 (Compagno *et al.*, 2009). The constitutive activation of NF- $\kappa$ B leads to the expression of IL6 or IL10 and to a subsequent autocrine activation of STAT3 (Davis *et al.*, 2001; Lam *et al.*, 2008). Besides this NF- $\kappa$ B-dependent JAK-STAT activation, STAT3 mutations are also found in ABC DLBCLs and indicate along with high IL10 serum levels a worse clinical outcome (Ding *et al.*, 2008; Lech-Maranda *et al.*, 2006).

For the therapeutic aspect, the PI3K pathway is a promising drug target in GCB DLBCLs similar to BLs (Pfeifer *et al.*, 2013). As the pathogenesis of GCB DLBCLs is not fully elucidated, it is not surprising that some GCB DLBCL cases with wild type PTEN show no PI3K-AKT-dependency. However, the response to PI3K pathway inhibitors can be traced back to the expression status of PTEN (Pfeifer *et al.*, 2013). In ABC DLBCLs the BCR-mediated NF-κB activation relies on BTK and PI3K activation. Inhibition of these kinases leads to a reduced proliferation *in vitro* except for cases with BCR-independent NF-κB activation (Wilson *et al.*, 2015). MyD88 or CARD11 mutations causing a BCR-independent NF-κB activation can be counteracted through the inhibition of MALT1 or IRAK (Young and Staudt, 2013). As BTK inhibitors are well tolerable, the addition to standard therapies showed good results for B cell malignancies in the first clinical trials (Hendriks *et al.*, 2014).

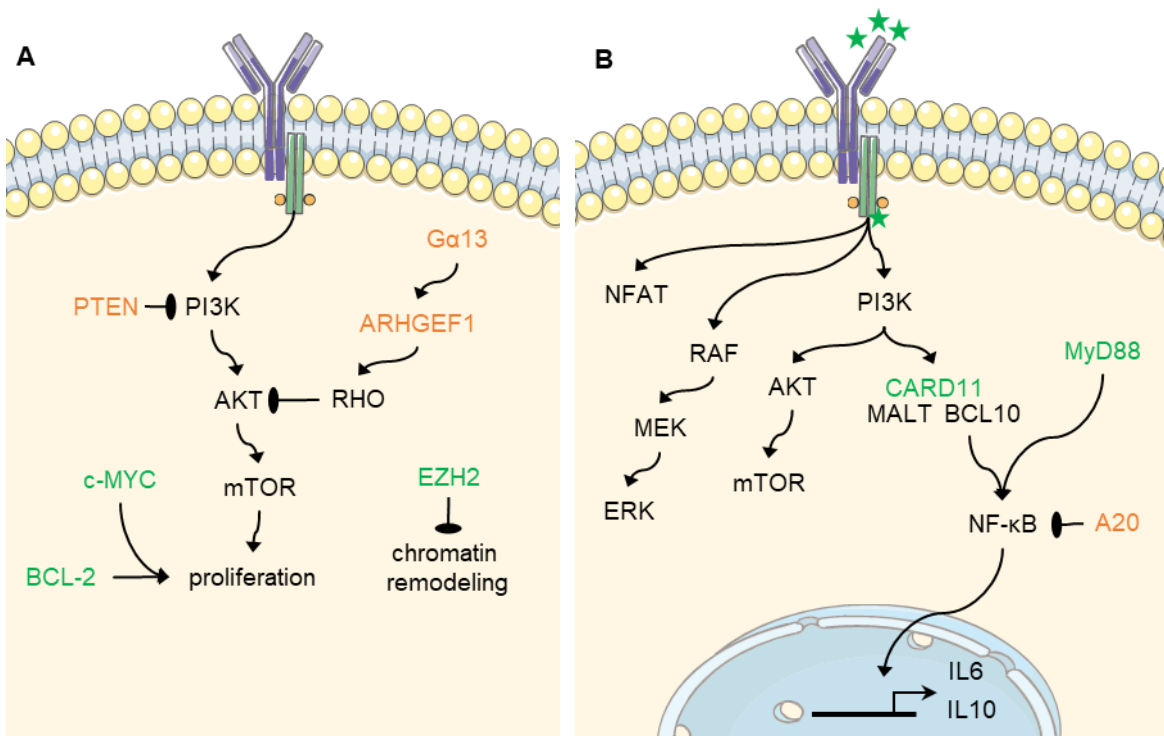


**Figure 2: Schematic overview of some known deregulated signaling pathways in DLBCLs.**

(A) The PI3K pathway is a major deregulated pathway of GCB DLBCLs. Missing negative interactions of  $G\alpha_{13}$  and PTEN contribute to the tonic BCR signaling. Aberrant regulation of c-MYC and BCL-2 enhance proliferation whereas EZH2 influences chromatin remodeling. (B) In ABC DLBCLs self-antigens and receptor mutations of CD79a/b initiate a BCR signaling with activation of the PI3K-AKT, NF-κB, ERK and NFAT pathways. CARD11, MyD88 or A20 mutations contribute to an enhanced NF-κB activation which induces IL6 or IL10 expression. Black lines represent the interaction. Upregulated and downregulated proteins are displayed in green and red, respectively. Adapted from Basso and Rickert (Basso and Dalla-Favera, 2015; Rickert, 2013).

## 1.5 Important pathway interactions and crosstalks

The inhibition of BCR-related kinases is promising for the treatment of several B cell malignancies. However, unexpected side effects and resistances occur consistently indicating disregarded feedback mechanisms (Blachly and Baiocchi, 2014). For cellular responses, the signal transmission from receptors to target gene expressions is not only a linear pathway. The signaling outcome is strongly regulated by different pathway kinetics and intensities. Thereby, the signal transduction from receptors to core kinase, the interaction between pathways and the modulation of feedbacks is essential to cause different reactions to extracellular stimuli (Bluthgen, 2015; Murphy and Blenis, 2006; Reth and Brummer, 2004). For this reason, signaling feedbacks and crosstalks can hamper targeted therapy through unknown effects. So far positive feedbacks of the BCR tyrosine kinases and the signalosome complex or negative feedbacks within one pathway have been described previously (Reth and Brummer, 2004). However, the downstream wiring of BCR-related pathways remains largely unexplored.

Beside its own negative feedback loop, the PI3K-AKT pathway interacts with the  $\beta$ -catenin pathway. AKT can phosphorylate and therefore inactivate glycogen synthase kinase-3 beta (GSK3 $\beta$ ) which is an inhibitory protein for  $\beta$ -catenin (Baracho *et al.*, 2011). This leads to increased expression of cell cycle regulators like c-MYC and cyclin D3 and constitutes a further opportunity of the PI3K-AKT pathway to promote proliferation (Cato *et al.*, 2011; Mazzoletti *et al.*, 2011). Besides, a similar negative impact of ERK1/2 to GSK3 $\beta$  is described (Ding *et al.*, 2005). The PI3K-AKT and MEK-ERK pathway share not only common downstream targets, they also influence each other. AKT can affect RAF phosphorylations leading to attenuation of the MEK-ERK pathway (Zimmermann and Moelling, 1999), whereas an ERK-dependent phosphorylation of MEK1 induces an interaction with PTEN at the membrane and causes a negative feedback on the PI3K-AKT pathway (Zmajkovicova *et al.*, 2013).

Positive and negative feedbacks are not exclusively mediated through phosphorylation of target proteins. Both kinases and phosphatases must be precisely regulated to determine the duration and intensity of pathways and thereby the signaling output. Several phosphatases are known to intervene at any tier of signal transduction, however, a large number of phosphatases regulate especially MAPKs (Bluthgen, 2015; Junnila *et al.*, 2008). Dual-specificity MAPK phosphatases (DUSP) specifically dephosphorylate threonine and tyrosine residues on different MAPK isoforms and can mediate the interplay between pathways (Jeffrey *et al.*, 2007). For instance, in lung cancer cells DUSP1 is induced in an ERK-dependent manner by cisplatin. DUSP1 then decreases the pathway activity of p38 MAPK and JNK (Low and Zhang, 2016). Furthermore, the PI3K-AKT

pathway can induce the degradation of the ERK-specific phosphatase DUSP6 and thus influences the ERK1/2 signal duration (Bermudez *et al.*, 2008).

Despite first approaches analyzing the interactions of pathways, interplays and feedback loops are often disregarded in signaling schemes. Classical genetic or modern loss-of-function experiments only reveal the linear order of signaling elements. Therefore, studies investigating pathway inhibitions are needed for the detection of feedbacks (Reth and Brummer, 2004). Our group previously generated a network model based on gene expression effects after different pathway perturbations (Pirkl *et al.*, 2016). However, this analysis could not fully elucidate the signaling network. To discover feedback loops and crosstalks the analysis of pathway activations seems to be indispensable.

## Aims

Many non-Hodgkin lymphomas are characterized by a strong dependency on the BCR signaling. The tonic BCR signaling is essential for the proliferation of Burkitt lymphoma and some GCB DLBCLs. In ABC DLBCLs mutations mimic a chronic active BCR, thereby causing NF- $\kappa$ B activation with subsequent JAK-STAT activation. While the proximal events and signaling cascades of the BCR are well studied, the downstream interplay of pathways is barely investigated although signaling feedbacks can promote or hinder the therapeutic success. Therefore, the establishment of reliable network models is useful to predict signaling alterations by external influences as well as therapeutic responses.

Our group has previously generated a Boolean Nested Effect model for BCR signaling from downstream gene expression changes of pathway perturbations (Pirkl *et al.*, 2016). To verify and complement the signaling network structure and to generate more accurate network models, the interplay of BCR-related signaling pathways was analyzed in B cell lymphomas. Thus, the primary objective of this study focused on the following questions:

1. Which pathway interplays exist downstream of the tonic BCR signaling in BLs?
2. Which pathway interplays occur after activation of the BCR in BLs?
3. Is it possible to construct a general network model with pathway interplays?
4. Do pathway interplays affect cellular functions like proliferation?
5. Are pathway interplays similar for tonic, activated and chronic active BCR signaling?

To address these aims, an antibody-based screen of phosphoproteins was used to compare different pathway perturbations and selected interactions were investigated in more detail.

In addition, our group has demonstrated that a simultaneous activation of TLR9 and IL10R signaling synergistically enhances proliferation by influencing cell cycle genes and metabolism (Feist, 2016). We proposed that in addition to NF- $\kappa$ B and STAT3 phosphorylation the interplay of TLR9 and IL10R activation led to hitherto unconsidered protein phosphorylations. Therefore, the second part of my thesis concentrated on the following questions:

1. Which other mediators beside NF- $\kappa$ B and STAT3 promote the proliferative boost?
2. Which cellular processes are directly influenced by the pathway activations?

For this purpose, comprehensive mass spectrometry analysis of the phosphoproteome was performed in the model cell line P493-6 after stimulation of TLR9 and IL10R to imitate a combined activation of NF- $\kappa$ B and STAT3.

## 2. Material and Methods

### 2.1 Material, recipes and equipment

#### 2.1.1 Biological material

Cell lines used in the study are listed in table 1.

**Table 1:** Cell lines

Cell line	Source	Distributor	Reference
BL-2	Homo sapiens Burkitt Lymphoma	DSMZ, Brunswick	(Bertrand <i>et al.</i> , 1981)
BL-41	Homo sapiens Burkitt Lymphoma	DSMZ, Brunswick	(Lenoir <i>et al.</i> , 1985)
CA-46	Homo sapiens Burkitt Lymphoma	DSMZ, Brunswick	(Magrath <i>et al.</i> , 1980)
HBL-1	Homo sapiens Diffuse Large B Cell Lymphoma (ABC)	Krappmann, Munich	(Nozawa <i>et al.</i> , 1988)
OCI-LY3	Homo sapiens Diffuse Large B Cell Lymphoma (ABC)	DSMZ, Brunswick	(Tweeddale <i>et al.</i> , 1987)
P493-6	Homo sapiens c-Myc transformed lymphoblastoid cell line	Bornkamm, Munich	(Polack <i>et al.</i> , 1996)

#### 2.1.2 Chemicals, solutions and consumable supplies

The chemicals, solutions and supplies used are recorded in table 2, 3 and 4, respectively.

**Table 2:** Chemicals

Chemical	Manufacturer
4-(2-hydroxyethyl)-1-piperazineethanesulfonic acid (HEPES)	Sigma-Aldrich, St. Louis, US
4-Iodophenylboronic acid (4-IPBA)	Sigma-Aldrich, St. Louis, US
Adenosine phosphosulfate (APS)	Serva, Heidelberg, DE
Albumin Fraction V (BSA)	Roth, Karlsruhe, DE
Ammonium sulfate	Merck KGaA, Darmstadt, DE
Bromophenol blue	Serva, Heidelberg, DE
Chameleon Duo Pre-stained Protein Ladder	LI-COR, Lincoln, US
cComplete Mini	Roche, Basel, CH
Desoxyribonucleosid triphosphate (dNTP)	PrimeTech LTD, Minsk, BY
Diethylpyrocarbonate (DEPC)	Roth, Karlsruhe, DE
Dimethyl sulfoxide (DMSO)	Sigma-Aldrich, St. Louis, US
Dithiothreitol (DTT)	Sigma-Aldrich, St. Louis, US

Chemical	Manufacturer
DMSO cell culture grade	Sigma-Aldrich, St. Louis, US
Ethanol	Roth, Karlsruhe, DE
Ethylenediaminetetraacetic acid (EDTA)	Merck KGaA, Darmstadt, DE
Ethylene glycol bis(2-aminoethyl ether) tetraacetic acid (EGTA)	Sigma-Aldrich, St. Louis, US
Full range rainbow molecular weight marker	GE Healthcare, Chicago, US
Glycerol	Merck KGaA, Darmstadt, DE
Glycine	Roth, Karlsruhe, DE
HEPES cell culture grade (Gibco)	Thermo Fisher, Waltham, US
Hot FIREpol DNA polymerase (5 U/ $\mu$ l)	PrimeTech LTD, Minsk, BY
Hydrochloric acid 37 %	Merck KGaA, Darmstadt, DE
Hydrogen peroxide 30 %	Sigma-Aldrich, St. Louis, US
Isopropanol	Roth, Karlsruhe, DE
L-Arginine:HCl unlabeled	Euriso-Top, Saarbrücken, DE
L-Arginine:HCl ( $^{13}\text{C}_6$ , 99 %; $^{15}\text{N}_4$ , 99 %)	Euriso-Top, Saarbrücken, DE
L-Lysine:2HCl unlabeled	Euriso-Top, Saarbrücken, DE
L-Lysine:2HCl ( $^{13}\text{C}_6$ , 99 %)	Euriso-Top, Saarbrücken, DE
L-Proline	Sigma-Aldrich, St. Louis, US
Luminol	Sigma-Aldrich, St. Louis, US
Magnesium chloride ( $\text{MgCl}_2$ )	Merck KGaA, Darmstadt, DE
Melisepol	B. Braun, Melsungen, DE
Methanol	Roth, Karlsruhe, DE
Nonylphenyl-polyethylene glycol (NP-40)	Sigma-Aldrich, St. Louis, US
Phenylmethanesulfonyl fluoride (PMSF)	Sigma-Aldrich, St. Louis, US
Phosphatase Inhibitor Cocktail 2	Sigma-Aldrich, St. Louis, US
Phosphatase Inhibitor Cocktail 3	Sigma-Aldrich, St. Louis, US
PhosSTOP	Roche, Basel, CH
Potassium chloride (KCl)	Merck KGaA, Darmstadt, DE
Sodium chloride (NaCl)	Roth, Karlsruhe, DE
Sodium dodecyl sulfate (SDS)	Serva, Heidelberg, DE
Sodium fluoride	Sigma-Aldrich, St. Louis, US
Sodium orthovanadate	Sigma-Aldrich, St. Louis, US
Sodium pyruvate	Sigma-Aldrich, St. Louis, US
SYBR green master mix fast	Applied Biosystems, Kalifornien, US
Tetramethylethylenediamine (TEMED)	Sigma-Aldrich, St. Louis, US
Trehalose dihydrate	Roth, Karlsruhe, DE
Tris(hydroxymethyl)-aminomethanhydrochlorid (Tris-HCl)	Roth, Karlsruhe, DE
TritonX-100	Roth, Karlsruhe, DE
Tween-20	Serva, Heidelberg, DE
Water HPLC grade	Th.Geyer, Renningen, DE
Urea	Sigma-Aldrich, St. Louis, US

**Table 3:** Solutions

Solution	Manufacturer
Acrylamide/Bis Solution 40 % (w/v)	Serva, Heidelberg, DE
Dulbecco's Phosphate Buffered Saline (DPBS)	Lonza, Basel, CH
Fetal Bovine Serum (FBS) (Gibco)	Thermo Fisher, Waltham, US
Fetal Bovine Serum (FBS) Dialyzed (Gibco)	Thermo Fisher, Waltham, US
Odyssey Blocking Buffer	LI-COR, Lincoln, US
Penicillin and Streptomycin	Lonza, Basel, CH
Ponceau S Solution	Sigma-Aldrich, St. Louis, US
Re-Blot Plus Mild Solution (10x)	Merck Millipore, Burlington, US
RPMI-1640 with L-Glutamine	Lonza, Basel, CH
RPMI 1640 Media for SILAC	Thermo Fisher, Waltham, US
Roti-Load 1 (4x)	Roth, Karlsruhe, DE
Roti-Quant (5x)	Roth, Karlsruhe, DE
Trypan Blue Solution 0.4 %	Sigma-Aldrich, St. Louis, US

**Table 4:** Consumables

Consumable	Manufacturer
Blotting paper BF3	Th.Geyer, Renningen, DE
C-Chip disposable hemocytometer NI	NanoEnTek, Waltham, US
Cell culture flasks, suspension (T25, T75, T175)	Sarstedt, Nümbrecht, DE
Combitips advanced (0.5, 5.0 ml)	Eppendorf, Hamburg, DE
Cryo tubes (2 ml)	Greiner Bio-One, Kremsmünster, AT
Eppendorf tubes (5.0 ml)	Eppendorf, Hamburg, DE
Falcon tubes (15, 50 ml)	Sarstedt, Nümbrecht, DE
Filtropur S 0.2	Sarstedt, Nümbrecht, DE
Immobilon-FL transfer membrane PVDF 0.45 µm	Merck KGaA, Darmstadt, DE
Immobilon-P transfer membrane PVDF 0.45 µm membranes (8 µm pores)	Merck KGaA, Darmstadt, DE
Micro tubes (0.5, 1.5, 2.0 ml)	Neuro Probe, Gaithersburg, US
Microplate PCR (384 well)	Sarstedt, Nümbrecht, DE
Microtest plate (96 well)	Greiner Bio-One, Kremsmünster, AT
Multiply- µStrip pro 8-strip	Sarstedt, Nümbrecht, DE
Optical adhesive covers	Sarstedt, Nümbrecht, DE
Pasteur pipettes (150, 230 mm)	Applied Biosystems, Kalifornien, US
Pipette tips (20, 200, 1000 µl)	Th.Geyer, Renningen, DE
Serological pipettes (5, 10, 25 ml)	Sarstedt, Nümbrecht, DE
Sterling nitrile powder-free exam gloves	Halyard Health, Georgia, US
Syringe (5.0, 50 ml)	B. Braun, Melsungen, DE
TipOne filter tips (10, 200, 1000 µl)	Starlab, Hamburg, DE
well plate, suspension, flat (6, 12, 96 well)	Sarstedt, Nümbrecht, DE
well plate, suspension, round (96 well)	Sarstedt, Nümbrecht, DE

### 2.1.3 Buffers and media

The recipes of buffers used in the study are presented in table 5. All buffers are water-based. For cell culture used media and supplements are listed in table 6.

**Table 5:** Recipes of buffers

Buffer	Recipe
chemiluminescence solution 1	100 mM Tris pH 8.8 2.5 mM Luminol 4 mM 4-IPBA
chemiluminescence solution 2	100 mM Tris pH 8.8 9 mM Hydrogen peroxide
NP-40 lysis buffer	50 mM Tris pH 7.4 150 mM NaCl 1 mM EDTA 0.50 % (v/v) NP-40 0.1 mg/ml PMSF 1 x cComplete Mini 1 x PhosSTOP 125 µM Sodium orthovanadate
NP-40 lysis buffer modified	50 mM Tris pH 7.8 150 mM NaCl 0.5 mM EDTA 1 % (v/v) NP-40 10 % (v/v) Glycerol 2 mM Sodium orthovanadate 1 mM Sodium fluoride 1 x cComplete Mini 1 x Phosphatase Inhibitor Cocktail 2 1 x Phosphatase Inhibitor Cocktail 3
nuclear extraction buffer A	10 mM HEPES pH 7.9 10 mM KCl 100 µM EDTA 100 µM EGTA 1 mM DTT 1 x cComplete Mini 1 x PhosSTOP
nuclear extraction buffer B	20 mM HEPES pH 7.9 400 mM KCl 1 mM EDTA 1 mM EGTA 1 mM DTT 1 x cComplete Mini 1 x PhosSTOP

Buffer	Recipe
PCR buffer	750 mM Tris pH 8.8 200 mM Ammonium sulfate 0.1 % (v/v) Tween-20 in 0.1% (w/v) depc water
resolving gel buffer	375 mM Tris pH 8.8 25 % (v/v) Acrylamide/Bis Solution (40%) 0.0004 % (w/v) APS 0.00125 % (v/v) TEMED
running buffer	25 mM Tris 192 mM Glycine 34.67 mM SDS
stacking gel buffer	125 mM Tris pH 6.8 12.5 % (v/v) Acrylamide/Bis Solution (40%) 0.0004 % (w/v) APS 0.00125 % (v/v) TEMED
SYBR green Mix	1 x PCR buffer 3 mM MgCl <sub>2</sub> 1:80000 SYBR green 0.2 mM dNTP each 20 U/ml Hot FIREpol DNA polymerase 0.25 % (v/v) TritonX-100 0.5 mM Trehalose dihydrate in 0.1% (w/v) depc water
Tris buffered saline (TBS) pH 7.6	20 mM Tris 137 mM NaCl
TBS-T	1 x TBS buffer 0.1 % (v/v) Tween-20
transfer buffer pH 8.3	25 mM Tris 192 mM Glycine 15 % (v/v) methanol
urea buffer	25 mM Tris pH 8.0 8 M urea 1 x cComplete Mini

**Table 6:** Media

Medium	Recipe (Manufacturer)
cell culture medium	RPMI-1640 with L-Glutamine (Lonza) 10 % (v/v) heat-inactivated FBS (Gibco) 100 U/ml Penicillin + 100 U/ml Streptomycin
cell labeling medium light	RPMI 1640 Media for SILAC (Thermo Fisher) 10 % (v/v) heat-inactivated FBS Dialyzed (Gibco) 100 U/ml Penicillin + 100 U/ml Streptomycin 0.824 mM L-Arginine:HCl unlabeled 0.275 mM L-Lysine:2HCl unlabeled 200 mg/l L-Proline
cell labeling medium heavy	RPMI 1640 Media for SILAC (Thermo Fisher) 10 % (v/v) heat-inactivated FBS Dialyzed (Gibco) 100 U/ml Penicillin + 100 U/ml Streptomycin 0.824 mM L-Arginine:HCl ( $^{13}\text{C}_6$ , 99 %; $^{15}\text{N}_4$ , 99 %) 0.275 mM L-Lysine:2HCl ( $^{13}\text{C}_6$ , 99 %) 200 mg/l L-Proline
cell freezing medium	90 % (v/v) heat-inactivated FBS (Gibco) 10 % (v/v) DMSO cell culture grade

#### 2.1.4 Cell culture supplements, inhibitors and siRNA

In this study, cells were stimulated with soluble factors under the conditions listed in table 7. Inhibitors used to reduce different pathway activities are presented in table 8 with their respective working concentrations. Table 9 includes the small interfering RNA (siRNA) used for transient transfection analyses.

**Table 7:** Stimulants used in cell culture

Stimulant	Working concentration	Manufacturer
anti-human IgM F(ab')2 (α-IgM) Fragment	13 µg/ml	Jackson ImmunoResearch, Cambridgeshire, GB
CpG ODN2006	0.5 µM	InvivoGen, San Diego, US
Doxycycline	1 ng/ml	Clontech, Saint-Germain-en-Laye, FR
recombinant human IL10	40 ng/ml	Peprotech, Rocky Hill, US

**Table 8:** Inhibitors used in cell culture

Inhibitor	Target	Working concentration	Manufacturer
(5Z)-7-Oxozeaenol	TAK1	0.5 µM	Tocris Bioscience, Bristol, GB
ACHP	IKK $\beta$	7 µM	Merck KGaA, Darmstadt, DE
AZD6244	MEK 1,2	1 µM	Selleckchem, Munich, DE
AZ-TAK1	TAK1	0.5 µM	Abcam, Cambridge, GB
BKM120	p100 $\alpha, \delta, \beta, \gamma$	1 µM	Selleckchem, Munich, DE
CAL-101	p100 $\delta, \gamma$	1 µM	Selleckchem, Munich, DE
Ibrutinib	BTK	10 µM	Selleckchem, Munich, DE
JNK Inhibitor VIII	JNK 3,1,2	5 µM	Merck KGaA, Darmstadt, DE
LY294002	p100 $\alpha, \delta, \beta$	10 µM	Merck KGaA, Darmstadt, DE
MK-2206	AKT 1,2,3	1 µM	Selleckchem, Munich, DE
MLN120B	IKK $\beta$	10 µM	MedChemExpress, Sollentuna, SE
Rapamycin	mTOR	1 µM	Selleckchem, Munich, DE
SB203580	p38 $\alpha, \beta$	2 µM	Sigma-Aldrich, St. Louis, US
SP600125	JNK 1,2,3	5 µM	Merck KGaA, Darmstadt, DE
U0126	MEK 2,1	10 µM	Sigma-Aldrich, St. Louis, US

**Table 9:** siRNA

siRNA	Manufacturer	Order no.
MAPK14 (p38 MAPK)	Dharmacon, Colorado, US	L-003512-00-0005
negative control (scrB)	Life Technologies, Carlsbad, US	4390844

### 2.1.5 Antibodies

The detection of phosphorylated or total proteins was conducted in the study with antibodies listed in table 10.

**Table 10:** Antibodies

Antibody against	Host species	Dilution	Order no.	Source
AKT	rabbit	1:1000	9272	Cell Signaling Technology, Leiden, NL
p-AKT (Ser473)	rabbit	1:1000	9271	Cell Signaling Technology, Leiden, NL
Histone Deacetylase 1 (HDAC1)	rabbit	1:1000	2062	Cell Signaling Technology, Leiden, NL
MEK1/2	rabbit	1:1000	9122	Cell Signaling Technology, Leiden, NL

Antibody against	Host species	Dilution	Order no.	Source
p-MEK1/2 (Ser217/221) (41G9)	rabbit	1:1000	9154	Cell Signaling Technology, Leiden, NL
Mouse IgG-HRP	goat	1:2000	sc-2005	Santa Cruz Biotechnology, Dallas, US
Mouse IRDye 680RD	goat	1:15000	925-68070	LI-COR, Lincoln, US
p38 MAPK	rabbit	1:1000	9212	Cell Signaling Technology, Leiden, NL
p-p38 MAPK (Thr180,Tyr182) (D3F9)	rabbit	1:1000	4511	Cell Signaling Technology, Leiden, NL
p44/p42 (ERK1/2) (L34F12)	mouse	1:1000	4696	Cell Signaling Technology, Leiden, NL
p-p44/p42 (pERK1/2) (Thr202/Tyr204) (197G2)	rabbit	1:1000	4377	Cell Signaling Technology, Leiden, NL
p70 S6 Kinase (49D7)	rabbit	1:1000	2708	Cell Signaling Technology, Leiden, NL
p-p70 S6 Kinase (Thr389) (108D2)	rabbit	1:1000	9234	Cell Signaling Technology, Leiden, NL
Rabbit IgG-HRP	goat	1:2000	sc-2004	Santa Cruz Biotechnology, Dallas, US
Rabbit IRDye 800CW	goat	1:15000	925-32211	LI-COR, Lincoln, US
p-Raf1 (Ser289/296/301)	rabbit	1:1000	9431	Cell Signaling Technology, Leiden, NL
p-Raf1 (Ser338) (56A6)	rabbit	1:1000	9427	Cell Signaling Technology, Leiden, NL
S6 ribosomal protein (54D2)	mouse	1:1000	2317	Cell Signaling Technology, Leiden, NL
p-S6 ribosomal protein (Ser240/244)	rabbit	1:1000	2215	Cell Signaling Technology, Leiden, NL
TAK1 (D94D7)	rabbit	1:1000	5206	Cell Signaling Technology, Leiden, NL
Tubulin	mouse	1:1000	05-829	Merck Millipore, Burlington, US

### 2.1.6 Oligonucleotides

For quantitative real-time PCR (qRT-PCR), oligonucleotides listed in table 11 were applied. All oligonucleotides were purchased from IBA Lifesciences (Goettingen, DE).

**Table 11:** Oligonucleotides

Gene	Forward primer (5' - 3')	Reverse primer (5' - 3')
<i>EGR2</i>	GCA CCA GCT GTC TGA CAA CAT CT	CAT GTC AAT GTT GAT CAT GCC ATC
<i>EGR3</i>	CGG TGA CCA TGA GCA GTT TG	GTA GGT CAC GGT CTT GTT GC
<i>FOS</i>	GCT TCA ACG CAG ACT ACG AG	AGT GAC CGT GGG AAT GAA GT
<i>GAPDH</i>	CAG CCT CAA GAT CAT CAG CA	CAT GAG TCC TTC CAC GAT ACC
<i>MAP2K6</i>	GTG AAG GCA GAT GAC CTG GAG	GGA TCC GCT TCA CTG CCA T
<i>PDP1</i>	CCA GAC GAA TTG GAA TCC CAG	AGT GCC ATA GAT CCT GCT CAG TTC
<i>PLD6</i>	CAA ATC GGT CTG CTG CGC	AGT GAT GAG CAC CCT CTT GTC C
<i>PTGS1</i>	AGC AGA GTT GGA GGA ATT GTA TGG	CAG GGT AGA ACT CCA ACG CAT C
<i>TNF<math>\alpha</math></i>	TCT CTA ATC AGC CCT CTG G	CTA CAA CAT GGG CTA CAG G
<i>ZFP36L1</i>	TCT GCC ACC ATC TTC GAC TT	GTC TTG TAG CGG CTG GAG TT

### 2.1.7 Ready to use reaction systems

Assays in the study were conducted with ready to use reaction systems which are shown in table 12.

**Table 12:** Reaction systems

Description	Manufacturer	Order no.
Amaxa Cell Line Nucleofector Kit V	Lonza, Basel, CH	VCA-1003
BCA Protein Assay	Thermo Fisher, Waltham, US	23225
Bio-Plex Pro Cell Signaling Reagent	BIO-RAD, Hercules, US	171-304006M
Calcein AM Cell Viability	R&D Systems, Minneapolis, US	
NucleoSpin RNA	Macherey-Nagel, Düren, DE	740.955.250
SuperScript II Reverse Transcriptase	Invitrogen, Carlsbad, US	18064-014

### 2.1.8 Equipment

Analyses in the study were done with the equipment listed in table 13.

**Table 13:** Equipment

Instrument	Manufacturer
7900HT Fast Real-Time PCR System	Thermo Fisher, Waltham, US
Balance Kern EW420-3NM	Kern&Sohn, Balingen, DE
Bio-Plex Protein Array system	BIO-RAD, Hercules, US
Centrifuge Heraeus Fresco 21	Thermo Fisher, Waltham, US
Centrifuge Heraeus Multifuge 3 L-R	Thermo Fisher, Waltham, US
Centrifuge Heraeus Multifuge X3R	Thermo Fisher, Waltham, US
Counting chamber Neubauer Improved	LO LaborOptik, Friedrichsdorf, DE
Freezer (-80°C)	Panasonic Corporation, Osaka, JP
Heraeus BB6220	Thermo Fisher, Waltham, US
IKAMAG RCT	IKA Works, Staufen, DE
Image Reader LAS-4000 mini	Fujifilm, Tokio, JP
Infinite F50	Tecan Group, Männedorf, CH
Laminar flow Telstar Bio-II-A	Prettl, Pfullingen, DE
Micro centrifuge 1-15K	Sigma-Aldrich, St. Louis, US
Micro centrifuge 220 VAC	Roth, Karlsruhe, DE
Micro centrifuge 5424	Eppendorf, Hamburg, DE
Micro Chemotaxis Chamber (48-well)	Neuro Probe, Gaithersburg, US
Microscope Telaval 31	Zeiss, Oberkochen, DE
Mini Trans-Blot Cell	BIO-RAD, Hercules, US
Multipette plus	Eppendorf, Hamburg, DE
Nalgene Cryo 1°C Freezing Container	Thermo Fisher, Waltham, US
Nucleofector 2b	Lonza, Basel, CH
Odyssey CLx	LI-COR, Lincoln, US
pH-Meter 761 Calimatic	Knick, Berlin, DE
Pipette 8-channel (1-10 µl)	Eppendorf, Hamburg, DE
Pipette 8-channel (10-100 µl) ErgoOne	Starlab, Hamburg, DE
Power Pac 300	BIO-RAD, Hercules, US
Power Supply EV202	Consort bvba, Turnhout, BE
Roller Mixer SRT6	Stuart, Staffordshire, GB
Shaker 3005	GFL, Burgwedel, DE
Spectrophotometer ND-1000	Thermo Fisher, Waltham, US
Synergy HTX multi-mode reader	BioTek, Winooski, US
Biometra Thermocycler T3000	Analytik Jena, Jena, DE
UVC/T-AR, DNA/RNA UV-cleaner box	BioSan, Riga, LV
Vortex Genius 3	IKA Works, Staufen, DE
Water bath	Köttermann, Uetze, DE

### 2.1.9 Software

Software presented in table 14 was used for analysis and visualization of the obtained data.

**Table 14:** Software

Software	Developer
ABI 7900HT SDS 2.4	Applied Biosystems, Kalifornien, US
ABI RQ Manager 1.2.1	Applied Biosystems, Kalifornien, US
Adobe Illustrator CS6 Version 16.0.0	Adobe Systems, Kalifornien, US
Adobe Photoshop CS2 Version 9.0	Adobe Systems, Kalifornien, US
Bio-Plex Manager Software	BIO-RAD, Hercules, US
EndNote X5	Clarivate Analytics, Pennsylvania, US
Gen5 2.0	BioTek, Winooski, US
GraphPad Prism Version 7.03	GraphPad Software, La Jolla, US
Image Studio Lite Version 5.2.5	LI-COR, Lincoln, US
Microsoft Office Professional Plus 2016 (Excel, Word, PowerPoint)	Microsoft, Washington, US
Magellan for F50 Version 7.0	Tecan Group, Männedorf, CH
LAS-4000 mini Version2.0	Fujifilm, Tokio, JP
NanoDrop 1000 3.8.1	Thermo Fisher, Waltham, US

## 2.2 Cell Biology

### 2.2.1 Cell Culture

All cell lines used in this study were grown in cell culture medium at 37°C and 5 % CO<sub>2</sub>. The cells were kept in culture for up to four weeks. BLs were cultivated at a density of 1.5 x 10<sup>5</sup> to 1.5 x 10<sup>6</sup> cells/ml by splitting three times a week. ABC DLBCLs and P493-6 cells were maintained at a higher density of 3 x 10<sup>5</sup> to 1.5 x 10<sup>6</sup> cells/ml. To determine the cell numbers a hemocytometer was used for counting and dead cells were excluded by trypan blue. For experiments, cells were freshly adjusted the day before. Furthermore, the MYC overexpressing P493-6 cells were supplemented with 1 ng/ml doxycycline 16 hours prior to the experiment to obtain a c-Myc depleted condition.

For long-term storage, the cell lines were frozen. For this propose, cells were centrifuged (100 x g, RT) for 5 minutes and resuspended in cell freezing medium. Suspensions of 1 ml containing 3 x 10<sup>6</sup> cells of BLs or 5 x 10<sup>6</sup> cells of DLBCLs/P493-6 were cooled down to -80°C using a cryo freezing container. The cryo freezing container filled with isopropanol provides a constant cooling of -1°C per minute. After 24 hours the cryo tubes were placed at -150°C for long-term storage. The thawing was performed rapidly in a

37°C water bath and the 1 ml cell suspension was transferred in 9 ml cell culture medium. After centrifugation (100 x g, RT) for 5 minutes the cells were resuspended in fresh cell culture medium and adjusted to their optimal density.

### **2.2.2 Stable isotope labeling by amino acids in cell culture**

For phosphoproteomics, stable isotope labeling by amino acids in cell culture (SILAC) was used to analyze two conditions simultaneously by mass spectrometry. The incorporation of <sup>13</sup>C- and <sup>15</sup>N-labeled amino acids during protein turnover leads to a distinct mass difference between the samples making them quantitative and accurate comparable (Mann, 2006). P493-6 cells were thawed and cultured in cell culture medium for three days. Afterwards the cell medium was replaced by either cell labeling medium light or cell labeling medium heavy for seven days to fully incorporate the label into proteins. To avoid an arginine to proline conversion, the labeling medium was supplemented with 200 mM L-proline. After six days and 16 hours prior to the experiment, the cells were centrifuged (100 x g, RT) for 5 minutes and freshly adjusted to  $8 \times 10^5$  cells/ml. Besides, the light-labeled cells were stimulated with 1 ng/ml doxycycline to obtain a c-Myc depleted condition.

### **2.2.3 Inhibitor treatment and stimulation of the BCR signaling**

The inhibition of distinct pathway activations was done with inhibitors which are displayed with their working concentrations in Table 8. As all inhibitors are solved in DMSO, the control cells were always treated with the equal volume of DMSO. The different cell lines were seeded in fresh cell culture medium and adjusted to a density of  $1 \times 10^6$  cells/ml. For studying protein phosphorylations, the cells were incubated with inhibitors for 3 hours. HBL-1 and OCI-LY3 were then harvested while BLs were incubated for additional 30 minutes with or without BCR activation. The BCR activation was done by stimulation with 13 µg/ml anti-human IgM F(ab')2 for 5 or 30 minutes. For RNA analysis, inhibitors were supplemented 3 hours before the BCR was activated for 1 - 3 hours.

### **2.2.4 IL10 and CpG stimulation**

For phosphoproteomics, isotope labeled P493-6 cells were counted and 20 million heavy-labeled cells stimulated with 40 ng/ml IL10 and 0.5 µM CpG as control reference. The light-labeled cells were divided in two samples of 10 million cells respectively. While one was treated with 40 ng/ml IL10 and 0.5 µM CpG, the other was equally stimulated with DPBS + 0.1 % BSA as control. After 30 minutes of pathway activation cells were harvested for mass spectrometry analysis.

For studying the impact of STAT3 and NF-κB activation on the migration capacity, c-Myc depleted P493-6 cells were counted and centrifuged (100 x g, RT) for 5 minutes. After adjustment to a density of  $1 \times 10^6$  cells/ml in FBS-free cell culture medium, P493-6 cells were supplemented with 1 ng/ml doxycycline to maintain the c-Myc depleted condition. Furthermore, the cells were stimulated with 40 ng/ml IL10 and 0.5 μM CpG and the control cells were treated with equal amounts of DPBS + 0.1 % BSA. The migration assay was performed immediately.

#### 2.2.5 RNA-interference-mediated gene knockdown

To down regulate specific proteins, small interfering RNAs (siRNA) were transferred by an electroporation-based method called Nucleofector™ Technology (Lonza). The combination of unique buffers with cell-specific electroporation programs ensures high transfection efficiencies especially for suspension cells. For the BL-2 cell line the Amixa Cell Line Nucleofector Kit V (Lonza) and the Nucleofector 2b (Lonza) with program R-013 was used. According to the manufacturer's transfection protocol, 2 million cells were centrifuged (90 x g, RT) for 10 minutes and resuspended in 100 μl Nucleofector Solution V with 2 μg siRNA. The cells were immediately transfected and received in pre-warmed cell culture medium supplemented with 10 mM HEPES and 1 mM sodium pyruvate. After 24 hours cells were stimulated with 13 μg/ml anti-human IgM F(ab')2 for 30 minutes and harvested for protein phosphorylation analysis.

#### 2.2.6 Cell viability assay

The cell viability after inhibitor treatment was determined using the Calcein AM Cell Viability Assay (R&D Systems). Calcein AM is a non-fluorescent, cell-permeable compound that is converted to a green-fluorescent dye by esterases of living cells. The inhibition of distinct pathway activations was done with inhibitors which are displayed with their working concentrations in Table 8. As all inhibitors are solved in DMSO, the control cells were always treated with the equal volume of DMSO. Inhibitor treated and control cells were seeded as triplicates in a 96-well plate. BLs were adjusted to  $7.5 \times 10^3$  cells/well and ABC DLBCLs to  $1.5 \times 10^4$  cells/well in a final volume of 50 μl. After certain time points, 50 μl 1 x Calcein buffer were added to each well and the plate was centrifuged (200 x g, RT) for 3 minutes. The supernatant was removed and the cells incubated in 100 μl 1 x Calcein buffer with 0.1 μM Calcein AM for 20 minutes at 37°C. Three wells without cells were additionally filled as blank value. Punctually, the absorption at 485 nm was measured and the viability calculated. For this purpose, the blank value was subtracted from sample values and all treatments normalized to the control.

### 2.2.7 Migration assay

The migration potential of cells towards a stimulus was studied with the Boyden Chamber assay (Chen, 2005). The boyden chamber consists of two chambers separated by a porous membrane. Therefore, the movement of cells through pores of a defined size can be regarded. For the P493-6 cell line, a 48-well micro chemotaxis chamber and membranes with 8 µm pore size were used. The lower wells were filled with either cell culture medium containing 10 % FCS as directed migration or medium without FCS as undirected condition. After placing the membrane and sealing the chamber, the upper wells were filled with cell suspension. The cell suspension contained  $1 \times 10^6$  cells/ml in FCS-free cell culture medium. The chamber was then incubated at 37°C and the cells were allowed to migrate for 6 hours. Afterwards, the chamber was disassembled and the cell concentration of the lower wells was determined. For each condition six technical replicates were evaluated by cell counting using disposable hemocytometer chips. The cell amount of each condition was normalized to the directed control condition.

## 2.3 Protein biochemistry

### 2.3.1 Preparation of cell lysates and cell fractionation for Western Blot analysis

After stimulation, inhibitor treatment or siRNA transfection cells were harvested for pathway analysis. To protect protein phosphorylation cells were firstly cooled down on ice by addition of the two-fold volume of ice-cold DPBS supplemented with 0.5 x PhosSTOP (Roche) and 100 µM sodium orthovanadate. Furthermore, the cells were centrifuged (500 x g, 4°C) for 5 minutes, washed once and the dry pellet stored at -80°C. For lysis, the cell pellet was resuspended in 50 µl cold NP-40 lysis buffer and shaken for 30 minutes on ice. The debris was removed by centrifugation (14.000 x g, 4°C) for 15 minutes and the supernatant transferred into new tubes. The protein concentration was determined with Roti-Quant (Roth) according to the manufacturer's instructions for use. Protein concentration of all samples were adjusted to each other with lysis buffer.

To separate cytosolic and nuclear fractions cells were burst by swelling and intact nuclei isolated as described by Schreiber *et al.* (Schreiber *et al.*, 1989). After stimulation or inhibitor treatment, cells were cooled down on ice by addition of the one-fold volume of ice-cold DPBS supplemented with 0.5 x PhosSTOP (Roche) and 100 µM sodium orthovanadate. The cells were centrifuged (500 x g, 4°C) for 5 minutes and washed once. In order to burst the cell membrane 200 µl nuclear extraction buffer A were added and samples were shaken 15 minutes on ice. Immediately, samples were supplemented with 12.5 µl 10 % NP-40, mixed by vortexing and the nuclei were collected by centrifugation

(14000 x g, 4°C) for 1 minute. The supernatant containing the cytosolic fraction was transferred to a new tube. The pellets were washed with 50 µl nuclear extraction buffer A and centrifuged (14000 x g, 4°C) for 1 minute. After discarding the supernatant pellets were lysed in 30 µl nuclear extraction buffer B for 25 minutes while shaking on ice. Finally, the debris was removed by centrifugation (14000 x g, 4°C) for 5 minutes and the supernatant with the nuclear fraction transferred to a new tube. The protein concentration of both fractions was determined with Roti-Quant (Roth) according to the manufacturer's instructions for use. Protein concentrations of all samples were adjusted to each other with the respective buffer.

### 2.3.2 SDS Page, Western Blot and Immunodetection

The separation of proteins was done by a discontinuous sodium dodecyl sulfate (SDS) polyacrylamide gel electrophoresis (Page) (Laemmli, 1970). For this purpose, modified buffers were used to generate a 10 % resolving gel with a 5 % stacking gel at least 24 hours in advance. The samples were supplemented with 1 x Roti-Load (Roth) and heated to 95°C for 5 minutes just before use. The gel was loaded with 20 µg protein and a molecular weight marker to determine protein size. For separation, the chamber was filled with 1 x running buffer and a current of 30 mA for 20 minutes was firstly used. Furthermore, the current was set to 20 mA for 1 hour. The voltage was limited to 150 V to avoid overheating and the run was stopped after the dye front had left the gel.

In order to transfer the separated proteins to a hydrophobic membrane, the tank transfer system was used (Towbin *et al.*, 1979). In deviation to this, a PVDF membrane was taken which needs to be activated by 100 % methanol for 20 seconds, to be rehydrated in ddH<sub>2</sub>O for 2 minutes and to be equilibrated in transfer buffer for 5 minutes. Meanwhile, the SDS page gels were incubated in transfer buffer and the stacking gel was cut off. After blotting at 4°C and 100 V for 1 hour the membranes were removed and air-dried for 30 minutes. For re-wetting, membranes were shortly incubated in 100 % methanol and washed twice with TBS for 5 minutes. Blocking of unspecific binding sites was done with Odyssey Blocking Buffer or 5 % BSA in TBS for 1 hour (RT).

To detect the protein of interest the membranes were incubated overnight (4°C) in 5 % BSA-TBS-T with the primary antibody (Table 10). After washing 3 times for 5 minutes with TBS-T the suitable secondary antibody in 5 % BSA-TBS-T was added for 1 hour (RT). Finally, the membranes were washed further 3 times and the secondary antibodies visualized either by chemiluminescence or fluorescence detection. For chemiluminescence, the self-prepared chemiluminescence solutions 1 and 2 were mixed in equal parts according to Haan & Behrmann (Haan and Behrmann, 2007) and the Image

Reader LAS-4000 mini (Fujifilm) was used. The detection of fluorescence was performed light-protected with the Odyssey CLx (LI-COR). After staining of protein phosphorylations, the membranes were reblotted 15 minutes in 1 x Re-Blot Plus Mild Solution and washed three times with TBS. Before analyzing the total protein, the membrane was blocked in Odyssey Blocking Buffer or 5 % BSA in TBS for 1 hour (RT). Then the next antibody detection could be performed overnight as described above.

### 2.3.3 Bio-Plex® Multiplex Immunoassay

To measure 15 different protein phosphorylations in one sample, the magnetic bead-based multiplex assay (BIO-RAD) was performed in close collaboration with the Blüthgen group of the Institute of Pathology (Charité – University Medicine Berlin). The principle is that a specific antibody coupled to a color-coded bead identifies the protein of interest while a second detection antibody determines the magnitude of a distinct phosphorylation. For this analysis, the Bio-Plex Pro Cell Signaling Reagent Kit (BIO-RAD) was used. The treated lymphoma cells were cooled down by addition of the three-fold volume of ice-cold DPBS supplemented with 1 x PhosSTOP (Roche) and 100 µM sodium orthovanadate. After 5 minutes centrifugation (500 x g, 4°C) the cells were washed once. According to the instruction manual the cells were lysed in the provided buffer containing 1 x factor QG and 2 mM PMSF. After shaking for 20 minutes at 4°C debris was removed by centrifugation (14000 x g, 4°C) for 15 minutes. The protein concentration was determined with the BCA Protein Assay Kit according to the user guide. In brief, the samples were diluted 1:8 and 1 part of solution B was mixed with 50 parts of solution A. 112 µl of the solution mix was added to 14 µl diluted sample, the samples were shaken for 30 seconds and then incubated for 30 minutes at 37°C. To determine the protein concentration the absorption was measured at 560 nm. Afterwards the samples were transferred in a 96 well plate, stored at -80°C and shipped on dry ice to the Blüthgen group for analysis.

The analysis with the Bio-Plex Protein Array system (BIO-RAD) was done by Anja Sieber of the Institute of Pathology (Charité – University Medicine Berlin) as published before (Klinger *et al.*, 2013) and according to the manufacturer's instructions. Specific beads were used for p-SYK (Y352), p-70 kDa zeta-chain associated protein (ZAP70) (Y319), p-BTK (Y223), p-AKT (S473), p-40S ribosomal protein S6 (RPS6) (S235/S236), p-Bcl2-associated agonist of cell death (BAD) (S136), p-MEK1 (S217/S221), p-ERK1/2 (T202/Y204, T185/Y187), p-90 kDa ribosomal protein S6 kinase (p90RSK) (S380), p-GSK3ab (S21/S9), p-p38 MAPK (T180/Y182), p-HSP27 (S78), p-JNK (T183/Y185), p-c-Jun (S63) and p-p65 NF-κB (S536). The Bio-Plex manager software was used for data acquisition. Subsequently, Bertram Klinger of the Institute of Pathology (Charité –

University Medicine Berlin) performed the evaluation and network modeling using Modular Response Analysis-based R package STASNet (Dorel *et al.*, 2018; Klinger *et al.*, 2013).

### 2.3.4 Mass spectrometry based phosphoproteomics

In order to ensure a complete incorporation of the isotope labeled amino acids, P493-6 cells were harvested after growing in cell labeling medium for 7 days. To that, 1 million cells were sedimented (500 x g, 4°C) and washed once with DPBS. The cell pellet was resuspended in 500 µl urea buffer and the protein concentration determined. An aliquot of each labeling was analyzed by mass spectrometry to ensure a protein labeling above 95 % and to exclude an arginine to proline conversion.

For phosphoproteomics, cells were harvested by centrifugation (500 x g, 4°C) for 5 minutes and washed once with ice-cold DPBS + 1 x PhosSTOP (Roche). The cell pellet was stored by -80°C until lysis. Afterwards the cell pellet was resuspended in 450 µl modified NP-40 lysis buffer for 30 minutes at 4°C. The cell debris was removed by 15 minutes centrifugation (14000 x g, 4°C) and the supernatant collected. The light and heavy labeled samples were mixed in equal parts, the protein concentration was determined with Roti-Quant (see 2.3.1) and the samples stored at -80°C until mass spectrometry analysis.

The further steps were executed by Jasmin Corso from the Bioanalytical Mass Spectrometry Group of Henning Urlaub (Max-Planck-Institute for Biophysical Chemistry, Goettingen) as described elsewhere (Corso *et al.*, 2016). In summary, a global enrichment of phosphopeptides was done and analyzed with liquid chromatography-tandem mass spectrometry. Raw data were analyzed with the MaxQuant software (Max Planck Institute for Biochemistry, DE) (Cox and Mann, 2008) and further processed using the Perseus software (Max Planck Institute for Biochemistry, DE) (Deshmukh *et al.*, 2015). Phosphorylation sites with a localization probability lower than 0.75 were removed and the logarithmic SILAC ratios displayed as described by Corso *et al.* (Corso *et al.*, 2016).

## 2.4 Molecular Biology

### 2.4.1 RNA isolation

For RNA analysis, cells were harvested by centrifugation (500 x g, 4°C) for 5 minutes and washed once with ice-cold DPBS. Total RNA was isolated from the cell pellets using the NucleoSpin RNA kit (Macherey-Nagel) and following the user manual. In brief, the cell pellet was lysed without β-mercaptoethanol, debris was removed and the RNA was

loaded to a spin column. After digestion of DNA and several washing steps the RNA was eluted in 50 µl RNase free H<sub>2</sub>O. The concentration was determined with the spectrophotometer ND-1000.

#### 2.4.2 Reverse transcription

The SuperScript II Reverse Transcriptase kit (Invitrogen) was used to generate complementary DNA (cDNA) from messenger RNA. First, 1 µg RNA was filled up with RNase free water to a total volume of 10 µl. After adding 2 µl random hexamer primers the samples were denatured at 70°C for 10 minutes. Furthermore, samples were cooled down on ice, supplemented with 8 µl master mix (Table 15) and the reverse transcription performed in a thermocycler following the program detailed in Table 16.

**Table 15:** Reverse transcriptase master mix

Substance	Amount
First strand buffer (5x)	4 µl
DTT (0.1 M)	2 µl
Super Script II RT	1 µl
dNTPs (10 mM)	1 µl

**Table 16:** Thermocycler program

Temperature	Cycle length
25°C	10 minutes
42°C	60 minutes
65°C	10 minutes
4°C	continuously

#### 2.4.3 Quantitative real-time polymerase chain reaction

To analyze distinct gene expressions a SYBR green-based qRT-PCR was performed in 384 well plates using the 7900HT Fast Real-Time PCR System. SYBR green is a nucleic acid binding dye emitting a much higher green fluorescence upon intercalation with double stranded DNA compared to single strands (Schneeberger *et al.*, 1995). As the amount of DNA rises exponentially with the number of amplification cycles, the fluorescence signal increases equally. Hence, the number of cycles crossing a fluorescence threshold is inversely proportional to the DNA amount and defined as CT-value. The comparison of CT-values allows a relative quantification of gene expression. For this purpose, 5.6 µl SYBR green mix were supplemented with 0.3 µM of each primer and filled up to 8 µl as

PCR master mix. The cDNA samples were diluted to 50 ng/ $\mu$ l and 10 ng of cDNA added to the PCR master mix. After closing the well plate with an optical adhesive cover, the analysis was done following the qRT-PCR program shown in Table 17.

**Table 17:** qRT-PCR program

Temperature	Cycle length	Cycle amount
95°C	15 minutes	
95°C	15 seconds	40 x
60°C	1 minute	
95°C	15 seconds	
60°C	15 seconds	
95°C	15 seconds	

The relative quantification of gene expression was determined using the software ABI 7900HT SDS 2.4 and ABI RQ Manager 1.2.1. Thereby, normalization was firstly implemented to the internal housekeeper glyceraldehyde-3-phosphate dehydrogenase (GAPDH) ( $\Delta CT$ ) in order to compensate technical differences:

$$\Delta CT = CT_{\text{gene of interest}} - CT_{\text{housekeeper}}$$

The relative gene expression changes were calculated by reference to the untreated control ( $\Delta\Delta CT$ ):

$$\Delta\Delta CT = CT_{\text{treatment}} - CT_{\text{control}}$$

As the number of cycles is inversely proportional to the DNA amount, the expression fold changes can be calculated as follows:

$$\text{relative expression} = 2^{-\Delta\Delta CT}$$

#### 2.4.4 RNA sequencing

RNA sequencing was conducted in three previous projects at the clinic for Hematology and medical Oncology (University Medical Centre, Goettingen). Hence, the implementation of the BL-2 analysis is described by Wolff *et al.* (Wolff *et al.*, 2018). For P493-6 and ABC DLBCLs, the RNA analysis was performed as described by Maren Feist (Feist, 2016) and Annekatrin Arlt (Arlt, 2018).

## 2.5 Statistics and bioinformatical analyses

Statistical and bioinformatical analyses of the multiplex immunoassay were performed by Bertram Klinger of the Institute of Pathology (Charité – University Medicine, Berlin).

For the phosphoproteomic experiment, phosphosites quantified in less than two replicates were excluded. Significance testing was done using the two-way ANOVA method and a two-stage step-up method of Benjamini, Krieger and Yekutieli to correct for multiple comparisons by a FDR threshold of 0.05. The calculation was performed with log<sub>2</sub>-transformed ratios and GraphPad Prism 7. Therefore, phosphosites altered in two or more replicates, with p-value of less than 0.05 and log<sub>2</sub> ratio above 0.58 (over 50 % fold change) were deemed significantly changed. The network representation of changed protein phosphorylations was created with STRING (Szklarczyk *et al.*, 2015). Furthermore, a gene set enrichment was performed with the online DAVID bioinformatics annotation tool (Huang da *et al.*, 2009). Thereby, a functional annotation clustering for biological processes (GOTERM\_BP\_Fat) was used with an EASE score of 0.1 and a medium classification stringency. Due to a long list of gene ontology terms, REVIGO was used with default settings and allowed similarity of 0.5 for summarization and visualization (Supek *et al.*, 2011). The changed protein phosphorylations were also used to predict possible kinase activities with a literature-based kinase-substrate library of the online Kinase Enrichment Analysis 2 (KEA2) tool (Lachmann and Ma'ayan, 2009).

### 3. Results

The result section is divided in two chapters. At first, the interplay of BCR-related signaling pathways was investigated to generate a semi-quantitative network by complementation of a literature-based model with the experimental data. Thereafter, the combined stimulation of IL10R and TLR9 was examined for their impact on the phosphoproteome to investigate the synergistic effects on proliferation in more detail.

#### 3.1 Tonic and active BCR signaling contains several feedback loops

In a previous analysis, our group applied the Boolean-Nested Effect Model framework to gene expression changes after pathway perturbations using the BL cell line BL-2 with a tonic or activated BCR signaling (Pirkl et al., 2016). The results provided a first unsupervised model of the distal BCR signaling nodes and a hypothesis explaining how downstream nodes of this pathway were affected. Nevertheless, this analysis could not fully elucidate the signaling network. For a better understanding and extension of the network structure, protein phosphorylation analyses of the BCR signaling were performed to uncover the interplay and feedback loops of downstream effector pathways.

For data consistency, we used BL-2 cells again and investigated pathway perturbations during a tonic or an activated BCR signaling. The tonic BCR signaling is next to c-MYC a hallmark of BLs and includes in particular the activation of the PI3K pathway (Schmitz et al., 2012; Srinivasan et al., 2009). However, a fully active BCR signaling can be achieved by stimulation of the receptor with antigens and in case of BL-2 with  $\alpha$ -IgM. This crosslinking of the BCR leads to an additional activation of the MAPK, NFAT and NF- $\kappa$ B pathways (Hendriks et al., 2014). For the inhibition of these signal transmissions, the same inhibitors were used as in the previous study and some new ones included. Beside the inhibition of PI3K $\alpha, \beta, \delta$  (Ly294002), MEK1/2 (U0126), TAK1 (5'-7-Oxozeanol), p38 MAPK (SB203580), JNK (SP600125) and IKK $\alpha, \beta$  (ACHP), the list was extended with the inhibition of BTK (Ibrutinib), PI3K $\alpha, \beta, \gamma, \delta$  (BKM120), PI3K $\gamma, \delta$  (CAL-101), AKT (MK-2206), mTOR (Rapamycin), MEK1/2 (AZD6244), JNK (JNK Inh VIII) and IKK $\alpha, \beta$  (MLN120b). Instead of analyzing gene expression changes, we detected the pathway activations by measuring specific kinase phosphorylations. For this purpose, we used an antibody-based multiplex immunoassay to quantify 15 different protein phosphorylations simultaneously in one sample. Thereby, the phosphorylations of the upstream kinases SYK, ZAP70 and BTK as well as the pathway activations of PI3K-AKT, MEK-ERK, p38 MAPK, JNK and NF- $\kappa$ B were determined. Only such an approach allowed us to

compare the thirteen inhibitor treatments during a tonic or active BCR signaling in BL-2 cells.

### 3.1.1 Determination of a suitable time point for pathway interaction analyses

As the kinetics of posttranslational modifications occur prior to the gene expression responses, the suitable time point to analyze protein phosphorylations had to be determined first. Therefore, protein phosphorylations of three major pathways were investigated after different durations of BCR activation. The phosphorylation of PI3K, AKT, pS6 kinase, MEK1, ERK1/2 and p38 MAPK was measured after 15, 30, 60 and 90 minutes of BCR stimulation with  $\alpha$ -IgM. The detection was done with immunoblot analysis (Figure 3 A) and the multiplex immunoassay in BL-2 cells (Figure 3 B).

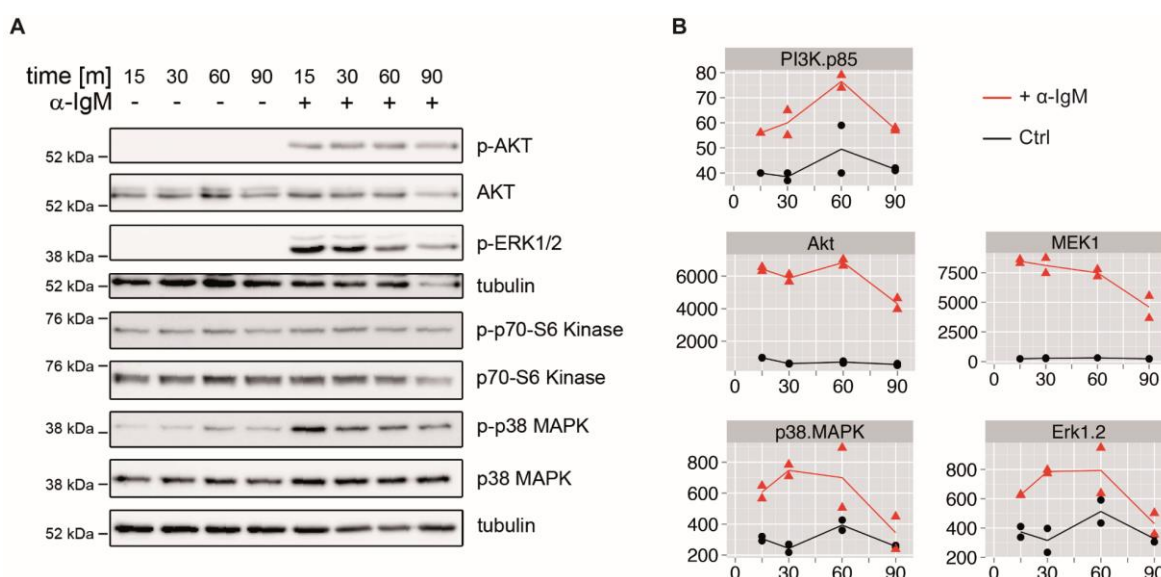


**Figure 3: Time dependent activation of specific signaling pathways after BCR activation.**

Protein phosphorylations were investigated after BCR activation by  $\alpha$ -IgM at the indicated time points. (A) Immunoblot analysis of AKT, ERK1/2, S6 kinase and p38 MAPK phosphorylation and total proteins. Tubulin served as loading control (n=1). (B) multiplex immunoassay for quantitative phosphorylation analysis of PI3K, MEK1, AKT, ERK1/2 and p38 MAPK. Data points displayed the mean fluorescence intensity of two technical replicates. The black line displays the unstimulated control (Ctrl), whereas the red line indicates BCR activation by  $\alpha$ -IgM stimulation (n=1).

Activation of the BCR led to an increasing phosphorylation of PI3K till 60 minutes in the multiplex immunoassay (Figure 3 B). In addition, both analyses clearly showed a phosphorylation of the PI3K target AKT by  $\alpha$ -IgM stimulation up to 60 minutes (Figure 3 A, B). After 90 minutes of BCR activation a declining phosphorylation was observed for PI3K and AKT. However, in the immunoblot analysis no phosphorylation changes were detected for the AKT downstream kinase S6 compared to the unstimulated control (Figure 3 A). The phosphorylation of MEK1, ERK1/2 and p38 MAPK was highest at 15 or

30 minutes of  $\alpha$ -IgM stimulation, decreased slightly till 60 minutes and showed a stronger decline after 90 minutes (Figure 3 A, B).

In conclusion, the PI3K activation increased up to 60 minutes of BCR activation, whereas the phosphorylations of the other kinases already decreased at this time point. In order to detect the most pathway activations and interactions, we decided to choose a time point suitable for all measured kinases. Therefore, 30 minutes of BCR activation was selected for further analysis.

### 3.1.2 Tonic BCR signaling is enhanced by positive feedback loop

We then analyzed the tonic BCR signaling in BL-2 cells with the multiplex immunoassay and the results are displayed in comparison to the untreated control in Figure 4. The quantitative values of this analysis are presented in the supplement (Figure A-1, Figure A-2). In BL-2 cells it was shown that the inhibition of BTK, PI3K, AKT and mTOR lowered all measured protein phosphorylations except for p38 MAPK (Figure 4 A). In detail, the affected phosphorylations belonged to the upstream kinases SYK, ZAP70 and BTK as well as the pathway activations of PI3K-AKT, MEK-ERK, JNK, NF- $\kappa$ B and GSK3 $\beta$ . As a signal inhibition of the PI3K pathway led to a decreased phosphorylation of downstream as well as upstream kinases, we hypothesized the existence of a positive feedback loop from mTOR to kinases nearby the BCR. However, the inhibition of MEK1/2 or p38 MAPK had nearly no effect on any detected phosphorylation. The impacts of JNK or NF- $\kappa$ B inhibition were also not notable and decreased only slightly the phosphorylations of SYK, ZAP70, BTK, GSK3 $\beta$  and the PI3K-AKT, MEK-ERK, JNK and NF- $\kappa$ B pathways. Therefore, no clear influences of the MAPKs or NF- $\kappa$ B on the other pathways were seen.

In order to confirm the obtained findings, a second BL cell line was investigated using a smaller set of inhibitors. Similar results were obtained in BL-41 cells compared to BL-2 cells (Figure 4 B). Only the MEK1/2 inhibition differed from the BL-2 data and rather induced a slight increase of the phosphorylation of SYK, ZAP70, BTK, GSK3 $\beta$  and the PI3K-AKT, MEK-ERK, p38 MAPK, JNK and NF- $\kappa$ B pathways.

In summary, we concluded that the PI3K pathway enhances its own activation by a positive feedback loop to the proximal kinases of the BCR. In addition, the MAPKs and NF- $\kappa$ B pathways are not interacting with other pathways during the tonic BCR signaling. As the PI3K pathway is the main driver of the tonic BCR signaling (Sander *et al.*, 2012; Schmitz *et al.*, 2012), we suspected that the other pathways are maybe not active enough to reveal pathway interplays.

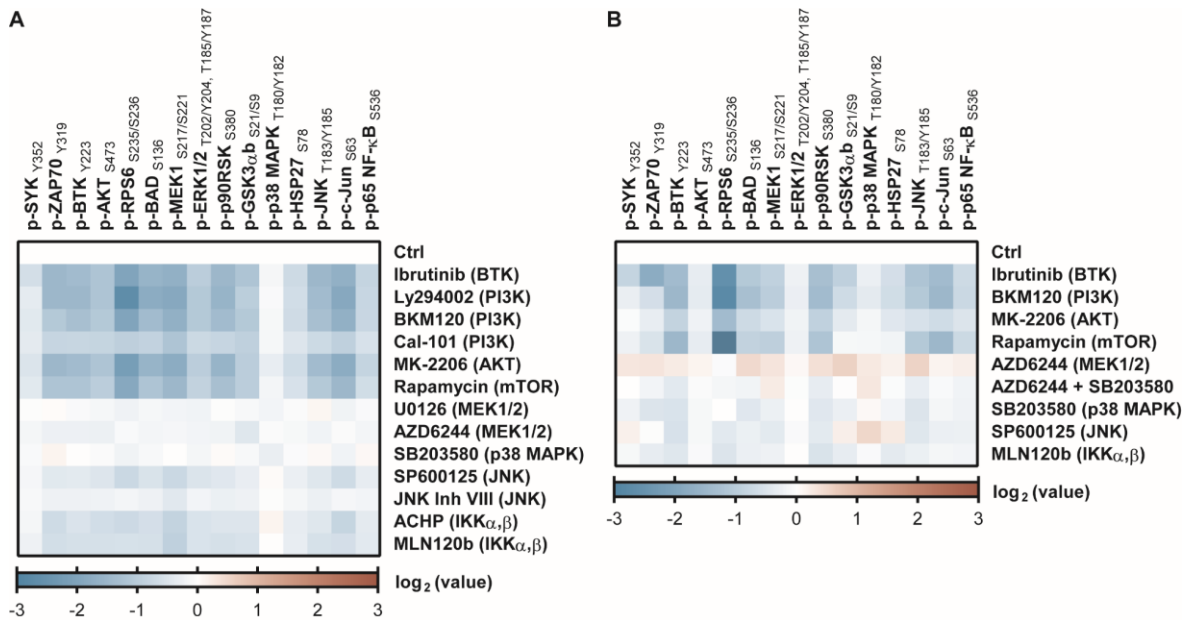


**Figure 4: Signaling changes by pathway perturbations during the tonic BCR signaling.**

Signal transduction was disrupted by inhibitors of BTK, PI3K, AKT, mTOR, MEK1/2, p38 MAPK, JNK and IKK $\alpha,\beta$  for 3.5 hours. Specific phosphorylations of SYK, ZAP70, BTK, AKT, RPS6, BAD, MEK1, ERK1/2, p90RSK, GSK3ab, p38 MAPK, HSP27, JNK, c-JUN and p65 NF- $\kappa$ B were measured with the multiplex immunoassay. The log<sub>2</sub> values normalized to control are shown for the BL cell lines BL-2 (**A**) and BL-41 (**n=3**).

In order to determine whether all PI3K-AKT pathway inhibitors hamper the proliferation of BLs, the cell viability was examined over 72 hours. Besides, a MEK1/2 inhibitor was included to confirm that this pathway is not pivotal for the proliferation of BLs. While the inhibition of AKT and mTOR clearly reduced the viability of BL-2 cells to 72 hours, the PI3K and MEK1/2 inhibitor showed nearly no influences (Figure 5 A). However, in BL-41 cells the inhibition of PI3K, AKT and mTOR decreased the cell viability, whereas only the MEK1/2 inhibition had no impact (Figure 5 B). This indicated that the PI3K-AKT pathway was altogether important for BL proliferation.

We concluded that the PI3K is indeed the main driver of the tonic BCR signaling and the MEK-ERK pathway is negligible or not active under these conditions.

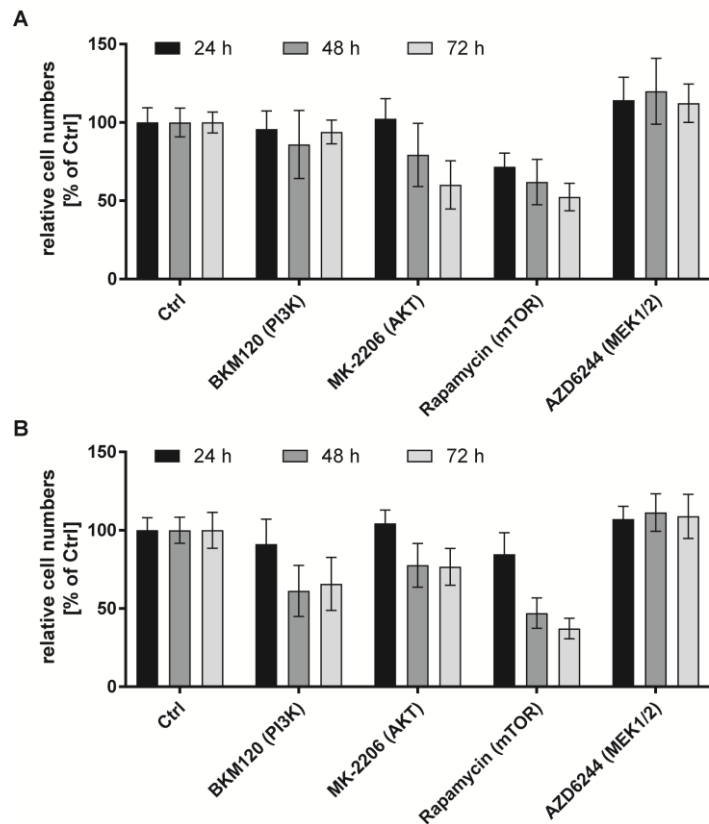


**Figure 5: Cell viability of BLs after pathway inhibition during the tonic BCR signaling.**

Cell viability assay was performed after 24, 48 and 72 hours with the fluorescence dye Calcein AM. The cells were treated with inhibitors of PI3K, AKT, mTOR and MEK1/2. The amount of viable cells was normalized to control and the mean +/- SD is displayed for the Burkitt lymphoma cell lines BL-2 (**A**) and BL-41 (**B**) (n=3).

### 3.1.3 Active BCR signaling is influenced by positive and negative interplays

Next we examined the pathway phosphorylations after 30 minutes of BCR activation in BL-2 cells with the multiplex immunoassay. The quantitative values of this analysis are presented in the supplement (Figure A-1, Figure A-2). The  $\alpha$ -IgM stimulation of the BCR increased all measured protein phosphorylations in comparison to the unstimulated control (Figure 6 A). More precisely, the activation of SYK, ZAP70, BTK, GSK3 $\beta$  and the PI3K-AKT, MEK-ERK, p38 MAPK, JNK and NF- $\kappa$ B pathways were heightened.

To verify these findings, BL-41 cells were included as well (Figure 6 B). Similar to BL-2, the phosphorylations of SYK, ZAP70, BTK, GSK3 $\beta$  and the PI3K-AKT, MEK-ERK and NF- $\kappa$ B pathways were stronger after  $\alpha$ -IgM stimulation compared to control cells. However, no phosphorylation changes were detected for p38 MAPK whereas the phosphorylation of the downstream target HSP27 was reduced. The JNK phosphorylation was not altered as well, while the phosphorylation of c-Jun was enhanced. As the exact

signal transduction to the MAPKs was still not fully clarified, we suggested that little differences in the activation of upstream kinases were an explanation for these variations.

In conclusion, activation of the BCR receptor induced the phosphorylation of SYK, ZAP70 and BTK as well as a further activation of the PI3K-AKT, MAPK and NF- $\kappa$ B pathways as described previously (Hendriks *et al.*, 2014). Besides, we assumed that the signal distribution to the MAPK pathways depend on the activity of upstream kinases and can differ between cell lines.

For an easier interpretation of the inhibitor effects, the values were normalized to the  $\alpha$ -IgM-stimulated control. Similar to the tonic BCR results, the inhibition of BTK, PI3K, AKT and mTOR diminished all measured protein phosphorylations in BL-2 cells (Figure 6 C). Thereby, the phosphorylations of the upstream kinases SYK, ZAP70 and BTK as well as the pathway activations of PI3K-AKT, MEK-ERK, p38 MAPK, JNK, NF- $\kappa$ B and GSK3 $\beta$  were affected. We concluded that the enhanced PI3K pathway after BCR activation also comprised a positive feedback loop from mTOR to the BCR.

In addition, a similar pattern like for PI3K inhibitors was seen after inhibition of MEK1/2 (Figure 6 C). The MEK1/2 inhibitor caused a lower phosphorylation of SYK, ZAP70, BTK, GSK3 $\beta$  and of the PI3K-AKT, p38 MAPK, JNK and NF- $\kappa$ B pathway, while its own phosphorylation was enhanced. As ERK1/2 is known to reduce its own pathway activity through inactivating phosphorylations of RAF-1 and MEK1/2 (Steelman *et al.*, 2011), we suggested that the signal inhibition to ERK1/2 provoked the increase of the activating MEK1 phosphorylation. Furthermore, the inhibition of p38 MAPK heightened strongly the phosphorylation of MEK1 and ERK1/2. In comparison to the other pathways only slight increased phosphorylations of ZAP70, BTK, AKT, GSK3 $\beta$ , JNK, c-Jun and NF- $\kappa$ B were detected. These pointed out that p38 MAPK attenuated especially the MEK-ERK pathway. Comparable with the tonic BCR signaling in BL-2 cells, JNK and NF- $\kappa$ B inhibition achieved only little phosphorylation changes. Thereby, the phosphorylations of SYK, ZAP70, BTK, GSK3 $\beta$  and the PI3K-AKT, MEK-ERK, JNK and NF- $\kappa$ B pathways were only slightly diminished. Thus, no clear influences of JNK and NF- $\kappa$ B were seen on the other pathways after BCR activation.

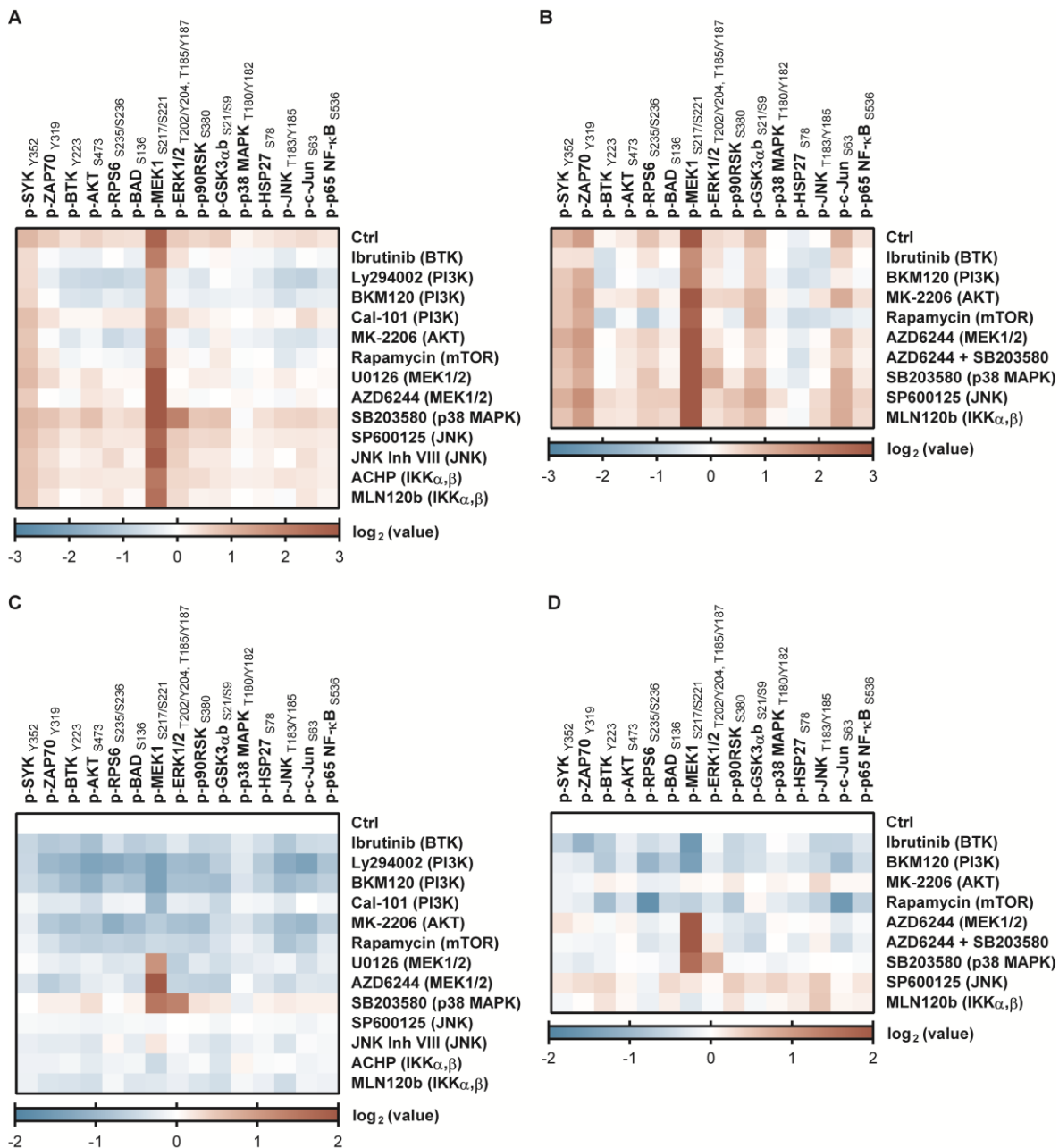


**Figure 6: Signaling changes by pathway perturbations during the active BCR signaling.**

The signal transduction was disrupted by inhibitors of BTK, PI3K, AKT, mTOR, MEK1/2, p38 MAPK, JNK and IKK $\alpha,\beta$  for 3 hours. Afterwards the BCR were activated by  $\alpha$ -IgM for 30 minutes. Specific phosphorylations of SYK, ZAP70, BTK, AKT, RPS6, BAD, MEK1, ERK1/2, p90RSK, GSK3ab, p38 MAPK, HSP27, JNK, c-JUN and p65 NF- $\kappa$ B were measured with the multiplex immunoassay. The log<sub>2</sub> values normalized to untreated control are shown for the Burkitt lymphoma cell line BL-2 (**A**) and BL-41 (**B**). Furthermore, the log<sub>2</sub> values of **A** and **B** were normalized to the  $\alpha$ -IgM-stimulated control and displayed for BL-2 (**C**) and BL-41 (**D**) (n=3).

For the verification of these results, a second BL cell line was examined with a smaller set of inhibitors. The BL-41 cells showed similar results in comparison with BL-2 cells (Figure 6 D). Therefore, only the differences are mentioned in the following. In contrast to the BL-2 results, the inhibition of AKT caused a stronger phosphorylation of p90RSK and JNK while the other kinase phosphorylations were not affected compared to the antigen-stimulated

control. In addition, the JNK inhibitor showing no effects in BL-2 led to increased phosphorylation of SYK, ZAP70, BTK, GSK3 $\beta$  and the PI3K-AKT, MEK-ERK, p38 MAPK, JNK and NF- $\kappa$ B pathways. After inhibition of NF- $\kappa$ B, the increased phosphorylation of BTK, p90RSK, HSP27 and JNK was contrary to the reduced phosphorylations in BL-2 cells. Another difference compared to the BL-2 analysis was the combined inhibition of MEK1/2 and p38 MAPK. As a negative impact from p38 MAPK was considered on MEK1 and ERK1/2, the inhibition of both kinases was performed to reveal whether p38 MAPK directly influences ERK1/2. The phosphorylation of ERK1/2 was over 80 % lower after inhibition of p38 MAPK and MEK1/2 compared to the p38 MAPK inhibition alone. This pointed out that p38 MAPK reduced mainly the phosphorylation of MEK1 or upstream components.

In summary, the PI3K pathway was also promoted by a positive feedback loop to proximal kinases of the BCR after receptor activation. Furthermore, the BCR activation induced negative feedbacks on the MEK-ERK pathway which are mediated by ERK1/2 and p38 MAPK on upstream kinases of ERK1/2.

### 3.1.4 Schematic model represents interactions of signaling pathways

Current literature-based networks present mostly a linear signal transduction from the receptor along the pathway components. Furthermore, the data collected from different publications often focus on a particular signaling or on protein complexes within the own pathway. For the BCR signaling, the proximal events are so far investigated in more detail (Satpathy *et al.*, 2015), even though a final network is still missing. In contrast, the distal signaling of the BCR is just partially understood. In order to refine the network structure, we used a literature-derived signaling network, depicted in a recent review, as a starting point (Figure A-3) (Hendriks *et al.*, 2014). In collaboration with Bertram Klinger (Institute of Pathology, Charité – University Medicine Berlin), a semi-quantitative network analysis was performed on the perturbation data using the modular response analysis and the profile likelihood (Klinger *et al.*, 2013). For this purpose, pathway interactions were included or excluded to achieve the best likelihood and network.

In Figure 7 the network for the BL-2 analysis is displayed. As the network analysis of BL-41 is comparable, it is presented in the appendix (Figure A-4). After BCR activation, the signal was transmitted through SYK, BTK and PI3K over AKT to mTOR (upper part of Figure 7). Furthermore, a link from mTORC1 to GSK3 $\beta$  and the BCR was proposed. The interaction between AKT and GSK3 $\beta$  was known before and confirmed by our analysis (Baracho *et al.*, 2011). While negative feedbacks were only described for the PI3K-AKT

pathway (Logue and Morrison, 2012), our results suggested a positive feedback loop from mTOR to the BCR in BLs.

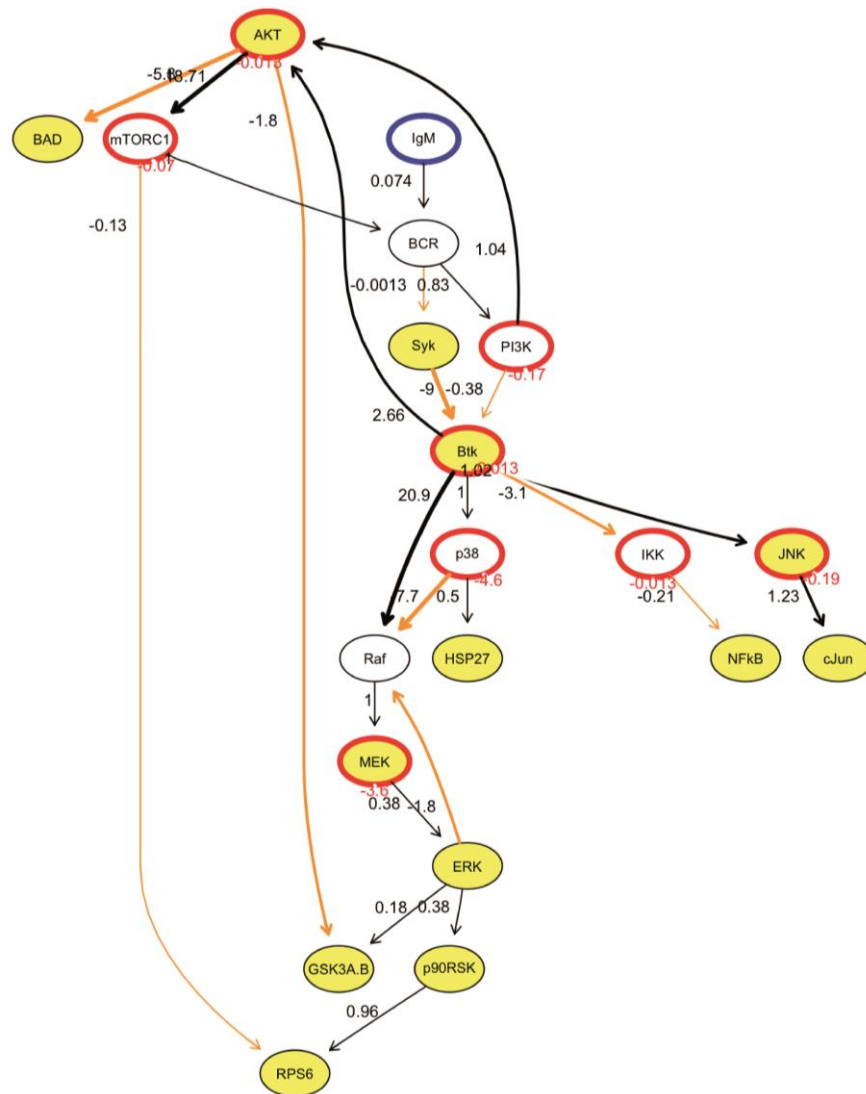


**Figure 7: Network model of BCR signaling interactions and feedbacks.**

Network model of BL-2 based on Modular Response Analysis by STASTNet was calculated by Bertram Klinger (Institute of Pathology, Charité – University Medicine Berlin). Stimulated (blue), inhibited (red) and measured (Yellow) nodes are displayed. The corresponding numbers reveal the inhibition strength (red) and the value of the local response coefficients (black). Arrows present interaction with positive (black) or negative (orange) local response coefficients.

The BCR signal was also transduced through SYK, PI3K and BTK to RAF-1, p38 MAPK, JNK and IKK (lower part of Figure 7). The activation of JNK led to the phosphorylation of c-Jun, whereas IKK subsequently activated NF- $\kappa$ B. For these both pathways, no feedbacks or other interactions were likely in our analyses. Besides, p38 MAPK induced HSP27 and influenced RAF-1. Although our results just implicated that p38 MAPK attenuates the MEK-ERK pathway upstream of ERK1/2, a connection from p38 MAPK to RAF-1 was assumed based on the literature. Finally, the activation of RAF-1 mediated the

phosphorylation of MEK1 and further ERK1/2. The activated ERK1/2 reduced then the activation of RAF-1 and GSK3 $\beta$ . Therefore, our findings confirmed the negative feedback from ERK1/2 to RAF-1 and validated the interaction with GSK3 $\beta$  in BLs.

To sum up, our signaling analyses revealed a positive feedback loop of the PI3K-AKT pathway which has not been described before. In addition, two negative feedbacks on the MEK-ERK pathway were mediated by ERK1/2 and p38 MAPK. The phosphorylation of GSK3 $\beta$  was both AKT- and ERK1/2-dependent. Therefore, the pathway analyses contribute to the validation of known feedbacks, to the discovery of new interactions and to a better understanding of the pathway interplays in BL cell lines.

### 3.2 p38 MAPK attenuates the MEK-ERK pathway

The importance of the PI3K pathway for BL proliferation is well studied (Sander *et al.*, 2012; Schmitz *et al.*, 2012) while the role of MAPKs is not elucidated and less is known about the attenuation of the MEK-ERK pathway. So far the capability of ERK1/2 to inhibit MEK1/2 and RAF-1 has been discovered (Dougherty *et al.*, 2005). An influence on the MEK-ERK pathway by p38 MAPK was only seen in other cell types and controversially discussed (Birkenkamp *et al.*, 2000; Zhang *et al.*, 2003). Therefore, we focused on the negative regulation of the MEK-ERK pathway in our next analyses.

#### 3.2.1 p38 $\alpha$ (MAPK14) limits the MEK-ERK pathway

As the RAF-1 activity increased linearly by raising concentration of the p38 MAPK inhibitor SB203580 above the required inhibitor concentrations to block p38 MAPK, this effect was referred to an unspecific inhibitory effect (Kalmes *et al.*, 1999). However, an increased MEK-ERK signaling after p38 inhibition was also observed with another inhibitor (Hirosawa *et al.*, 2009) and with dominant negative p38 MAPK expression (Aguirre-Ghiso *et al.*, 2001). Thus, we validated the p38 MAPK influence on the MEK-ERK pathway in BL-2 cells first. As shown in Figure 8 A, the phosphorylation of MEK1 and ERK1/2 was induced by antigen stimulation. Additionally, the inhibition of p38 MAPK (SB203580) led to much higher levels of MEK1 and ERK1/2 phosphorylations compared to the antigen-stimulated control. To confirm this effect, p38 MAPK was downregulated with specific siRNAs. p38 MAPK comprises four subunits and the p38 inhibitor SB203580 is known to block the  $\alpha$ - and  $\beta$ -subunit (Bain *et al.*, 2007). Therefore, siRNAs for p38 $\alpha$  (MAPK14) were chosen as the  $\beta$ -subunit is only expressed to a small extent in BL-2 cells (Figure 8 C). The immunoblot analysis (Figure 8 B) and the summary of three independent siRNA transfections (Figure 8 D) revealed that a downregulation of p38 $\alpha$  induced two-fold higher

ERK1/2 phosphorylations compared to the antigen-stimulated control. We concluded that the p38 $\alpha$  (MAPK14) subunit was involved in the attenuation of the MEK-ERK pathway and that the effect was not an inhibitory side effect.

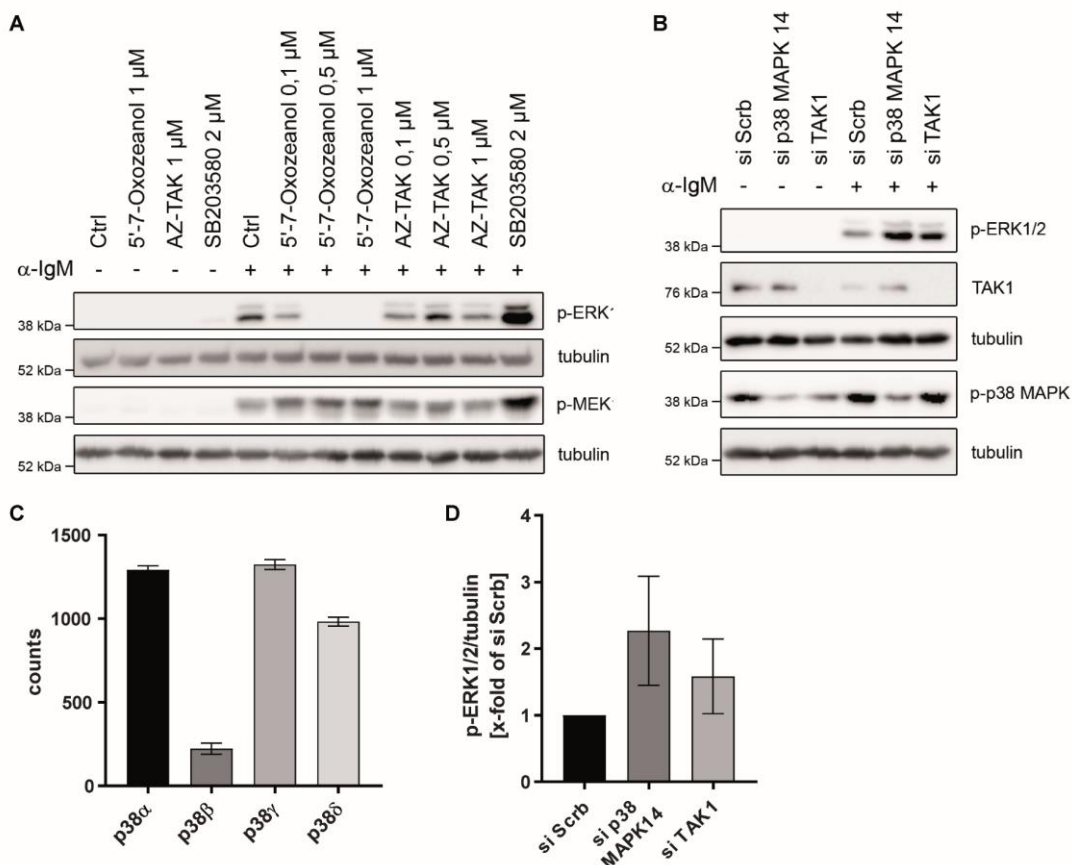


**Figure 8: Verification of TAK-1 and p38 MAPK influence on the MEK-ERK pathway**

(A) Representative immunoblot analysis of TAK-1 (5'-7-Oxozeanol, AZ-TAK) or p38 MAPK (SB203580) inhibition in BL-2 cells. Kinases were inhibited for 3 hours and the BCR additionally activated for 30 minutes with  $\alpha$ -IgM. Tubulin served as loading control (n=2). (B) Representative immunoblot analysis of TAK-1 and p38 $\alpha$  (MAPK14) knockdowns with specific siRNAs. Protein phosphorylation was measured after 24 hours of transfection and 30 minutes  $\alpha$ -IgM stimulation. Tubulin served as loading control (n=3). (C) Total reads of the p38 subunits  $\alpha$  (MAPK14),  $\beta$  (MAPK11),  $\gamma$  (MAPK12),  $\delta$  (MAPK13) are displayed from RNA sequencing analysis of BL-2 cells (n=3). (D) Quantification of phosphorylated ERK1/2 of the immunoblot analyses from B.

Besides, a second effect of the p38 MAPK activating kinase TAK-1 was observed. Inhibition of TAK-1 led to an increased MEK1 but not ERK1/2 phosphorylation (data not shown) and was more similar to a MEK1/2 than to a p38 MAPK inhibition. As an upstream activation of p38 MAPK was expected to obtain comparable results, the role of TAK-1 on ERK1/2 was analyzed. As shown in Figure 8 A, inhibition of TAK-1 with 5'-7-Oxozeanol caused a slight increase of MEK1 phosphorylation and a diminished ERK1/2 phosphorylation after BCR activation. However, an additional TAK-1 inhibitor (AZ-TAK) did not show comparable results. In addition, downregulation of TAK-1 with specific

siRNAs could also not confirm the effects of 5'-7-Oxozeanol (Figure 8 B,D). We suggested that the effect of TAK-1 inhibition on MEK1 and ERK1/2 was an inhibitor specificity and hence 5'-7-Oxozeanol was excluded from the analyses.

### 3.2.2 RAF-1 phosphorylations are affected by ERK1/2 but not by p38 MAPK

To investigate whether the p38 MAPK effect on the MEK-ERK pathway occurred directly after BCR activation, an earlier time point was chosen. Apart from 30 minutes of  $\alpha$ -IgM stimulation, the ERK phosphorylation was analyzed after 5 minutes of BCR activation (Figure 9 A). In all three tested cell lines the ERK1/2 phosphorylation was higher at 5 minutes of  $\alpha$ -IgM stimulation compared to 30 minutes. Additionally, inhibition of p38 MAPK (SB203580) caused a stronger increased of phosphorylated ERK1/2 at any time point compared to the antigen stimulated control. Therefore, we assumed that p38 MAPK attenuated directly or through phosphatases the MEK-ERK pathway although transcriptional changes by p38 MAPK inhibition were not excluded.

As purified p38 MAPK was shown to inhibit RAF-1 activity (Hutchison, 2012), we further investigated the phosphorylations of RAF-1. Over 50 phosphorylation sites were described for RAF-1. However, one study suggested that the activating phosphorylation on serine 338 of RAF-1 was heightened by p38 MAPK inhibition (Zhang *et al.*, 2003). A slight phosphorylation of RAF-1 on serine 338 was detectable in BL-2 and BL-41 cells after BCR activation (Figure 9 A). The stimulation with  $\alpha$ -IgM for 5 or 30 minutes showed no differences and no additional influences were shown on this activating phosphorylation of RAF-1 by p38 MAPK inhibition (SB203580).

Apart from many activating phosphorylations, the phosphorylations of serine 289, 296 and 301 are described to induce an inactive conformation of RAF-1. This inactive conformation is enhanced by active ERK1/2 and known as negative feedback for the MEK-ERK pathway (Dougherty *et al.*, 2005). We further examined whether this inactive conformation was promoted by p38 MAPK (Figure 9 A). While an increase of these phosphorylations was measured up to 30 minutes after  $\alpha$ -IgM stimulation, the inhibition of p38 MAPK (SB203580) had no effect. Therefore, we tested whether the inactive conformation of RAF-1 was ERK1/2 dependent or only induced by BCR activation (Figure 9 B,C). After 30 minutes of  $\alpha$ -IgM stimulation, the inactive phosphorylations of RAF-1 were clearly detectable in BL-41 cells and diminished by MEK1/2 inhibition (AZD6244). As before, no impacts on the ERK-dependent phosphorylation of RAF-1 were found by p38 MAPK inhibition.

This indicated that p38 MAPK attenuates the MEK-ERK pathway directly after BCR activation while the negative feedback from ERK to RAF-1 increases up to 30 minutes. Furthermore, p38 MAPK had no impacts on the activating serine 338 or the inactivating serine 289, 296 and 301 phosphorylations of RAF-1. The interaction of p38 MAPK to the MEK-ERK pathway and the involvement of RAF-1 requires further investigations.

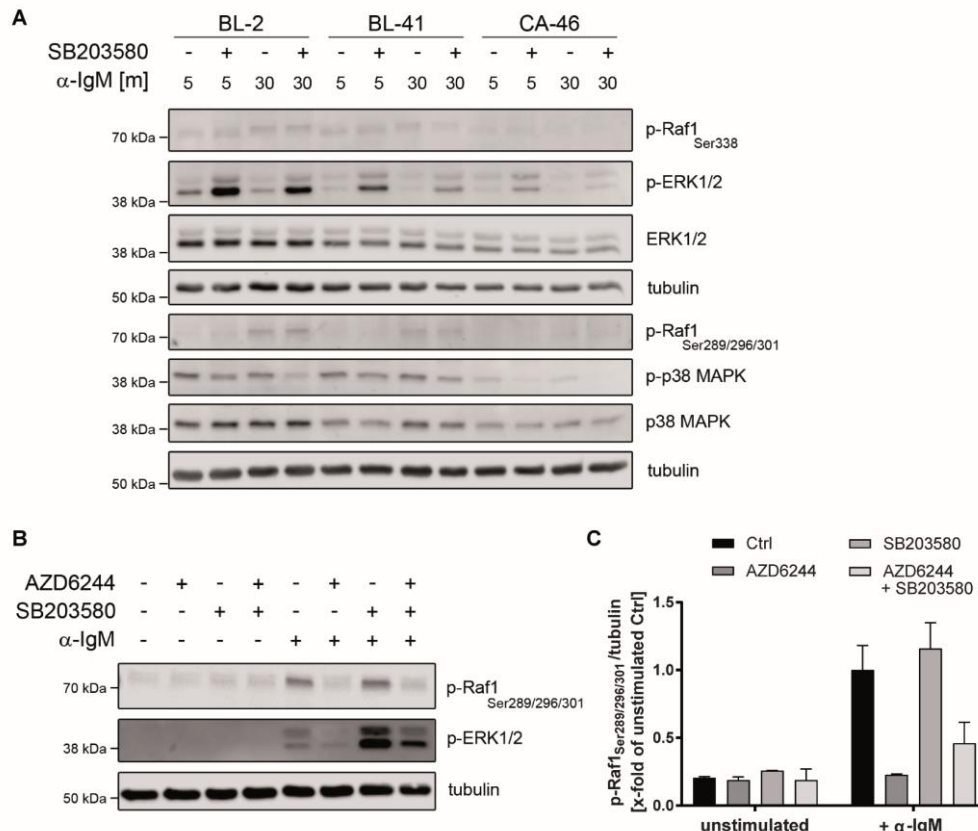


**Figure 9: p38 MAPK and ERK1/2 impact on RAF-1 phosphorylations**

(A) Representative immunoblot analysis of 3 hours p38 MAPK (SB203580) inhibition in the BL cell lines BL-2, BL-41 and CA-46. The BCR was stimulated with  $\alpha$ -IgM for 5 and 30 minutes. Tubulin served as loading control and imaging was done with fluorescence antibodies ( $n=2$ ). (B) Representative immunoblot analysis of MEK1/2 (AZD6244) and p38 MAPK (SB203580) inhibition in BL-41. After 3 hours inhibitor treatment, the BCR was activated with  $\alpha$ -IgM for 30 minutes. Tubulin served as loading control and imaging was done with fluorescence antibodies ( $n=2$ ). (C) Quantification of the inactivating RAF-1 phosphorylations of the immunoblot analyses from B.

### 3.2.3 p38 MAPK reduces activation and duration of the MEK-ERK pathway

Beside the connection of p38 MAPK to the MEK-ERK pathway, the question was also whether p38 MAPK limited the ERK1/2 activity. Firstly, the signaling duration of ERK1/2 was investigated more precisely. Once activated, the ERK1/2 signal diminished during the first 5 to 30 minutes but was still present over hours (data not shown). Therefore, an

experiment was planned whereby the BCR was activated for 5 minutes following a signal disruption by inhibition of the upstream kinase BTK. This analysis enabled us to monitor and compare the dephosphorylation of ERK1/2 between control and p38 MAPK inhibited BL-2 cells at several time points (Figure 10 A). After 5 minutes of  $\alpha$ -IgM stimulation ERK1/2 was phosphorylated and this signal started to decline after 10 minutes of BTK inhibition by ibrutinib. In comparison to the respective control, inhibition of p38 MAPK (SB203580) caused stronger ERK1/2 phosphorylations at each time point. However, the dephosphorylation of ERK1/2 was not prevented and only delayed by p38 MAPK inhibition.

As the dephosphorylation did not provide sufficient insights into ERK1/2 activity, ERK1/2 was immune-precipitated and the kinase activity measured in BL-2 cells (data of our collaboration partner and not shown). After stimulation of the BCR with  $\alpha$ -IgM for 30 minutes, the ERK1/2 activity was about two-fold higher in p38 inhibited cells. Furthermore, *in vitro* stimulation of purified ERK1/2 revealed that the p38 MAPK inhibitor (SB203580) alone had no influence on the activity. In conclusion, p38 MAPK caused a reduced kinase activity of ERK1/2 and an unspecific inhibitor effect on ERK1/2 was excluded.

In order to evaluate whether the increased ERK1/2 activity is limited to cytosolic functions or could also affect nuclear tasks, the translocation of ERK1/2 was investigated in CA-46 cells (Figure 10 B). The stimulation of the BCR with  $\alpha$ -IgM for 5 minutes led to phosphorylation and translocation of ERK1/2 to the nucleus. In comparison, a higher amount of phosphorylated ERK1/2 was detected in the nucleus after inhibition of p38 MAPK (SB203580). Nevertheless, the ERK1/2 phosphorylation was also increased in the cytosolic fraction after p38 MAPK inhibition in comparison to the antigen-stimulated control. We assumed that p38 MAPK could alter cytosolic as well as nuclear tasks of ERK1/2.

To sum up, p38 MAPK not only diminished the phosphorylation of MEK1 and ERK1/2 after BCR activation but also reduced the pathway activity. We concluded that p38 MAPK shortens the signal duration and activity of ERK1/2 thus influencing ERK targets.

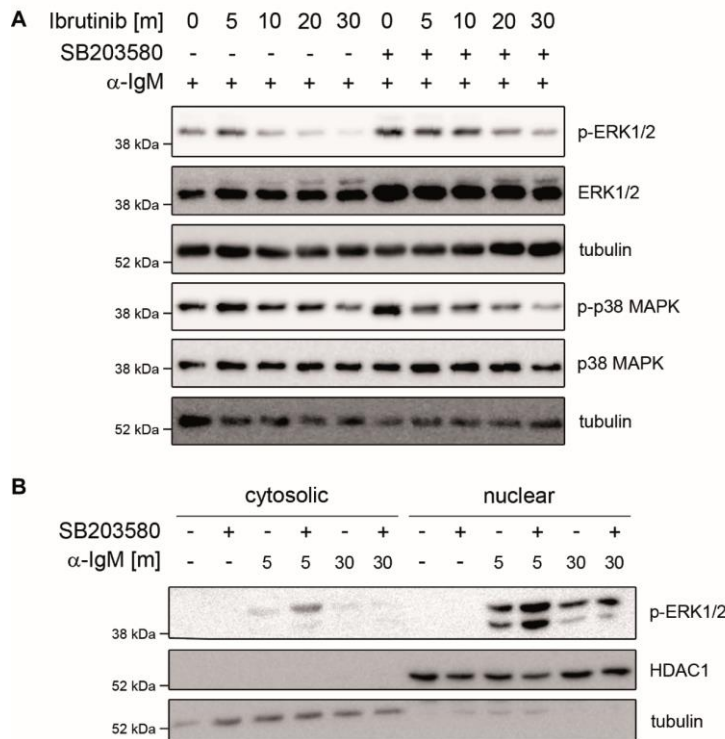


**Figure 10: Alteration of ERK1/2 activity after p38 MAPK inhibition**

(A) Representative immunoblot analysis of 3 hours p38 MAPK (SB203580) inhibition in BL-2 cells. The BCR was activated for 5 minutes by  $\alpha$ -IgM stimulation followed by a signal disruption through inhibition of the BCR-related kinase BTK for the indicated time points. Tubulin served as loading control (n=3). (B) Representative immunoblot analysis of nuclear and cytosolic fractions after p38 MAPK (SB203580) inhibition in CA-46. After 3 hours inhibitor treatment the BCR was stimulated with  $\alpha$ -IgM for 5 and 30 minutes. HDAC1 and tubulin served as loading controls (n=3).

### 3.2.4 Early target gene expression of ERK1/2 is not influenced by p38 MAPK

To examine whether ERK1/2 targets were affected by p38 MAPK, we investigated the expression of well-known target genes. The expression of several genes is mediated by ERK1/2 through binding to promotor regions or through activation of transcription factors (Fukunaga and Hunter, 1997; Shaul and Seger, 2007). We analyzed the target genes *FOS*, *early growth response 2* (*EGR2*) and *early growth response 3* (*EGR3*) because ERK1/2 can bind to the promotor region and quickly induces their expression (Yasuda et al., 2008). The activation of the BCR with  $\alpha$ -IgM for 3 hours strongly increased the expression of *EGR2*, *EGR3* and *FOS* in BL-2 and CA-46 compared to the unstimulated control (Figure 11). In addition, all three gene expressions were ERK-dependent and diminished by inhibition of MEK1/2 (AZD6244, U0126). The p38 MAPK inhibition (SB203580) did not affect the gene expression compared to the antigen-stimulated control in BL-2 cells (Figure 11 A-C). In CA-46 cells the expression of *FOS* was also not altered by p38 MAPK inhibition (Figure 11 F). However, a slight increase was detectable for

*EGR2* and *EGR3* expression after p38 MAPK inhibition compared to the antigen-stimulated control in CA-46 (Figure 11 D-E). Although *EGR2*, *EGR3* and *FOS* expression was induced by ERK1/2, the higher activity of ERK1/2 after p38 MAPK inhibition only led to a stronger expression of *EGR2* and *EGR3* in CA-46 cells.

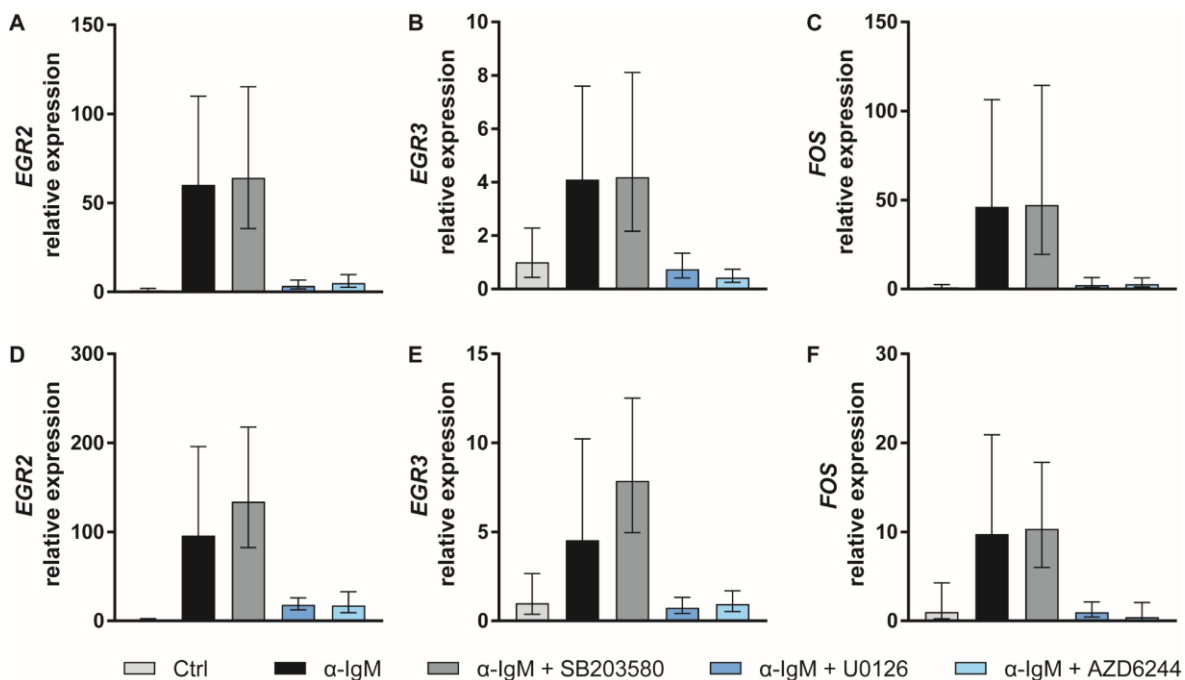


**Figure 11: Impact on early target gene expressions by ERK1/2 and p38 MAPK**

Gene expression analyses of early target genes were investigated after 3 hours inhibitor treatment with additionally 3 hours BCR activation. Data were normalized to *GAPDH* (housekeeper) and the untreated control. The mean +/- SD is shown for *EGR2* (A, D), *EGR3* (B, E) and *FOS* (C, F) for the BL cell lines BL-2 (A - C) or CA-46 (D - F) (n=3).

In order to reduce the possibility of feedbacks or secondary effects that influence or limit the target gene expressions after 3 hours of BCR activation, the expression of *EGR2* and *EGR3* was analyzed after 1 hour of BCR activation (Figure 12). Due to the observed differences between BL-2 and CA-46 cells, a third lymphoma cell line, BL-41, was included. In all three lymphoma cell lines the stimulation with α-IgM for 1 hour increased the expression of *EGR2* and *EGR3*. Furthermore, the target gene expressions were ERK1/2-dependent (AZD6244, U0126) in all three cell lines. Unlike as before, the p38 MAPK inhibition (SB203580) resulted in a reduced expression of *EGR2* and *EGR3* compared to the antigen-stimulated control in BL-41 and CA-46 (Figure 12 B-C,E-F), while almost no difference was found in BL-2 cells (Figure 12 A,D).

In conclusion, *EGR2*, *EGR3* and *FOS* are ERK1/2 target genes. However, the limiting effect of p38 MAPK on the *EGR2* and *EGR3* expression in CA-46 cells after 3 hours of BCR activation could not be verified after 1 hour of BCR activation. Interestingly, the

fold changes revealed that the *EGR2* expression increased up to 3 hours of BCR activation (Figure 11 A,D; Figure 12 A,C), whereas the *EGR3* expression seemed to be terminated after 3 hours of BCR activation (Figure 11 A,D; Figure 12 A,C). Therefore, we suggested that p38 MAPK is not limiting the *EGR2* expression and due to a peaking expression at an earlier time point, *EGR3* remains to be further examined.

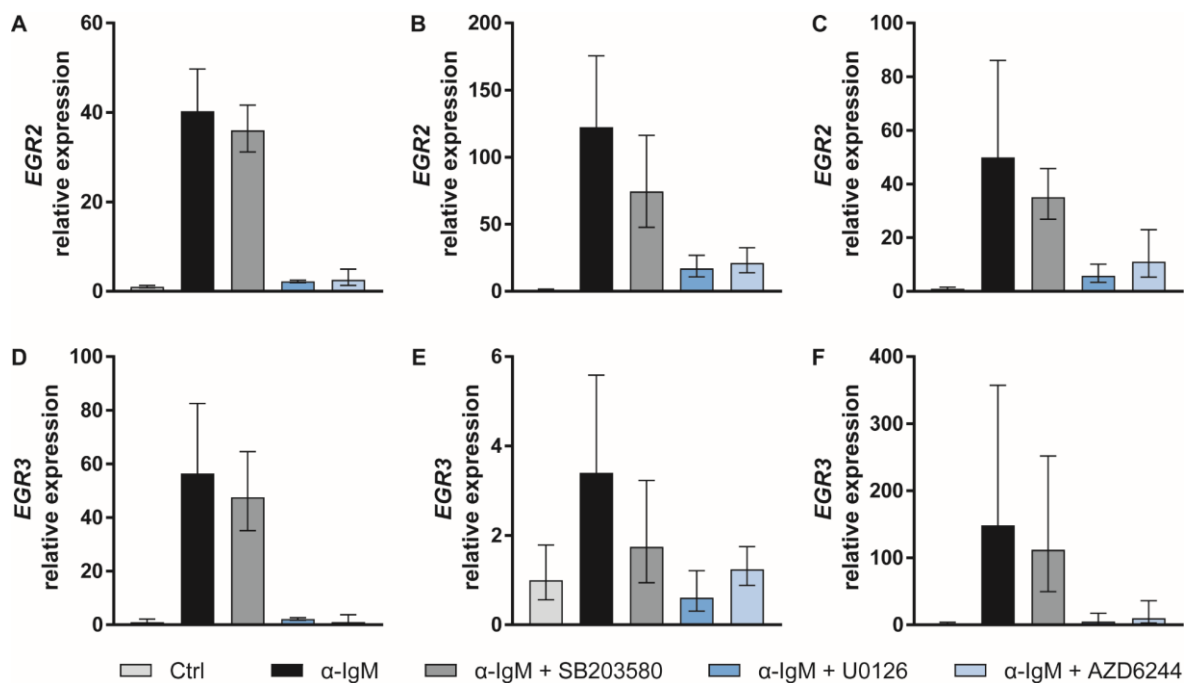


**Figure 12: Impact of ERK1/2 and p38 MAPK on early target gene expression**

Gene expression of early target genes was analyzed after 3 hours inhibitor treatment following 1 hour BCR activation. Data were normalized to *GAPDH* (housekeeper) and the untreated control. The mean +/- SD is shown for *EGR2* (A - C) and *EGR3* (D - F) for the BL cell lines BL-2 (A, D), BL-41 (B, E) or CA-46 (C, F) (n=3).

### 3.2.5 p38 MAPK attenuates ERK1/2-regulated gene expression of the kinase MKK6

To further pursue the analysis of ERK1/2 targets affected by p38 MAPK, we used and re-evaluated the previous generated microarray analyses. In this project, gene expression changes were examined after pathway perturbations during the BCR signaling in BL-2 cells to achieve a network structure indirectly from downstream effects (Hand, 2013). Therefore, we could compare the gene expression changes of MEK1/2 (U0126) and p38 MAPK (SB203580) inhibition during an activated BCR. As p38 MAPK increased the ERK1/2 activity, we examined the expression data for oppositely regulated genes. This comparison and evaluation of the microarray data was performed by Maren Sitte (Statistical Bioinformatics Department Medical Statistics, University Medical Centre Goettingen). The following genes were found to be contrarily regulated after MEK1/2 and

p38 MAPK inhibition: *zinc finger protein 800* (*ZNF800*), *pyruvate dehydrogenase phosphatase 1* (*PDP1*), *special AT-rich sequence-binding protein 1* (*SATB1*), *zinc finger protein 36 C3H1 type-like 1* (*ZFP36L1*), *EGR3*, *phospholipase D6* (*PLD6*), *myotubularin-related protein 4* (*MTMR4*), *NACHT, LRR and PYD domains-containing protein 11* (*NLRP11*), *neurogenic locus notch homolog protein 2* (*NOTCH2*), *prostaglandin-endoperoxide synthase 1* (*PTGS1*), *CD40* and *MAP2K6*.

For the validation of these 12 target genes, BL-2 cells were treated in the same way as performed for the microarray analyses and then analyzed with qRT-PCR. Namely, BL-2 cells were pretreated with MEK1/2 or p38 MAPK inhibitors for 3 hours and then the BCR was activated with  $\alpha$ -IgM for additional 3 hours. The CA-46 cell line was also included in the analyses. The found targets *MTMR4*, *NOTCH2*, *CD40* were not ERK1/2 or p38 MAPK regulated (data not shown). *SATB1* was an ERK target gene but the expression was not altered by p38 MAPK inhibition (data not shown). The expression of *EGR3* was already displayed in the previous chapter 3.2.4 while the examination of the other candidates is shown in Figure 13. The microarray data proposed a downregulation of *PLD6* by ERK1/2 whereas all other target gene expressions were suggested to be upregulated. A decreased expression of *PLD6* was measured after  $\alpha$ -IgM stimulation in both cell lines (Figure 13 A,D). In addition, p38 MAPK inhibition (SB203580) induced no changes and MEK1/2 inhibition (AZD6244, U0126) was not able to rescue the gene expression to the level of the untreated control.

The expression of the other targets *PDP1*, *ZFP36L1*, *PTGS1* and *MAP2K6* were clearly increased by  $\alpha$ -IgM stimulation in both cell lines (Figure 13 B-C,E-F,G-H,J-K). Besides, the expressions were induced to a higher extent in BL-2 cells compared to CA-46 cells. The inhibition of MEK1/2 (AZD6244, U0126) reduced the gene expression of *PDP1*, *ZFP36L1*, *PTGS1* and *MAP2K6* to the unstimulated control level thus revealing the dependence on ERK1/2. However, the inhibition of p38 MAPK (SB203580) caused no differences compared to the antigen-stimulated control except for *MAP2K6* in CA-46. The expression of *MAP2K6* was almost doubled after p38 MAPK inhibition compared with the antigen-stimulated control (Figure 13 K). As TNF $\alpha$  can lead to MKK6 (*MAP2K6*) activation and the expression is known to be ERK1/2 as well as p38 MAPK regulated (Sabio and Davis, 2014), the TNF $\alpha$  gene expression was further investigated (Figure 13 I,L). Interestingly, TNF $\alpha$  was strongly upregulated by BCR and especially ERK1/2 activation (AZD6244, U0126). An influence on the expression of TNF $\alpha$  by p38 MAPK inhibition (SB203580) was not detected.

To sum up, the target gene expressions of *PDP1*, *ZFP36L1*, *PTGS1*, *MAP2K6* and *TNF $\alpha$*  depended on ERK1/2 activity. However, the increased ERK1/2 activity after p38 MAPK inhibition was only reflected by an increased expression of *MAP2K6* in CA-46 cells.

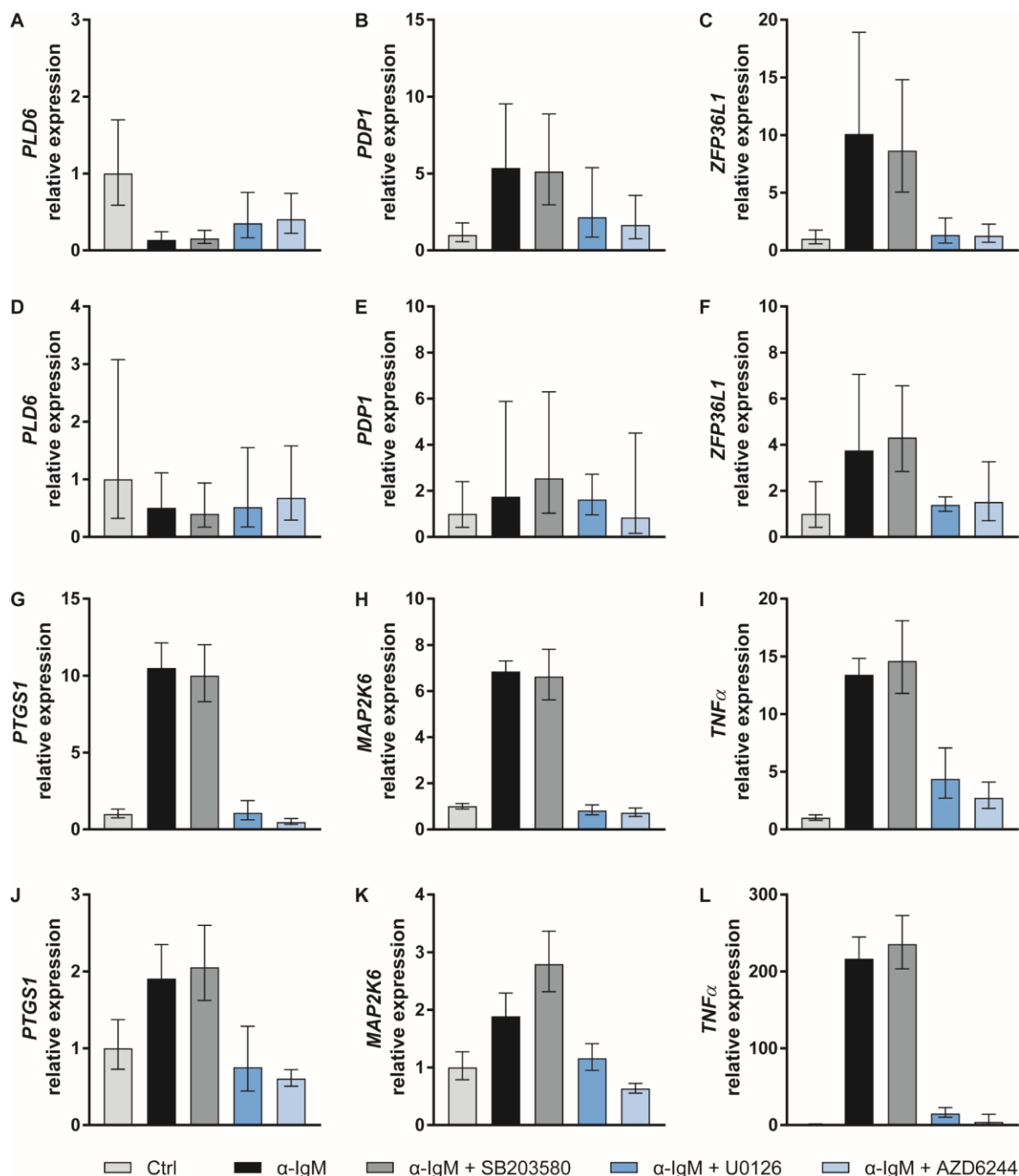


**Figure 13: p38 MAPK influence on ERK1/2 target gene expression**

Expression of ERK1/2 target genes was measured after 3 hours inhibitor treatment and additional 3 hours BCR activation. Data were normalized to *GAPDH* (housekeeper) and the untreated control. The mean +/- SD is shown for *PLD6* (A, D), *PDP1* (B, E), *ZFP36L1* (C, F), *PTGS1* (G, J), *MAP2K6* (H, K) and *TNF $\alpha$*  (I, L) for the BL cell lines BL-2 (A – C, G – I) or CA-46 (D – F, J – L) (n=3).

Not to overlook gene expression differences in BL-2 at an earlier time point, the expression of *MAP2K6* (MKK6) and the MKK6 activator *TNF $\alpha$*  was examined after 1 hour of BCR activation (Figure 14). Due to the observed differences between BL-2 and CA-46 cells, the lymphoma cell line BL-41 was included in the analysis. In all three cell lines the *TNF $\alpha$*  expression was induced by  $\alpha$ -IgM stimulation in an ERK-dependent manner (AZD6244, U0126) (Figure 14 A-C). The inhibition of p38 MAPK (SB203580) showed no notable impacts on *TNF $\alpha$*  expression compared to the antigen-stimulated control in BL-2 and CA-46 cells (Figure 14 A,C), while in BL-41 cells p38 MAPK inhibition reduced the expression similar to MEK1/2 inhibition (Figure 14 B). The expression analysis of *MAP2K6* revealed that BCR activation by  $\alpha$ -IgM caused a clear induction in BL-2 cells (Figure 14 D) and a slight increase in BL-41 cells (Figure 14 E). While in BL-2 cells the ERK1/2 dependence (AZD6244, U0126) was obvious, it was only supposed in BL-41 cells. On the contrary, in CA-46 no increased *MAP2K6* expression was observed and therefore no ERK1/2-dependence is concluded (Figure 14 F). Nevertheless, the inhibition of p38 MAPK (SB203580) resulted in a stronger expression of *MAP2K6* in all three cell lines (Figure 14 C-F).

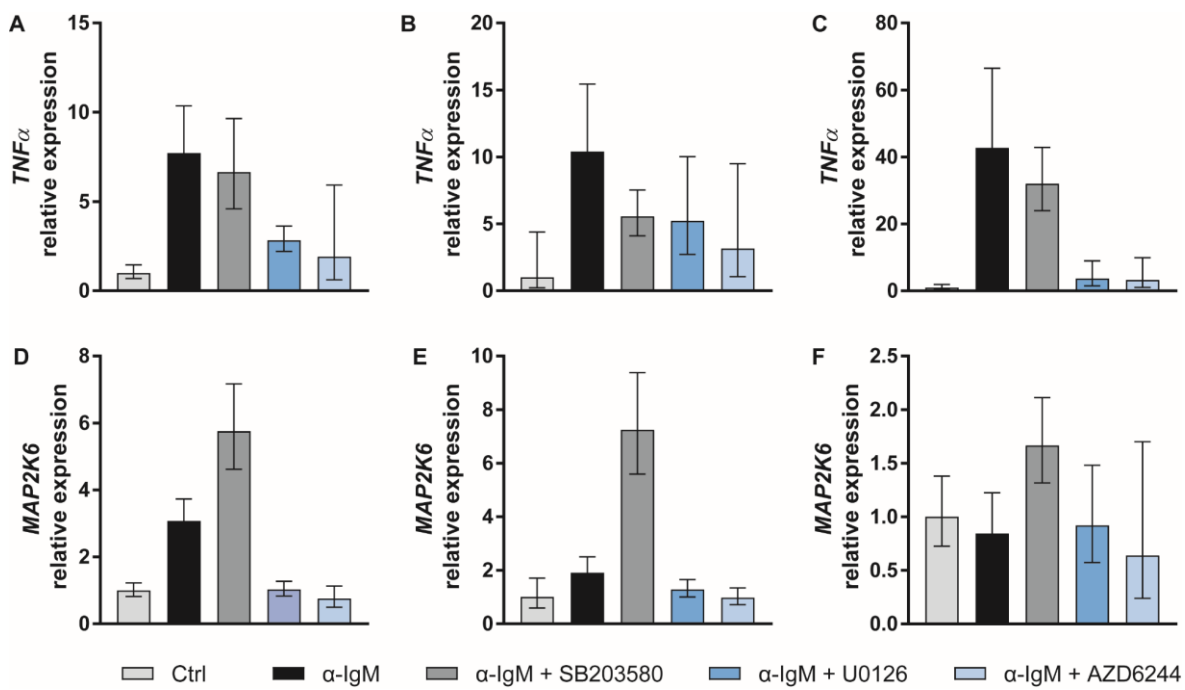


**Figure 14: p38 MAPK influence on ERK1/2 target gene expression**

Expression of ERK1/2 target genes was investigated after 3 hours inhibitor treatment and additional 1 hour BCR activation. Data were normalized to *GAPDH* (housekeeper) and the untreated control. The mean +/- SD is shown for *TNF $\alpha$*  (A - C) and *MAP2K6* (D - F) for the BL cell lines BL-2 (A, D), BL-41 (B, E) or CA-46 (C, F) (n=3).

To sum up, p38 MAPK not only attenuated the MEK-ERK pathway, the target gene expression of *MAP2K6* was also limited by p38 MAPK after 1 hour of BCR activation.

Interestingly, *MAP2K6* transcribes for the kinase MKK6 which can be activated by TNF $\alpha$  and which is known as upstream activator of p38 MAPK (Sabio and Davis, 2014). Due to the ERK-dependent upregulation of TNF $\alpha$  and MKK6, we suggested that the negative feedback of p38 MAPK on the MEK-ERK pathway can be further promoted by high ERK1/2 activities but this remains to be elucidated.

### 3.3 DLBCLs with chronic active BCR contain divers feedback loops

Unstimulated BLs showed a positive feedback loop of the PI3K pathway and only after BCR activation with antigens two negative feedbacks on the MEK-ERK pathway were revealed. Therefore, the question was whether B cell lymphomas with a chronic active BCR involve the same pathway interplays. In ABC DLBCLs mutations of CD79b, MyD88 or CARD11 mimic an active BCR with subsequent activation of NF- $\kappa$ B (Davis *et al.*, 2010; Ngo *et al.*, 2011). As different mutations in ABC DLBCLs can cause similar pathway activations, the cell lines HBL-1 and OCI-LY3 were chosen. HBL-1 cells harbor mutations in MyD88 and CD79b, while the OCI-LY3 cells are characterized by a receptor-independent activation of NF- $\kappa$ B due to mutations in MyD88 and CARD11 (Paul *et al.*, 2017).

#### 3.3.1 Positive and negative feedbacks influence chronic active BCR signaling

In order to compare the feedbacks with BLs, pathway phosphorylations during a chronic active BCR signaling were examined like before using a smaller set of inhibitors than for the BL-2 analysis. The quantitative values of this analysis are presented in the supplement (Figure A-5). In HBL-1 cells we observed that the inhibition of BTK, PI3K, mTOR and JNK reduced the phosphorylation of all measured protein phosphorylations (Figure 15 A). More precisely, the activation of SYK, ZAP70, BTK, GSK3 $\beta$  and the PI3K-AKT, MEK-ERK, p38 MAPK, JNK and NF- $\kappa$ B pathways were decreased. On the contrary, the inhibition of AKT increased the phosphorylation of SYK, ZAP70, BTK, GSK3 $\beta$ , MEK1, ERK1/2, JNK and c-Jun while the amount of phosphorylated RPS6 was reduced. As a signal inhibition at PI3K or mTOR led to a decreased phosphorylation of downstream and upstream kinases, we suggested that a positive feedback loop from mTOR to the BCR enhanced the signal as observed in BL cells. However, the JNK inhibitor had similar effects like a PI3K inhibitor and the inhibition of AKT revealed an opposite effect although no phosphorylation changes of the downstream target RPS6 were measured.

Besides, the inhibition of MEK1/2 diminished clearly the ERK1/2 and p90RSK phosphorylation and heightened the MEK1 phosphorylation. This indicated the negative feedback loop from ERK1/2 on its own pathway. The p38 MAPK inhibition heightened strongly the MEK1 and ERK1/2 phosphorylation suggesting that p38 MAPK had even a negative impact on the MEK-ERK pathway. The simultaneous inhibition of p38 MAPK and MEK1/2 revealed that the influence on the pathway occurred mainly upstream of ERK1/2 as ERK1/2 phosphorylation was reduced around 85 % compared to p38 MAPK inhibition alone. Finally, the NF- $\kappa$ B inhibition just slightly reduced the phosphorylation of SYK, ZAP70, BTK and of the PI3K-AKT, p38 MAPK and NF- $\kappa$ B pathway, whereas an increased phosphorylation of MEK1 was detected. However, NF- $\kappa$ B seemed not to be a further regulator of the MEK-ERK pathway because no effects on ERK1/2 were measured.

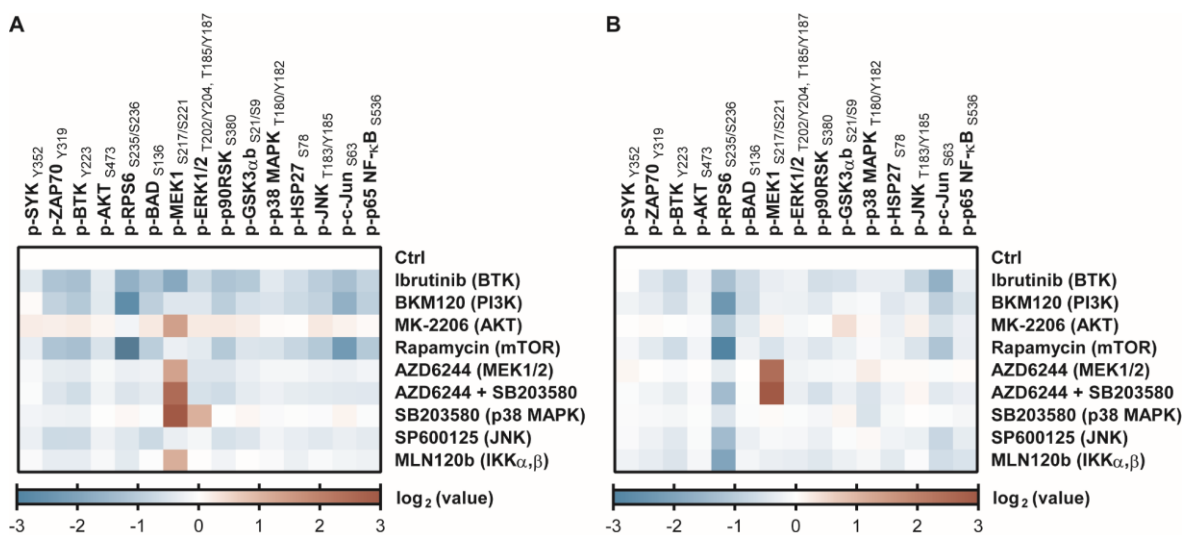


**Figure 15: Signaling changes by pathway perturbations during the chronic active BCR signaling.**

The signal transduction were disrupted by inhibitors of BTK, PI3K, AKT, mTOR, MEK1/2, p38 MAPK, JNK and IKK $\alpha$ , $\beta$  for 3 hours. Specific phosphorylations of SYK, ZAP70, BTK, AKT, RPS6, BAD, MEK1, ERK1/2, p90RSK, GSK3 $\alpha$ b, p38 MAPK, HSP27, JNK, c-JUN and p65 NF- $\kappa$ B were measured with the multiplex immunoassay. The log<sub>2</sub> values for the ABC DLBCL lymphoma cell line HBL-1 (**A**) or OCI-LY3 (**B**) are shown normalized to the control (n=3).

The treatment of OCI-LY3 cells caused mostly the same effects though the overall phosphorylation changes were smaller (Figure 15 B). Therefore, only the differences to HBL-1 cells are described. The inhibition of AKT caused a diminished phosphorylation of RPS6 and similar effects like PI3K and mTOR inhibition. Only the phosphorylation of GSK3 $\beta$  was raised and therefore controversial to HBL-1 cells. The inhibition of MEK1/2 had no influence on p38 MAPK in HBL-1 cells, whereas in OCI-LY3 cells a slight increased phosphorylation was observed. Furthermore, the NF- $\kappa$ B inhibition did not lead

to higher MEK1 phosphorylations as seen in HBL-1 cells. However, the most obvious difference was that inhibition of p38 MAPK had no impact on the MEK-ERK pathway.

In conclusion, we suggested that the positive feedback of the PI3K signaling and the negative feedback from ERK1/2 on the MEK-ERK pathway is conserved in B cell lymphomas. Nevertheless, we assumed that due to genetic variations the regulation of the MEK-ERK pathway by p38 MAPK differs between the ABC DLBCL cell lines. This indicated that the genetic background can influence possible interactions and feedbacks and thereby the signal distribution.

The obvious assumption for the missing influence of p38 MAPK on the MEK-ERK pathway could be that the p38 MAPK inhibitor was not functioning. But due to the slight reduction of phosphorylated p38 MAPK after the inhibitor treatment in several analyses, the three biological replicates and the simultaneously performed HBL-1 analyses, this possibility was excluded. Furthermore, the missing effect could be explained by an inactive MEK-ERK signaling. Comparing BL-2, HBL-1 and OCI-LY3 cells, it was shown that OCI-LY3 had phosphorylated ERK1/2 and furthermore high levels of phosphorylated p38 MAPK (Figure 16 A). Therefore, the cellular state of OCI-LY3 cells were suggested to be responsible for the missing negative feedback on the MEK-ERK pathway. One explanation can be that different mutations like the mutation of CARD11 entail an altered expression of some proteins. However, this would not be an explanation for the missing p38 MAPK effect if p38 MAPK directly interacted with RAF-1. But due to the not known interaction between p38 MAPK and RAF-1, we suggested that a p38 MAPK regulated phosphatase would rather explain the cell line differences as it could reduce any phosphosites in the MEK-ERK pathway.

In order to investigate kinases or phosphatases differently expressed in HBL-1 and OCI-LY3 cells, the gene expression of two previous RNA-sequencing projects were analyzed. Therefore, the estimated RNA sequencing reads of BL-2, HBL-1 and OCI-LY3 cells were compared to find a missing kinase or phosphatase expression in OCI-LY3 cells (Figure 16 B). An overview of phosphatases and kinases with more than 50 % differential expression between HBL-1 and OCI-LY3 cells is displayed. The extract of the gene list revealed that some phosphatases were highly expressed by HBL-1 and BL-2 cells and nearly absent in OCI-LY3 cells. For instance, the lymphocyte cell-specific protein tyrosine kinase (LCK), paladin (PALD1), tyrosine protein phosphatase non-receptor type 22 (PTPN22) and PTPN7 were barely expressed in OCI-LY3 cells which could explain the missing p38 MAPK influence on the MEK-ERK pathway. However, this hypothesis remained to be proven.

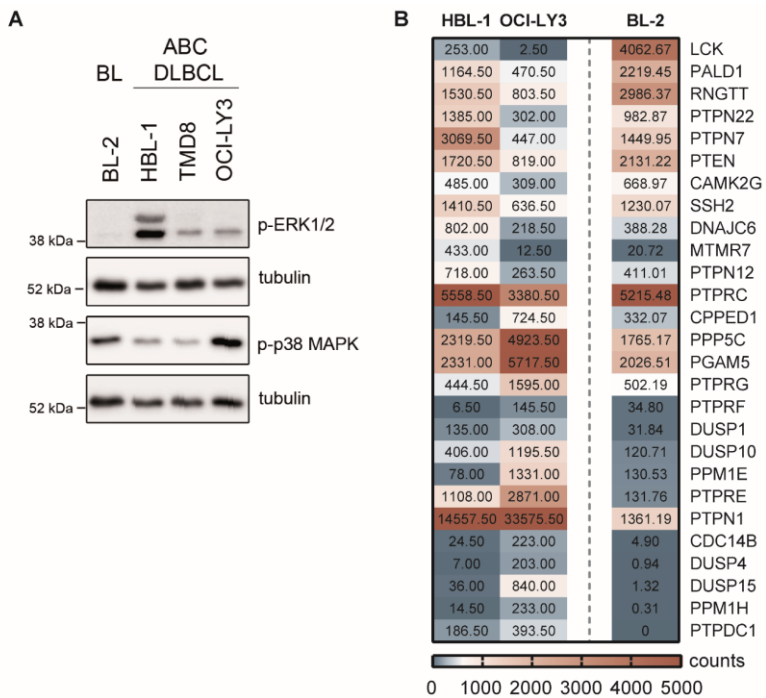


**Figure 16: Comparison of BL-2, HBL-1 and OCI-LY3 cells on protein and RNA level**

To explain the cell line differences of the multiplex immunoassay BL-2, HBL-1 and OCI-LY3 cells were compared on protein and RNA level. **(A)** Representative immunoblot analysis of the different, untreated lymphoma cell lines. Tubulin served as loading control (n=3). **(B)** An extract of phosphatases and kinases of the RNA sequencing analyses with mean of estimated counts are displayed for HBL-1, OCI-LY3 and BL-2 cells (n=3).

### 3.3.2 Negative feedbacks of the chronic active BCR signaling have no impacts on proliferation

While the inhibition of BTK, PI3K, JNK and NF- $\kappa$ B is well studied in DLBCLs (Gururajan *et al.*, 2005; Kloo *et al.*, 2011; Young and Staudt, 2013), less is known about the impact of MEK1/2 or p38 MAPK inhibition on proliferation. Only one paper indicated that inhibition of MEK1/2 with the AZD6244 inhibitor induced apoptosis in OCI-LY3 cells after 48 hours (Bhalla *et al.*, 2011). Therefore, the inhibition of MEK1/2 and p38 MAPK was analyzed on cell viability over 72 hours (Figure 17). No influences on cell viability of HBL-1 cells were detectable (Figure 17 A) and OCI-LY3 cells showed only a small decrease of cell viability about 15 - 20 % after MEK1/2 and p38 MAPK inhibition (Figure 17 B). Consequently, the inhibition of ERK1/2 or p38 MAPK did not reduce considerably the cell viability.

This indicated that the negative feedbacks on the MEK-ERK pathway are not involved in the regulation of cell proliferation and therefore the specific role of MAPKs in lymphoma needs to be further elucidated.

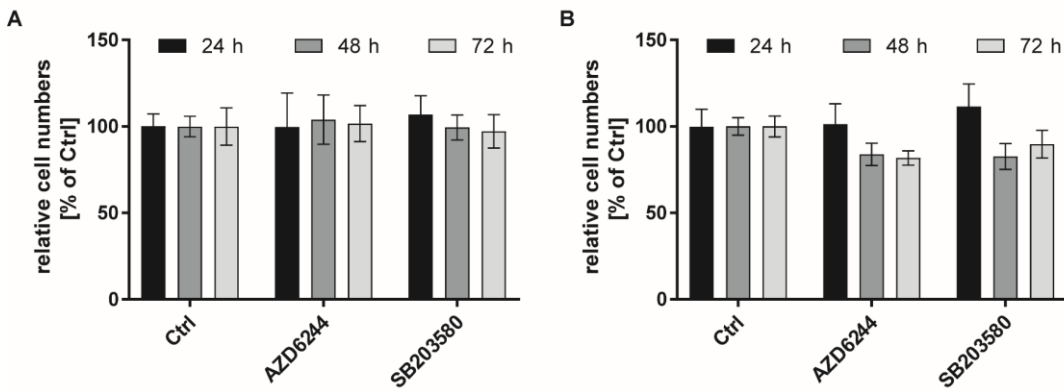


**Figure 17: Cell viability of HBL-1 and OCI-LY3 cells after MEK1/2 or p38 MAPK inhibition**

Cell viability assay was performed after 24, 48 and 72 hours with the fluorescence dye Calcein AM. The amount of viable cells was normalized to control and the mean +/- SD is displayed for HBL-1 (**A**) and OCI-LY3 (**B**) cells (n=3).

### 3.4 IL10R and TLR9 activation modify cell response and behavior

Apart from the several signaling pathways of the chronic active BCR, ABC DLBCLs contain an autocrine JAK-STAT activation. This is mediated by a BCR-dependent NF- $\kappa$ B signaling which causes an increased expression of ILs and thereby subsequently stimulates IL receptors and JAKs (Gupta *et al.*, 2012; Jost and Ruland, 2007). Our group has previously described that only the combined activation of NF- $\kappa$ B and STAT3 induces proliferation in a synergistic manner (Feist *et al.*, 2017; Feist *et al.*, 2018). To further examine mediators of the proliferative boost and the directly altered cellular processes after receptor activation, a phosphoproteomics analysis was performed. As ABC DLBCLs differ in their behavior due to cell line specific mutations, the analyses were done with the model cell line P493-6. This allows a direct comparison of cells with active or inactive NF- $\kappa$ B and STAT3 without variations resulting from mutations.

#### 3.4.1 IL10R and TLR9 activation change 239 protein phosphorylations

The examination of global protein phosphorylations was done after TLR9 and IL10R activation with mass spectrometry. For an accurate comparison of two conditions, the cells were labelled with stable isotopes (SILAC). In Figure 18 A the workflow is presented, the heavy labeled P493-6 cells ( $\text{Myc}^{\text{high}}$ ) were left untreated while the light labeled cells were supplemented with doxycycline to reduce the amount of c-MYC ( $\text{Myc}^{\text{low}}$ ). Afterwards  $\text{Myc}^{\text{low}}$  cells were stimulated with IL10+CpG to activate TLR9 and IL10R for 30 minutes or left untreated as control (Ctrl). The  $\text{Myc}^{\text{high}}$  cells served as a reference control for normalization and thus were also activated by IL10+CpG stimulation for 30 minutes to

obtain sufficient protein phosphorylations. Heavy and light labeled conditions were mixed in equal parts, the protein phosphorylation was determined and the phosphorylation changes of control or IL10+CpG stimulated Myc<sup>low</sup> cells in relation to Myc<sup>high</sup> cells were calculated.

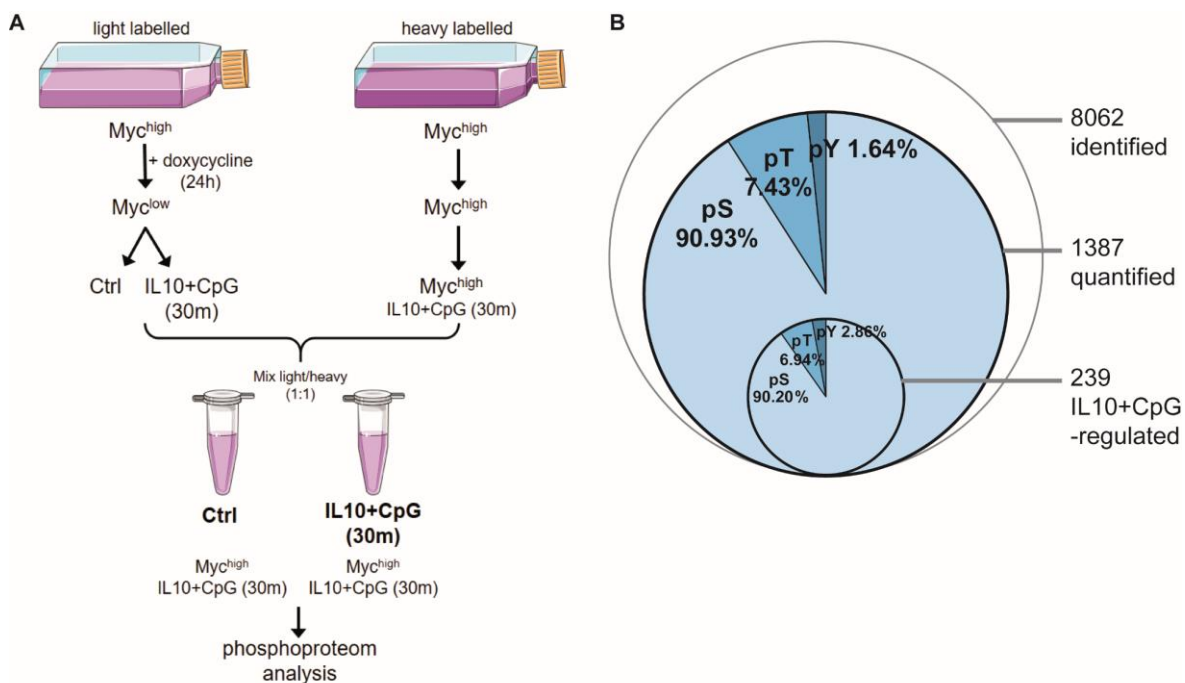


**Figure 18: Workflow and global phosphosites identification of mass spectrometry analysis**  
To reveal protein phosphorylations Ctrl and IL10+CpG stimulated Myc<sup>low</sup> cells were analyzed in relation to Myc<sup>high</sup> cells with mass spectrometry (n=3). **(A)** Schematic workflow for labeling, stimulating and harvesting of Myc<sup>low</sup> and Myc<sup>high</sup> cells. **(B)** Proportion of phosphorylated residues of quantified and IL10+CpG-regulated proteins.

Out of 8062 detected phosphosites, 1387 were quantified in at least two out of three replicates and with a p-value less than 0.05 (Figure 18 B). The stimulation of TLR9 and IL10R led to significant change of 239 phosphosites with a phosphorylation differences between Ctrl and IL10+CpG stimulated Myc<sup>low</sup> cells of more than 50 %. Thereby, the proportion of threonine, tyrosine and serine phosphorylated residues was not altered between quantified and IL10+CpG-regulated phosphosites. This proportion accurately reflects the relative abundance of serine, tyrosine and threonine phosphorylations after receptor activation (Olsen *et al.*, 2006).

In order to compare the results of the biological replicates, the phosphorylation ratios for the Ctrl (Figure 19 A) and IL10+CpG stimulated (Figure 19 B) Myc<sup>low</sup> cells in relation to Myc<sup>high</sup> cells were plotted for each biological replicate against the other replicates. The

Pearson's correlation coefficient was similar for each comparison of the biological replicates and ranged from 0.78 to 0.88 indicating an acceptable reproducibility.

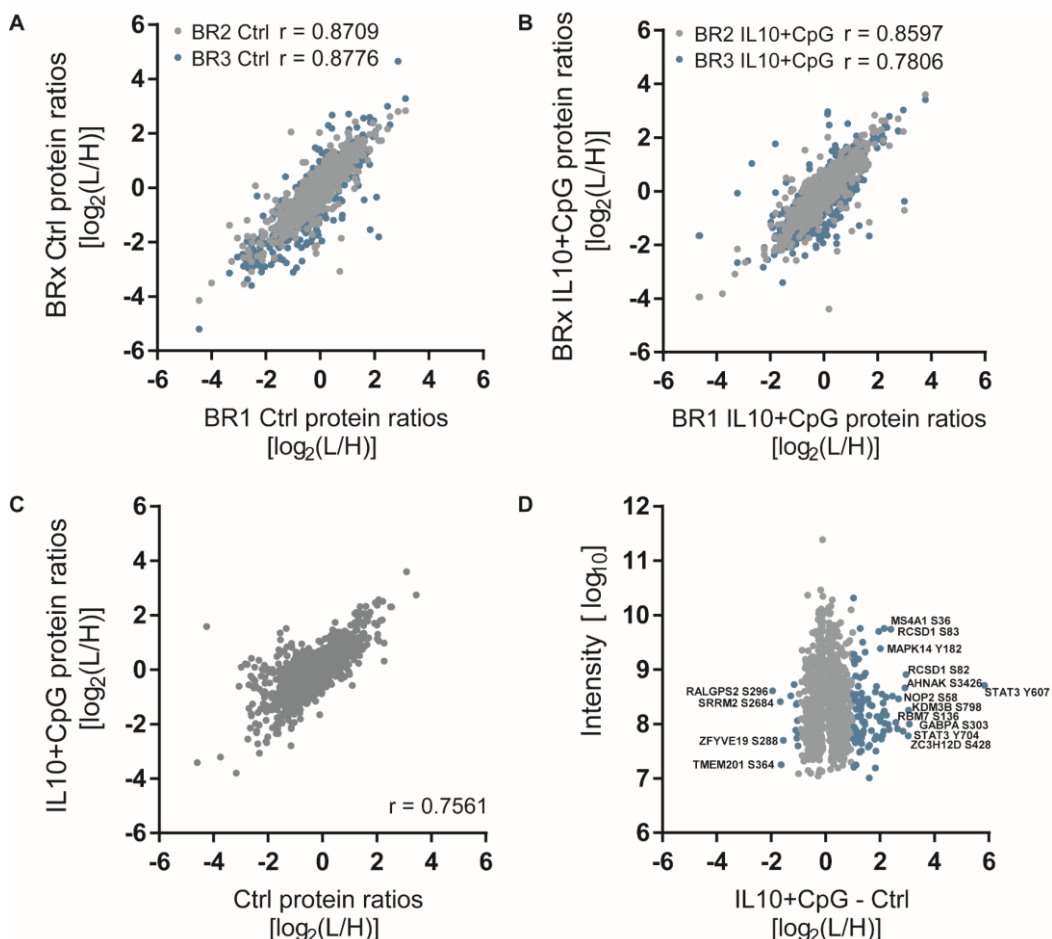


**Figure 19: Global phosphoproteomics results of Ctrl and IL10+CpG stimulated Myc<sup>low</sup> cells**  
Scatter Plots with Pearson's correlation coefficients were demonstrating the reproducibility of biological replicates for Ctrl (**A**) or IL10+CpG stimulated (**B**) Myc<sup>low</sup> cells. (**C**) Scatter Plot with Pearson correlation coefficients compared the values of quantified phosphosites of Ctrl and IL10+CpG stimulated Myc<sup>low</sup> cells. (**D**) Scatter plot showed the measured intensities for the log<sub>2</sub> ratios of IL10+CpG stimulated Myc<sup>low</sup> cells in relation to the Ctrl. Log<sub>2</sub> ratios with difference above 1.0 are indicated in blue. All quantified phosphosites are listed in the supplement.

To present the phosphosite changes after IL10+CpG stimulation, the phosphorylation ratios of the IL10+CpG stimulated Myc<sup>low</sup> cells were displayed to the ratios of the Ctrl Myc<sup>low</sup> cells (Figure 19 C). As more phosphosite ratios were higher in IL10+CpG stimulated cells compared to Ctrl, we suggested that the stimulation of cells clearly induced a phosphorylation of proteins while only few sites were dephosphorylated. The precision of quantitation increased with the protein abundance, therefore the measured intensities were displayed over the relation of IL10+CpG stimulation to the Ctrl Myc<sup>low</sup> cells (Figure 19 D). Protein phosphorylations with a log<sub>2</sub> change higher than 1.0 are marked (blue dots). For example, the STAT3 tyrosine phosphorylation known to be induced by

IL10 was strongly increased after IL10+CpG stimulation as well as some further sites of p38 MAPK (MAPK14), capZ-interacting protein 1 (RCSD1) and nucleolar protein 2 homolog (NOP2). The full list of the 239 changed phosphosites is presented in Table A-1.

### 3.4.2 Phosphoproteome reveals influence on cell cycle, metabolism and migration

Identifying the connection of regulated proteins is valuable in order to build a network which can help to reveal closely related proteins and altered protein groups. Therefore, the IL10+CpG-influenced phosphosites were used for a network generation with STRING (Figure 20).

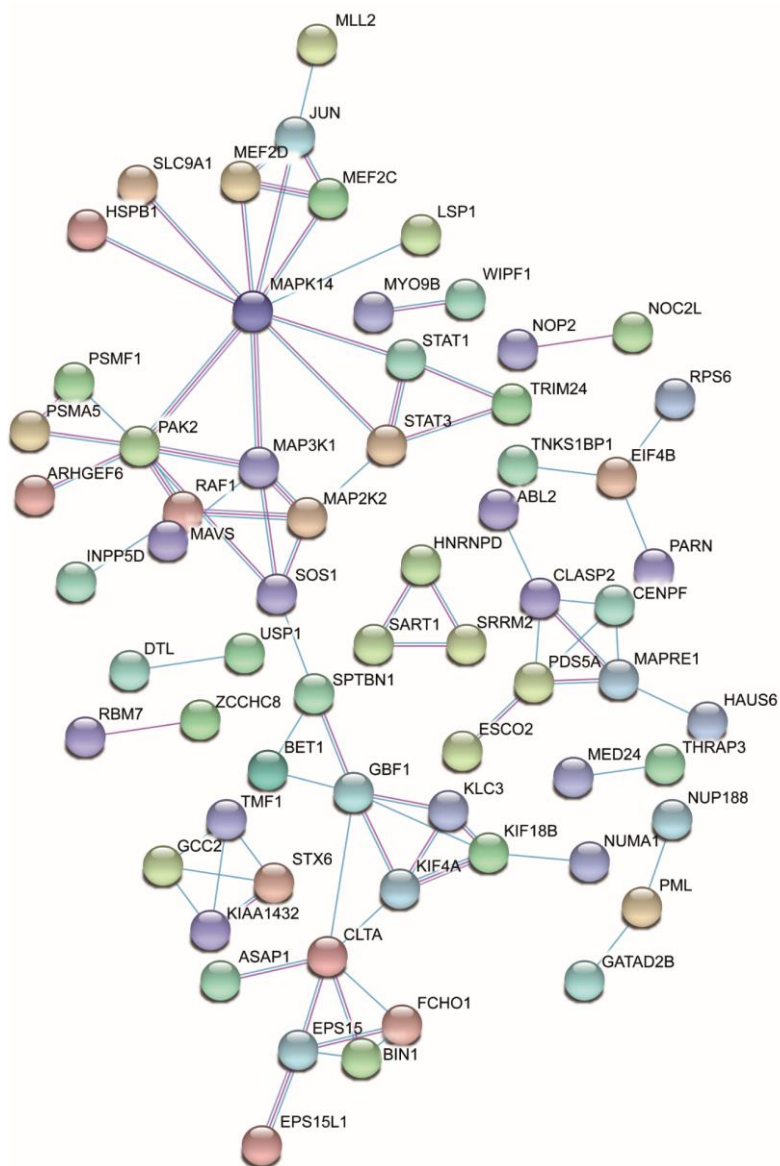


**Figure 20: Network of affected phosphoproteins after IL10+CpG stimulation**

Phosphoproteins that were up- or down-regulated by stimulation with IL10+CpG were used for an interaction analysis with STRING. The known interactions from curated databases (blue) and experimentally determined (red) are displayed.

The network revealed an interaction of proliferation associated proteins like RPS6, Poly(A)-specific ribonuclease (PARN) and EIF4B. Some MAPK-related proteins such as JUN, MAP3K1 and MAP2K2 clustered around p38 MAPK (MAPK14). This pointed out that, beside NF- $\kappa$ B and STAT3 activation, MAPKs were affected by TLR9 and IL10R activation to probably induce proliferation-associated proteins.

Previously, our group showed by RNA sequencing analyses that the impact of IL10+CpG stimulation alters the expression of cell cycle and metabolism-related genes (Feist, 2016). On the basis of phosphorylated proteins we further investigated the biological processes affected by the TLR9 and IL10R activation. Therefore, the 239 phosphosites altered after IL10+CpG stimulation were used for an enrichment of Gene Ontology (GO) terms with the functional annotation clustering tool of DAVID (Table A-2; Figure A-6). As the regulated phosphosites were part of many different biological processes, the list of GO terms was visualized in a tree map by REVIGO (Figure 21). Interestingly, the main altered biological process was also cell cycle. Furthermore, positive regulation of molecular function, cellular localization and protein phosphorylation were influenced by IL10+CpG stimulation. More precisely, DNA or mRNA metabolism, signal transduction, ameboidal-type cell migration as well as cell-cell adhesion belonged to altered processes.

In conclusion, we assumed that MAPK activation and the induction of proliferation-associated proteins may contribute to the proliferative effect after IL10+CpG stimulation. In addition, the protein phosphorylation after 30 minutes of receptor activation pointed to influences on cell cycle, metabolism and movement of cells.

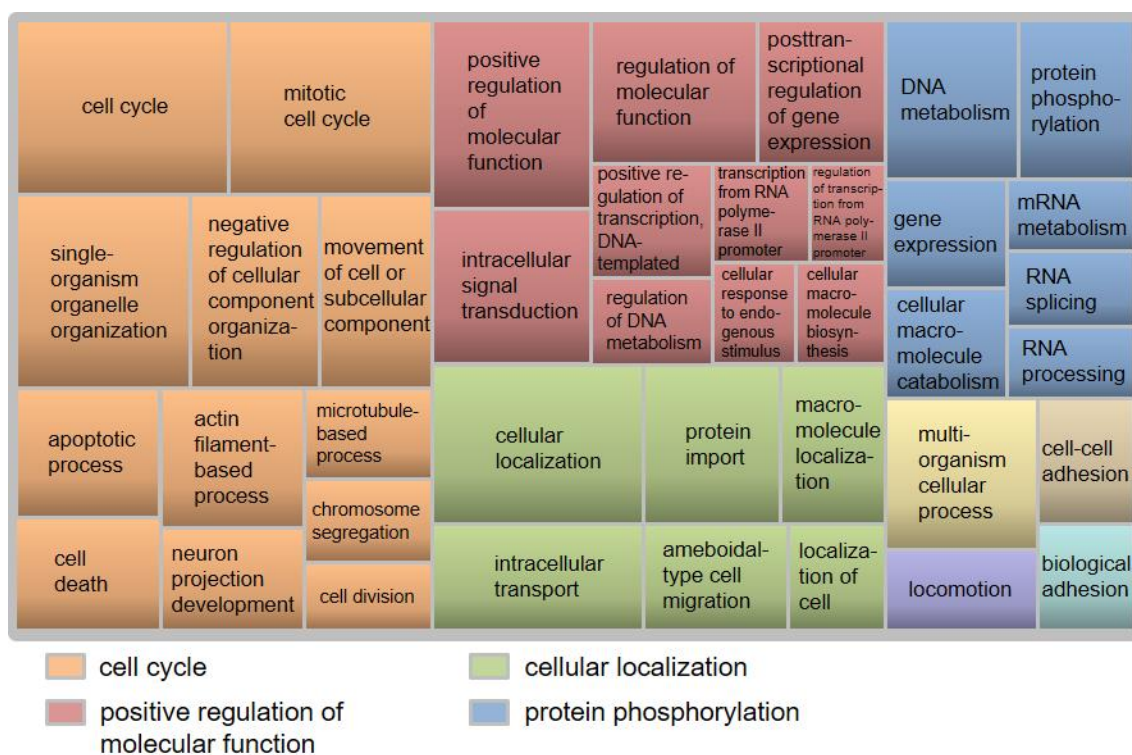


**Figure 21: GO annotation of biological process changed by IL10+CpG stimulation**

Biological processes that were up- or down-regulated by stimulation with IL10+CpG were identified using the 239 regulated phosphosites and the annotation tool DAVID. REVIGO was used for summarization and visualization of GO terms in a tree map. Clusters of related terms are marked with the same color and the size of boxes displays the p-values.

### 3.4.3 Phosphoproteome analysis indicates MAP kinase involvement

To reveal further mediators of the proliferative effect, an overview of the involved signaling components was required. Therefore, the phosphoproteins altered after TLR9 and IL10R activation were analyzed with the KEA2 tool to identify the possible upstream kinases and activated pathways (Figure 22 A). Beside the STAT3 activating kinases JAK1 and JAK2, the MAPK activation seemed to be further involved through JNK (MAPK9), MKK6 (MAP2K6) and p21-activated kinase 2 (PAK2). Furthermore, the cell cycle regulator CDK2 was listed. The kinase enrichment led to the assumption that MAPK as well as a direct phosphorylation of CDK2 were involved in the initiation of proliferation. As previous findings of our group uncovered that the combined activation of STAT3 and NF- $\kappa$ B induced the gene expression of CDK4 and thereby enhanced the proliferation of cells, the gene expression changes of these predicted kinases were considered (Figure 22 B). Similar to CDK4 and CDK6, the expression of CDK2 was enhanced and to a lower extent the expression of JAK1, JAK2, MAPK9 and PAK2 after IL10+CpG stimulation in Myc<sup>low</sup> cells.

We concluded that the stimulation with IL10+CpG induces probably not only CDK4 and CDK6 expression as published before (Feist, 2016), furthermore, some proliferation associated proteins seem to be enhanced in their expression as well as in their direct phosphorylation. The impact of these possible mediators remains to be investigated.

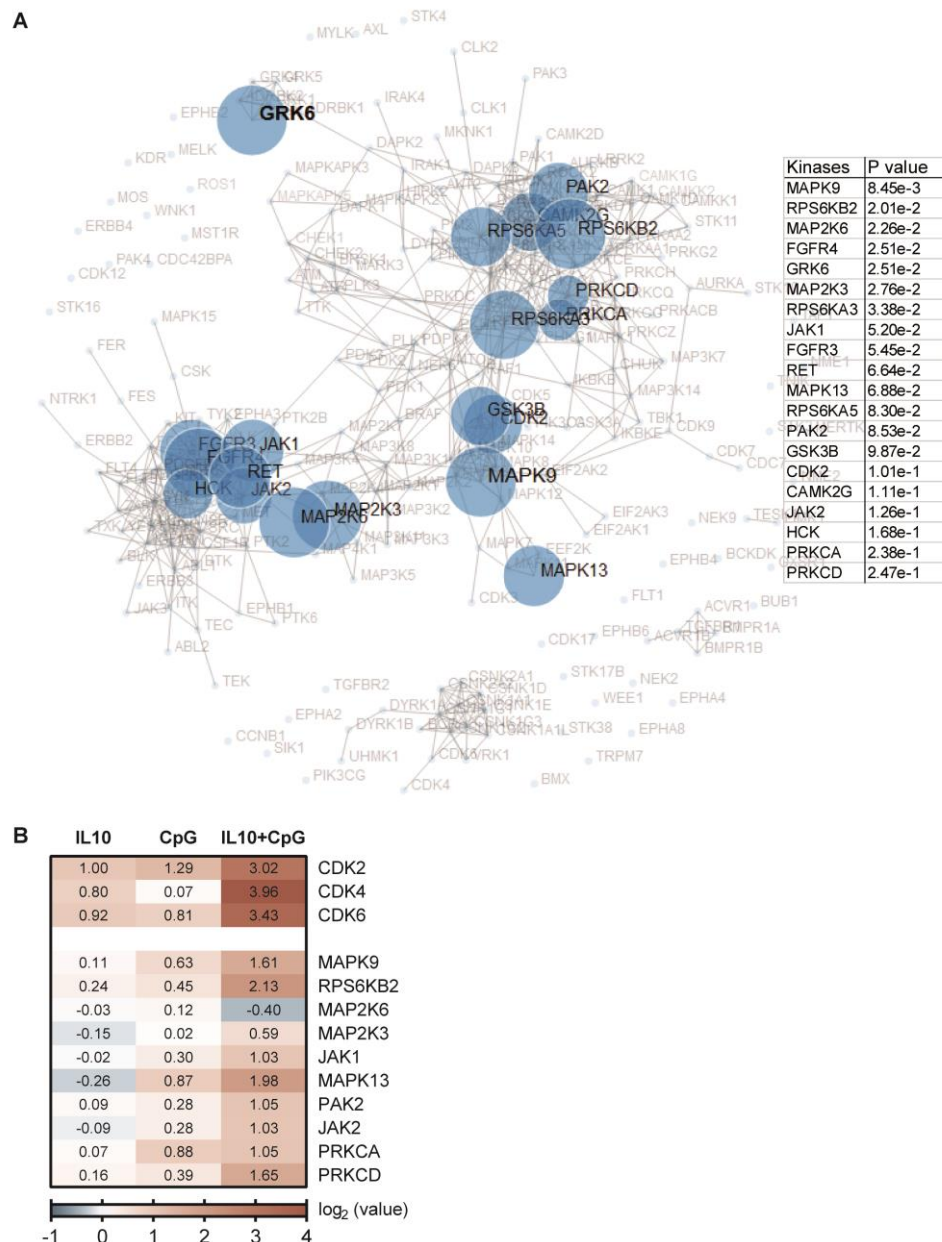


**Figure 22: IL10+CpG stimulation caused phosphorylation and expression of CDKs and MAPKs**

(A) Network of predicted upstream kinases for the changed 239 phosphosites using the kinase enrichment analysis (KEA) tool. Node size indicated the number of changed phosphosites which were predicted to be phosphorylated by that kinase. (B) RNA expression after 24 hours of proteins relevant in A. Displayed are the log<sub>2</sub> fold changes after different stimulations normalized to Ctrl Myc<sup>low</sup> cells (n=3).

### 3.4.4 IL10R and TLR9 activation reduce migration capacity of P493-6 cells

Beside the known influence on cell cycle and metabolism, the phosphoproteomics analysis pointed to an altered movement of cells. To investigate which phosphoproteins were involved in this process, those out of the 239 changed phosphosites are displayed that were annotated to the GO term “movement of cell or subcellular component” (Figure 23 A). The receptor activations mainly led to an increased phosphorylation of movement associated proteins. Several proteins well-known to play a role in migration were listed like p21-activated kinase 1 (PAK1), STAT3 and SOS1. Therefore, the cell movement was analyzed with the Boyden chamber assay (Figure 23 B). The migration potential of stimulated Myc<sup>low</sup> cells through 8 µm membranes for 6 hours was shown in relation to the migration potential of the unstimulated Ctrl Myc<sup>low</sup> cells. While IL10 stimulation alone had no effect on the migration, the TLR9 activation by CpG reduced the movement potential of Myc<sup>low</sup> cells about 30 %. Nevertheless, combined receptor activation led to a reduction of 50 % in comparison to Myc<sup>low</sup> cells.

In conclusion, many proteins associated with migration were changed by IL10+CpG stimulation. The phosphorylation of these proteins was mainly upregulated. Interestingly, the overall effect of this upregulation after stimulation was a reduced migration of the cells. The effect of the identified phosphorylations and how these proteins interact to regulate migration will need further investigations.

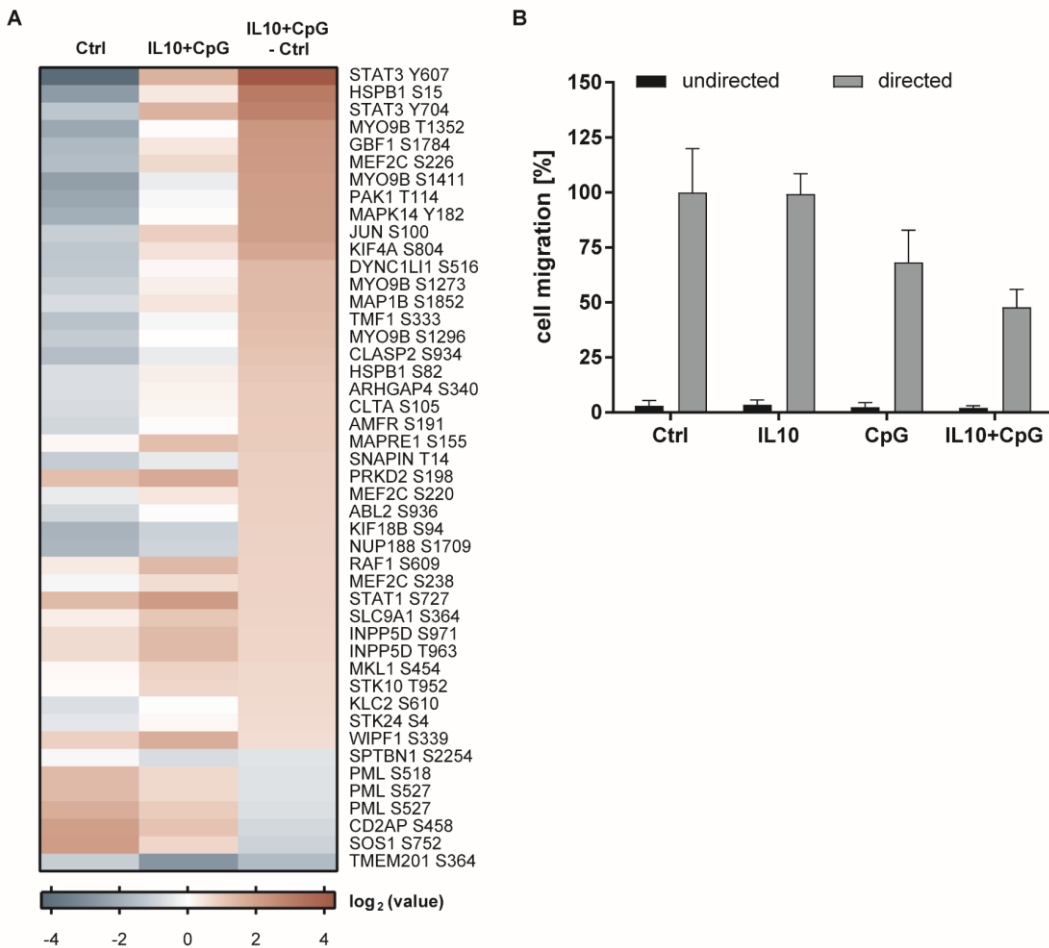


**Figure 23: IL10+CpG impact on movement associated proteins and the migration potential**

Investigation of the influence on movement associated proteins by TLR9 and IL10R activation. **(A)** Phosphoprotein changes of Ctrl and IL10+CpG stimulated Myc<sup>low</sup> cells were displayed as well as the difference between the values of Ctrl and IL10+CpG stimulated Myc<sup>low</sup> cells. **(B)** Boyden chamber analysis with 8 µm pore size membrane. Myc<sup>low</sup> cells were allowed to migrate for 6 hours towards 10 % FCS (directed) or 0 % FCS (undirected) after IL10, CpG or combined stimulation. Cell counts were normalized to the directed migration of the Ctrl Myc<sup>low</sup> cells (n=3).

## 4. Discussion

Many B cell non-Hodgkin lymphomas depend on the BCR signaling (Young and Staudt, 2013). Targeting BCR-related kinases emerges as a promising therapeutic strategy for several B cell malignancies (Smith, 2015). Nevertheless, the occurrence of unexpected side effects and toxicities is limiting the therapeutic success as feedback mechanisms are often disregarded (Blachly and Baiocchi, 2014). In the literature, mostly the linear signaling cascade from the receptor to the nucleus is displayed, while the interplays and feedback loops of pathways are often neglected (Reth and Brummer, 2004). This is also the case for the BCR signaling as the proximal events after receptor activation are well investigated but an accurate network model is still missing (Corso *et al.*, 2016; Satpathy *et al.*, 2015). Therefore, the downstream interplay of pathways remains to be examined for a further refinement of the signaling network. First approaches were performed by our group with Boolean-Nested Effect Models on the basis of gene expression changes after pathway perturbations (Pirkl *et al.*, 2016). However, pathway interplays and feedbacks hampered the network elucidation and thus an additional examination of pathway activations was required. The aim of this thesis was to uncover pathway interplays and feedbacks during the tonic, activated and chronic active BCR signaling to generate a semi-quantitative network model. In addition, the BCR-induced NF- $\kappa$ B activation with subsequent JAK-STAT activation is so far not examined for further pathway interactions. Thus, the interplay of TLR9 and IL10R signaling was investigated to identify additional mediators contributing to the NF- $\kappa$ B and JAK-STAT-dependent proliferative effect in the model cell line P493-6.

### 4.1 Positive feedback loop enhances tonic BCR signaling

The tonic BCR signaling is essential for the survival of BLs (Schmitz *et al.*, 2012). Aberrant regulation of c-MYC with additional activation of the PI3K pathway is sufficient to cause BL-like lymphomagenesis (Sander *et al.*, 2012; Schmitz *et al.*, 2012). An enhanced PI3K pathway activation is caused by several different mutations. Aberrations increasing E2A activity enhance the tonic BCR signaling by regulation of the BCR-related phosphatase SHP-1 (Basso and Dalla-Favera, 2015; Schmitz *et al.*, 2012). Besides, an inactivation or missing expression of PTEN, a negative regulator of PI3K, is common to increase the PI3K-AKT pathway (Lenz *et al.*, 2008c; Schmitz *et al.*, 2012). The main finding of our pathway analyses suggested a positive feedback loop of the PI3K-AKT pathway to the BCR to enhance its own pathway activation (Figure 4, Figure 24). However, the described negative feedback loop of the PI3K-AKT pathway could not be

concluded from our results (Logue and Morrison, 2012). We assume that the negative feedback loop is missing or overlaid by the positive feedback loop in BLs.

Besides, no further interplays of pathways or feedback loops were found during the tonic BCR in BLs (Figure 4). One limitation could be that, except for the PI3K pathway, the pathway activations and protein phosphorylations were too weak to uncover pathway interplays. However, this is in accordance with the suggestion that the PI3K pathway is the pivotal cascade of the tonic BCR signaling (Sander *et al.*, 2012; Schmitz *et al.*, 2012). Therefore, it is not surprising that inhibition of the PI3K-AKT pathway reduced the cell viability of BLs whereas a MEK inhibition had no effect (Figure 5). Our findings confirmed previous analyses demonstrating the dependency of BLs on PI3K, AKT and mTOR (Schmitz *et al.*, 2012; Spender and Inman, 2012). Only in BL-2 cells, we could not observe an effect of PI3K inhibition on cell viability. However, Schmitz *et al.* demonstrated that the double PI3K inhibitor concentration also reduced BL-2 cell viability after 96 hours (Schmitz *et al.*, 2012). Furthermore, we assume that especially the positive feedback loop of the PI3K pathway to the BCR contributes to the potent and survival-reducing effect of PI3K pathway inhibitors. As negative feedback loop hamper the inhibitory effect through upregulation of AKT as it was shown in breast cancer (Logue and Morrison, 2012), we suggested that PI3K, AKT and mTOR inhibitors are considered as additional treatment strategy for BLs due to the positive feedback loop (Spender and Inman, 2014).

In conclusion, mutations of BLs contribute not only to the PI3K pathway activation but also enhance this pathway activation through a positive feedback loop probably to the BCR. As other BCR-related pathways seem to be negligible, we also assume that the PI3K pathway is the central component of the tonic BCR signaling in BLs (Figure 24). However, the exact feedback mechanism to the BCR remains to be investigated and can be achieved by phosphorylation analyses of the upstream kinases using for example mass spectrometry. In addition, it has not been elucidated yet whether mTOR or downstream signaling components are responsible for the feedback.

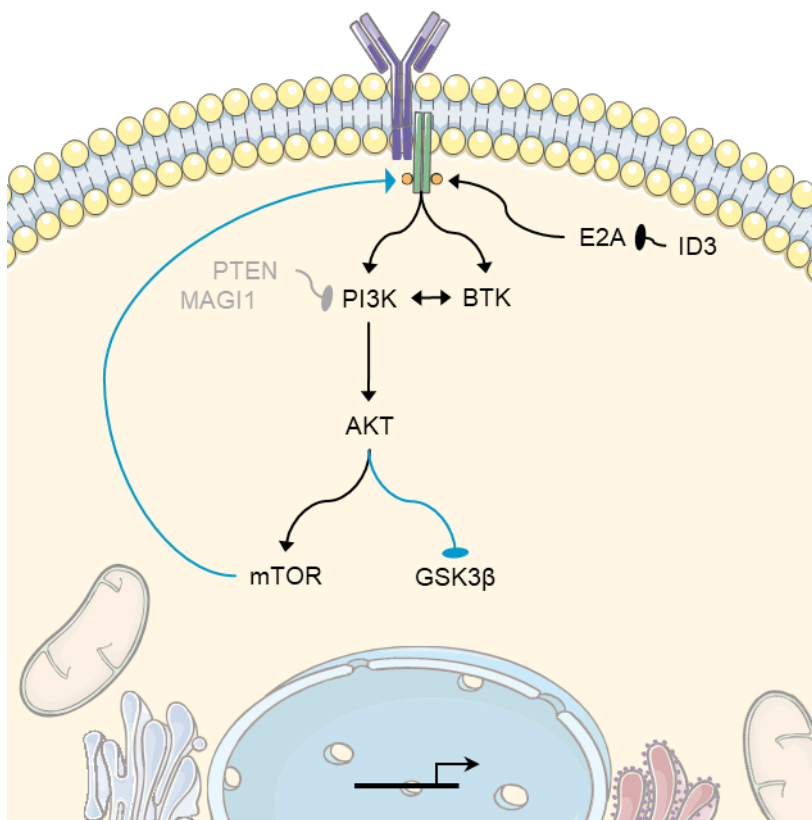


**Figure 24: Proposed network scheme of pathway interplays for the tonic BCR signaling**

Tonic BCR signaling in BLs includes an intrinsic induction of the PI3K pathway with a further signal transmission to AKT and mTOR. E2A activity, missing PTEN activity and a positive feedback loop downstream from mTOR to the BCR enhance the PI3K pathway. The black lines indicate the known linear signal transductions and the blue lines represent the analyzed pathway interplays and feedback loops. Proteins, which are not expressed in BL-2 cells, and the absence of pathway interactions are indicated in grey.

## 4.2 BCR signaling contains crosstalk from AKT and ERK1/2 to GSK3 $\beta$

As only the PI3K pathway was essential for the tonic BCR signaling, we additionally investigated the pathway activations after BCR stimulation in BLs. The outcome of BCR activation by antigens and induction of proximal kinases is known to increase the activity of the NF- $\kappa$ B, PI3K, MAPK and NFAT pathway (Kurosaki, 2011; Niilo and Clark, 2002). Our analyses confirmed the pathway activations of NF- $\kappa$ B, PI3K and MAPK after stimulation of the BCR with antigens (Figure 6). Interestingly, we further discovered that the positive feedback loop of the PI3K pathway was not limited to the tonic BCR signaling and was also present after receptor activation (Figure 6). As the upstream kinases were involved in the signal distribution to the different effector pathways, it was not surprising that the PI3K-AKT pathway inhibitors caused a decrease of all measured pathway activities. However, the exact mechanism and kinases which determined the signal

distribution to the effector pathways are not fully elucidated and are still under investigation.

The PI3K-AKT pathway is not exclusively regulating its own activity. An ERK-mediated phosphorylation of MEK1 was shown to recruit and activate PTEN with subsequent negative impact on the AKT pathway (Zmajkovicova *et al.*, 2013). Our results indicate that the activated BCR signaling contained no MEK-dependent inhibition of AKT (Figure 6). However, this could be due to mutations or absence of PTEN which is often described for BLs (Lenz *et al.*, 2008c; Schmitz *et al.*, 2012). Furthermore, a known interaction of AKT attenuates the MEK-ERK pathway activation by changing RAF phosphorylations (Zimmermann and Moelling, 1999). As all PI3K-AKT pathway inhibitors reduced the MEK1 and ERK1/2 phosphorylations, we could not identify a negative impact on the MEK-ERK pathway by AKT (Figure 6). Therefore, we assumed that the PI3K-AKT pathway was necessary for the MEK-ERK pathway activation during activated BCR signaling. One explanation for this pathway interplay is the regulation of an ERK-specific phosphatase by mTOR. mTOR induces the degradation of the ERK-specific phosphatase DUSP6 and therefore prolongs the ERK signaling (Bermudez *et al.*, 2008). Nevertheless, since DUSP6 is not expressed in BL-2 cells we suggest that the decreased ERK signal was rather mediated by the positive feedback loop of the PI3K-AKT pathway to the BCR (data not shown).

Although we could not discover any interaction between the AKT and the MEK-ERK pathway in the BL cell lines, the common influence on GSK3 $\beta$  was confirmed (Figure 6). Our pathway analyses validated a reduced GSK3 $\beta$  phosphorylation through inhibition of PI3K, AKT, mTOR and MEK1/2. The influence of the AKT and MEK-ERK pathway on GSK3 $\beta$  modulates the  $\beta$ -catenin pathway through a double-negative feedback inducing c-MYC and cyclin D3 expression (Baracho *et al.*, 2011; Cato *et al.*, 2011; Ding *et al.*, 2005; Mazzoletti *et al.*, 2011). Therefore, the PI3K-AKT and MEK-ERK pathways were reducing GSK3 $\beta$  probably to induce cell cycle progression of BLs. Despite the fact that AKT was suggested to mediate the GSK3 $\beta$  phosphorylation, we also detected a reduced GSK3 $\beta$  phosphorylation by mTOR inhibition (Figure 6). However, this effect could be mediated by the inhibition of the positive feedback loop of the PI3K pathway as mTOR inhibition caused also reduced AKT phosphorylation.

In summary, we assume that after BCR activation the positive feedback loop of the PI3K pathway also influences the pathway activation of NF- $\kappa$ B and MAPKs. Although the PI3K-AKT and MEK-ERK pathway regulate GSK3 $\beta$  phosphorylation possibly to enhance cell proliferation, a direct interplay of the AKT and ERK pathway does not exist in BLs (Figure 25 left part).

### 4.3 MEK-ERK pathway is diminished by several negative feedbacks

For cell fate decisions, the precise regulation of MAPK signal strength and duration is essential (Murphy and Blenis, 2006). Therefore, MAPKs are involved in many feedback mechanisms (Steelman *et al.*, 2011). Due to a strong negative impact on its upstream kinases, the feedbacks of the MEK-ERK pathway were uncovered early. The common feedbacks of ERK1/2 are responsible for distinct phosphorylations of RAF as well as MEK1/2. The ERK-dependent phosphorylations of RAF-1 cause a conformation change to an inactive state (Wartmann *et al.*, 1997), whereas the ERK-mediated MEK1/2 phosphorylation decreases the binding affinity to ERK1/2 (Lake *et al.*, 2016). In our pathway analyses only the activating MEK1 phosphorylation were investigated. Interestingly, a strong increase in this phosphorylation was measured after MEK1/2 inhibition during the activated BCR signaling (Figure 6). This is in accordance with the well-known effect that ERK1/2 decreases the binding affinity and thus the activating phosphorylations of MEK1/2 (Lake *et al.*, 2016). Therefore, the signal inhibition to ERK1/2 causes an increase of the active MEK1/2 phosphorylations (Fritzsche-Guenther *et al.*, 2011). As the increased MEK1 phosphorylation indicates the existence of the negative feedback loops, the ERK1/2 mediated RAF-1 phosphorylations were also investigated. The RAF-1 phosphorylation of the inactive state increased till 30 minutes after BCR activation in an ERK-dependent manner (Figure 9). While the ERK signaling is activated after few minutes, the increasing RAF-1 phosphorylation until 30 minutes further validates its ERK1/2 dependency due to the delayed induction. However, the signal duration of ERK1/2 indicates further negative regulators, as ERK1/2 activity peaks after few minutes of receptor activation followed by an intermediate activation before the signal is turned off (Figure 3) (Bluthgen, 2015). Another possibility how ERK1/2 decreases its own pathway activity could be mediated by regulation of gene expression. For instance, the gene expression of the negative regulator Sprouty2 is initiated by ERK1/2. Sprouty2 inhibits SOS and therefore the activation of RAF. However, Sprouty2 is downregulated in some lymphomas and was also not expressed in BL-2 cells (data not shown) (Frank *et al.*, 2009). This indicates that the MEK-ERK pathway activation is quickly decreased by negative feedbacks on RAF-1 and MEK but the signal duration might be still prolonged at an intermediate activation in BLs due to the missing expression of Sprouty2.

Furthermore, the regulation of phosphatases plays a pivotal role to determine the signal strength and duration of MAPKs and to constitute pathway interplays. Several phosphatases are known to intervene at any tier of signal transduction, however some regulate especially MAPKs (Junttila *et al.*, 2008). For instance, in lung cancer ERK induces DUSP1 after cisplatin treatment. DUSP1 in turn attenuates the pathway activity of

p38 MAPK and JNK (Low and Zhang, 2016). However, in B cells we could not detect an ERK-dependent phosphorylation of p38 MAPK and JNK after BCR activation (Figure 6), which is in agreement with a low expression of DUSP1 in BL-2 cells (Figure 16). We assume that the interaction from ERK1/2 over DUSP1 to p38 MAPK and JNK is missing in BLs.

In addition to the positive feedback loop of the PI3K pathway, we add a negative feedback loop from ERK1/2 to RAF and MEK1/2 to the network scheme after BCR activation (Figure 25 middle part). While the positive feedback loop enhanced the PI3K pathway, the negative feedback loops of ERK diminished the MEK-ERK pathway activity after an initially peak.

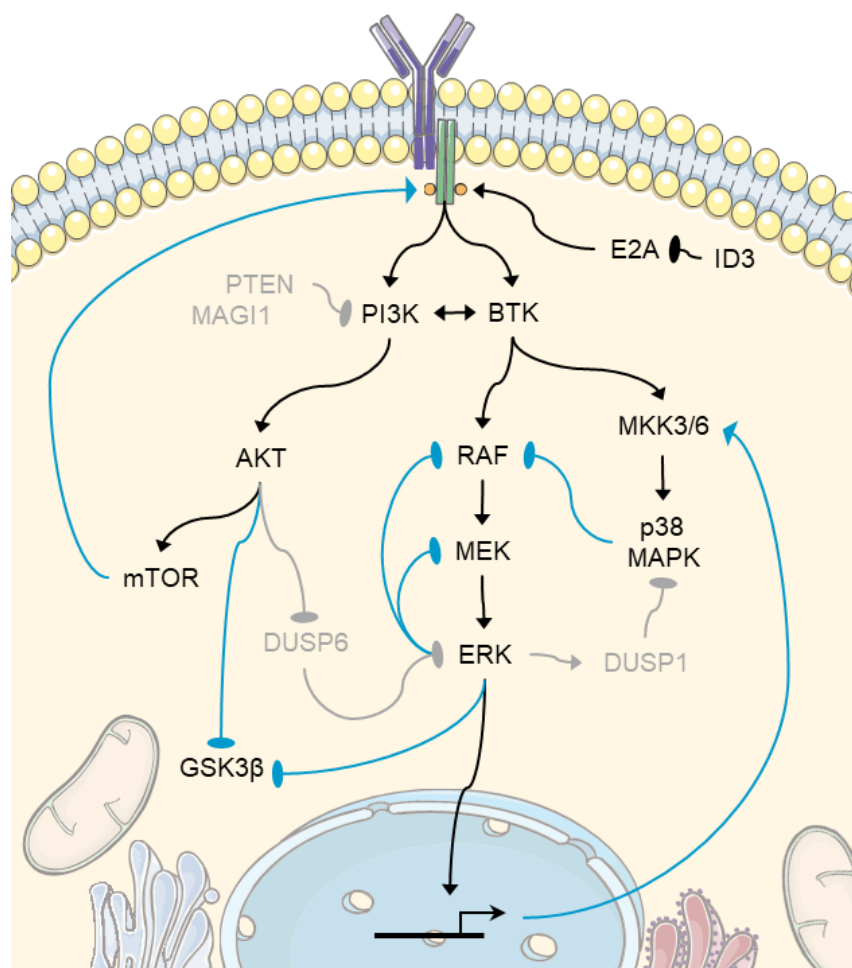


**Figure 25: Proposed network scheme of pathway interplays for the activated BCR signaling**

BCR signaling after antigen stimulation in BLs includes the activation of the PI3K, MEK-ERK and p38 MAPK pathway. E2A activity, missing PTEN activity and a positive feedback loop downstream from mTOR to the BCR enhance the PI3K pathway. The MEK-ERK pathway reduces its own activity by negative feedback loops to its upstream kinases. p38 MAPK negatively influences the MEK-ERK pathway, while an ERK-dependent expression of MKK6 is suggested to increase p38 MAPK activation. The black lines indicate the known linear signal transductions and the blue lines represent the analyzed pathway interplays and feedback loops. Proteins, which are not expressed in BL-2 cells, and the absence of pathway interactions are indicated in grey.

#### 4.4 p38 MAPK attenuates the MEK-ERK pathway

Beside the positive feedback loop of the PI3K pathway and the negative feedback loop of the MEK-ERK pathway, the negative influence of p38 MAPK on the MEK-ERK pathway was another major finding (Figure 6). The interaction of p38 MAPK to the MEK-ERK pathway is controversially discussed and is so far not described for BLs. Due to a linear increasing RAF activity with raising p38 MAPK inhibitor concentrations higher than the concentration necessary to block p38 MAPK, the influence of p38 MAPK on the MEK-ERK pathway was referred to an unspecific inhibitor effect (Kalmes *et al.*, 1999). However, an increasing ERK1/2 phosphorylation was also provoked by inhibition of p38 MAPK with a different inhibitor (Hirosawa *et al.*, 2009) or by expression of a dominant negative p38 MAPK variant (Aguirre-Ghiso *et al.*, 2001). Furthermore, our knock-down analysis of the p38 $\alpha$  subunit caused higher ERK1/2 phosphorylations after BCR activation and thereby indicated a specific effect (Figure 8). A modulation of the MEK-ERK pathway by p38 MAPK was previously described at any kinase of the signaling cascade. In chondrocytes an immunoprecipitation of p38 MAPK and RAF-1 revealed a direct modulation of RAF-1 activity by p38 MAPK (Hutchison, 2012). Furthermore, in HL-60 cells an increased phosphorylation of RAF-1 on serine 338 was detected after p38 MAPK inhibition (Zhang *et al.*, 2003). However, in our BL cell lines no phosphorylation changes of RAF-1 serine 338 were identified during the activated BCR signaling (Figure 9). In addition, p38 MAPK also showed no influence on the inactive state of RAF-1. As RAF-1 comprises more than 50 different phosphorylation sites, analysis of the activity could provide more insights whether p38 MAPK influences RAF-1. Furthermore, it cannot be excluded that p38 MAPK interacts with other RAF family members or upstream of RAF-1 and regulates for instance RAS activity.

Although many analyses suggested an induction of the upstream signaling compounds of MEK1/2 by p38 MAPK, a p38 MAPK-mediated activation of the phosphatase PP2A was shown to reduce the MEK1/2 phosphorylation (Wang *et al.*, 2006). However, Wang *et al.* only compared the effects of a p38 MAPK inhibitor with those of a PP2A inhibitor while it was shown by others that a combinatorial inhibition still caused higher levels of phosphorylated ERK1/2 (Birkenkamp *et al.*, 2000). Other possibilities of p38 MAPK to regulate ERK1/2 are the stabilization of phosphorylations or the induction of phosphatases. So far, no p38 MAPK-mediated effect on ERK1/2 is described. Therefore, BL-41 cells were treated with a combination of p38 MAPK and MEK1/2 inhibitors to investigate a direct influence of p38 MAPK on ERK1/2 after BCR activation (Figure 6). The addition of the p38 MAPK inhibitor to the MEK inhibitor caused little more ERK1/2 phosphorylation compared to the MEK inhibitor alone. However, the ERK1/2

phosphorylation after combinatorial treatment amounted only 20 % of the ERK1/2 phosphorylation after p38 MAPK inhibition. In conclusion, we suggest that the negative interaction of p38 MAPK to the MEK-ERK pathway is upstream of MEK1/2, however, the exact mechanism remains to be elucidated (Figure 25).

Beside the ERK-mediated negative feedbacks, we assume that p38 MAPK further contributes to the fine tuning of the MEK-ERK pathway. Until now, ERK signal durations and strengths were connected to some different signaling outputs (Bluthgen, 2015), but how feedbacks influence the cellular outcomes is so far not achieved. In BLs p38 MAPK inhibition prolonged the phosphorylation of ERK1/2 but it could not be excluded that this is only due to higher initial levels of phosphorylated ERK1/2 after BCR activation (Figure 10). Besides, p38 MAPK inhibition increased the ERK1/2 activity and nuclear amounts of phosphorylated ERK1/2 after BCR activation (Figure 10). Therefore, we investigated whether p38 MAPK limits ERK1/2 target gene expression. For p38 MAPK as well as ERK1/2 more than 100 targets are described (Roskoski, 2012; Tremppolec *et al.*, 2013b). As in a previous project gene expression changes after pathway perturbations were investigated, we validated ERK1/2 target genes which were inversely regulated by p38 MAPK inhibition. Many targets were identified as ERK1/2-dependent but only MAP2K6 expression was further attenuated by p38 MAPK after BCR activation for 1 hour (Figure 14). MAP2K6 encodes the kinase MKK6, an upstream activator of p38 MAPK (Sabio and Davis, 2014). Therefore, we hypothesized that the activation of ERK1/2 upregulates MKK6 and thereby modulates p38 MAPK activation. However, the activation of MKK6 and subsequently of p38 MAPK is so far not analyzed with regard to ERK1/2 activity.

In conclusion, the activated BCR signaling contains a further negative interplay from p38 MAPK to the MEK-ERK pathway (Figure 25 right part). Thereby, we assume that p38 MAPK probably interacts with RAF-1. The attenuation of the MEK-ERK pathway by p38 MAPK reduces not only the ERK1/2 activity but also modulates ERK1/2 target gene expressions. Through the ERK-dependent expression of MKK6 an additional interaction from ERK1/2 to p38 MAPK was hypothesized. These results suggest that the balance between the MEK-ERK and p38 MAPK pathway is strongly regulated, which contributes to the pathway durations and thus determines the signaling output.

#### 4.5 Feedback loops differ in ABC DLBCLs with chronic active BCR signaling

As in BLs more pathway interplays were analyzed after BCR activation, we further investigated the pathway interactions in lymphoma cell lines with a chronic active BCR signaling. While in ABC DLBCLs no deregulations of PTEN or E2A are found, the PI3K pathway is still increased due to receptor mutations of CD79a/b (Kloo *et al.*, 2011; Schmitz *et al.*, 2012). These mutations and the activation with self-antigens contribute to a constitutive activation of NF- $\kappa$ B, ERK and NFAT (Davis *et al.*, 2010; Young *et al.*, 2015). In addition, NF- $\kappa$ B can also be activated by aberrant inductions of CARD11 or MyD88 (Lenz *et al.*, 2008a; Ngo *et al.*, 2011). The cell lines used for this study were selected based on different mutation profiles. HBL-1 cells carry a CD79b and MyD88 mutation, whereas OCI-LY3 cells are characterized by CARD11 and MyD88 mutations (Paul *et al.*, 2017).

The pathway analyses after distinct perturbations in HBL-1 cells validated the discovered pathway interplays in BLs. The PI3K-AKT pathway was enhanced through a positive feedback loop, ERK1/2 negatively influenced MEK1 phosphorylation and p38 MAPK attenuated the MEK-ERK pathway (Figure 15). However, the inhibition of AKT in HBL-1 cells led to different outcomes in comparison to BL cell lines. One explanation might be that the regulation and feedbacks of the mTORC1 and mTORC2 are different compared to BLs but this hypothesis is so far not elucidated. As HBL-1 cells have no PTEN aberration, a negative influence of MEK1 along with PTEN on the PI3K pathway was expected (Zmajkovicova *et al.*, 2013). However, no increased PI3K-AKT pathway activation was identified following MEK1/2 inhibition (Figure 15). Interestingly, in T cells it was recently discovered that the negative influence of MEK1 on PI3K required aside from PTEN the protein MAGI1 (Kozakai *et al.*, 2018). As MAGI1 is not expressed in HBL-1 cells, this can be an explanation for the missing interplay from MEK1 to PI3K (data not shown).

Although OCI-LY3 cells are not PI3K-dependent like HBL-1 cells (Kloo *et al.*, 2011), the positive feedback loop of the PI3K-AKT pathway was also present, however, to a lesser extent (Figure 15). This indicates that this feedback mechanism is characteristic for lymphomas even though the proliferation of OCI-LY3 cells is mediated by other pathway activations. Furthermore, the negative feedback loop of the MEK-ERK pathway was consistent in all examined cell lines, while the influence of p38 MAPK on the MEK-ERK pathway was not present in OCI-LY3 cells (Figure 15). As the absence of phosphorylation of p38 MAPK and ERK1/2 could be excluded (Figure 16), we assumed that the lack of

interplay of p38 MAPK to the MEK-ERK pathway might be due to genetic differences and that p38 MAPK did not directly interact with RAF-1. We assume that p38 MAPK regulates rather a phosphatase or kinase and thereby influences the MEK-ERK pathway. The comparison of phosphorylation-related protein expressions led to the hypothesis that PTPN22, PTPN7, PALD1 or LCK, which were highly expressed in HBL-1 and BL-2 cells but not in OCI-LY3 cells, could mediate the interaction from p38 MAPK to the MEK-ERK pathway (Figure 16). LCK is involved in the aryl hydrocarbon receptor-mediated impairment of immunoglobulin secretion in human primary B cells (Zhou *et al.*, 2018). In BL cell lines high expression levels of LCK were reported but so far the benefit or reason is not known (Von Knethen *et al.*, 1997). However, in T cells an interaction of p38 MAPK to ZAP70 regulates the signaling duration of the MEK-ERK pathway (Giardino Torchia *et al.*, 2018). As ZAP70 and LCK are known to interact with each other, we hypothesize that LCK and ZAP70 probably regulate the signal duration of the MEK-ERK pathway in a p38 MAPK-dependent manner. Nevertheless, the interaction of p38 MAPK and LCK or ZAP70 as well as the ZAP70-triggered MEK-ERK pathway activation remains to be elucidated in B cell lymphomas.

In another DLBCL lymphoma cell line, DB cells, it was shown that p38 MAPK inhibition had also no impact on the ERK1/2 phosphorylation (Wojciechowski *et al.*, 2005). Because this lymphoma cell line is a GCB DLBCL, the CARD11 mutation of OCI-LY3 cannot be responsible for the missing interplay. One similarity between OCI-LY3 and DB cells is the expression of immunoglobulin IgG, whereas the other cell lines with p38 MAPK to ERK1/2 interplay express IgM. Mature B cells express IgM in a monomeric form on their cell surface prior to activation. Afterwards, B cells undergo clonal expansion and class switch recombination causing a downregulation of IgM and an upregulation of the IgG isotype (Engels *et al.*, 2009). The class switch occurs during the germinal center reaction and the IgM expression is essential for the proliferation of B cells, while IgG expression is connected to differentiation (Rickert, 2013). Therefore, we suggest that the B cell state of origin comprises different signaling interplays and feedbacks which are reflected in B cell lymphomas.

To examine whether the different interplays of HBL-1 and OCI-LY3 cells had different cellular outcomes, the MEK1/2 and p38 MAPK inhibition was analyzed in relation to the cell viability. An impact of MEK-ERK or p38 MAPK pathway inhibition on proliferation has so far not been described. While in BLs the activation of the BCR led to a cell cycle arrest which complicates the analysis of the interplays and feedbacks with regard to proliferation (Marches *et al.*, 1998), an increased rate of apoptosis was identified after MEK1/2 inhibition in OCI-LY3 cells (Bhalla *et al.*, 2011). Although the same MEK1/2 inhibitor was

used, the inhibition of MEK1/2 did not affect cell viability of OCI-LY3 cells over 72 hours (Figure 17). Furthermore, no effect on cell viability of HBL-1 and OCI-LY3 were detected after p38 MAPK or MEK1/2 inhibition. However, p38 MAPK is known to cause an increased ERK1/2 activation and tumor volume in prostate cancer (Aguirre-Ghiso *et al.*, 2003). Although no impact on the proliferation of HBL-1 and OCI-LY3 cells was identified, further analysis regarding tumor volume, stress response or differentiation might reveal the role of p38 MAPK and ERK1/2 in B cell lymphomas.

In summary, the positive feedback loop of the PI3K pathway and the negative feedback loop of the MEK-ERK pathway seem to be conserved across the tested B cell lymphoma cell lines. The p38 MAPK influence on the MEK-ERK pathway is assumed to be Ig-dependent and might even include some unknown effector proteins.

#### 4.6 Interplay of TLR9 and IL10R activation induces CDK2 and JNK

In ABC DLBCLs the constitutive activation of NF- $\kappa$ B leads to the expression of IL6 or IL10 and to a subsequent autocrine activation of the JAK-STAT signaling (Davis *et al.*, 2001). In the model cell line P493-6 it was shown that especially the combined activation of NF- $\kappa$ B and STAT3 by TLR9 and IL10R stimulation induced proliferation in a synergistic manner through expression changes of cell cycle genes (Feist *et al.*, 2017). In addition, we showed that TLR9 and IL10R activation induced over 200 phosphorylation changes in the proteome (Figure 19). Several differences in phosphorylation were detected in the MAPK pathways (Figure 22). Therefore, we assume that the activation of MAPKs and especially JNK contributes in addition to NF- $\kappa$ B and STAT3 activation to the proliferative effect in the model cell line. The dependency of ABC DLBCL proliferation on JNK is already known (Gururajan *et al.*, 2005), which further supports our hypothesis that JNK contributes to the NF- $\kappa$ B and STAT3-dependent proliferation of the cells. Nevertheless, the role of JNK regarding proliferation of the model cell line P493-6 after TLR9 and IL10R activation remains to be examined. Furthermore, cell cycle regulators like CDK4 were shown to be expressed after TLR9 and IL10R activation and to be essential for the proliferative effect in the model cell line P493-6 (Feist *et al.*, 2017). Interestingly, we demonstrated that the cell cycle regulator CDK2 displayed not only higher expression levels after TLR9 and IL10R activation, but was also directly phosphorylated after receptor stimulation (Figure 22). Therefore, we suggest that the cell cycle is directly induced by TLR9 and IL10R activation and the upregulation of the cell cycle genes is only one further aspect that enhances the proliferation rate. Although a reduced proliferation in DLBCLs was already shown after CDK2 inhibition (Faber and Chiles, 2007), the explicit

dependence of proliferation on CDK2 remains to be investigated in our model cell line P493-6.

Beside the influence on proliferation, the changed protein phosphorylations after TLR9 and IL10R activation indicated an altered cell adhesion and movement (Figure 21). For GCB DLBCLs, it was shown that modulation of cell movement resulted from Ga13 mutations (Muppidi *et al.*, 2014). However, less is known for the migration capacity of ABC DLBCLs. One recent publication investigated the migration speed in ABC DLBCLs which was enhanced by STAT3 activation (Pan *et al.*, 2018). Our findings of IL10R activation with subsequent STAT3 activation showed no higher migration rates of the model cell line P493-6 (Figure 23). Nevertheless, we cannot exclude an influence on the migration speed. Therefore, the cell movement requires further examinations using time-lapse microscopy. In addition, the impact of NF- $\kappa$ B pathway activation on cell migration of B cell lymphomas was so far not reported. The migration rate of the model cell line P493-6 was reduced after TLR9 activation (Figure 23). Furthermore, the combined activation of TLR9 and IL10R activation showed a stronger reduction of the migration rate compared to TLR9 activation alone. This is in accordance with phosphorylation of PAK2 which was identified in our phosphoproteome analysis and is described to inactivate the protein and thereby reduce the migration capacity. Nevertheless, the TLR9 and IL10R activation led mainly to a higher phosphorylation of migration-associate proteins and it remains to be elucidated whether these phosphorylations have a negative impact on the migration of cells. Controversially, inhibition of NF- $\kappa$ B was reported to reduce the migration of for instance lung cancer stem cells (Zakaria *et al.*, 2018). This emphasizes the need of further investigations to fully explain the migration capacity of the model cell line after TLR9 and IL10R activation as well as of ABC DLBCLs in relation to NF- $\kappa$ B activation.

## 5. Summary and Conclusion

In conclusion, this study provides a general network model of pathway interplays for B cell lymphomas. Three major interplays and feedback loops were uncovered downstream of the BCR. A positive feedback loop from mTOR or downstream targets to proximal kinases of the BCR enhances the PI3K pathway. Further investigations like phosphoproteome analyses are required to disclose the involved and affected kinases. A negative feedback loop of the MEK-ERK pathway to MEK1/2 and RAF-1 was consistently detected in all tested B cell lymphoma cell lines. While a negative influence from p38 MAPK on the MEK-ERK pathway was uncovered in B cell lymphomas expressing IgM, this interplay was missing in IgG expressing B cell lymphomas. To further illuminate the negative influence of p38 MAPK on the MEK-ERK pathway, analyses of the p38 MAPK interactome are necessary to uncover the affected pathway components. In addition, the validation of our findings in other lymphoma types like GCB DLBCLs, follicular lymphoma or mantle cell lymphoma can be a further aim to confirm the general network model. Nevertheless, these pathway interplays and feedback loops contribute to a better understanding and refinement of the BCR signaling network model. As pathway interplays and feedbacks alter signaling durations and strengths to achieve distinct responses to external influences, the improvement of computational network models is advantageous to predict the signaling outcome and furthermore the response of therapies. As the heterogeneity of lymphomas was shown to contain different pathway interplays, a further perspective is to include the genetic background for more accurate network models. Gene mutation and expression analyses will be useful tools to examine which pathway interplays and feedbacks occur and will hopefully provide deeper insights to improve the targeted therapies for lymphoma patients.

In the second approach, the pathway interplays after TLR9 and IL10R activation was investigated to uncover further mediators of the proliferative effect in the model cell line P493-6. Beside NF-κB and STAT3 activation, the stimulation of TLR9 and IL10R changed over 200 protein phosphorylations. A first network model of activated proteins was proposed and an impact on cell proliferation, metabolism and migration validated. Interestingly, the TLR9 and IL10R activation influence directly JNK and the cell cycle protein CDK2 to probably induce proliferation whereas the induction of proliferation-associated genes seems to be only a further aspect to increase the proliferation rate. However, a knock-out screening is required to confirm the phosphoproteom results and further possible mediators of the proliferative effect.

## 6. References

- Aguirre-Ghiso, J.A., Estrada, Y., Liu, D., and Ossowski, L. (2003). ERK(MAPK) activity as a determinant of tumor growth and dormancy; regulation by p38(SAPK). *Cancer research* 63, 1684-1695.
- Aguirre-Ghiso, J.A., Liu, D., Mignatti, A., Kovalski, K., and Ossowski, L. (2001). Urokinase receptor and fibronectin regulate the ERK(MAPK) to p38(MAPK) activity ratios that determine carcinoma cell proliferation or dormancy in vivo. *Molecular biology of the cell* 12, 863-879.
- Aldoss, I.T., Weisenburger, D.D., Fu, K., Chan, W.C., Vose, J.M., Bierman, P.J., Bociek, R.G., and Armitage, J.O. (2008). Adult Burkitt lymphoma: advances in diagnosis and treatment. *Oncology (Williston Park)* 22, 1508-1517.
- Alessi, D.R., Saito, Y., Campbell, D.G., Cohen, P., Sithanandam, G., Rapp, U., Ashworth, A., Marshall, C.J., and Cowley, S. (1994). Identification of the sites in MAP kinase kinase-1 phosphorylated by p74raf-1. *The EMBO journal* 13, 1610-1619.
- Alizadeh, A.A., Eisen, M.B., Davis, R.E., Ma, C., Lossos, I.S., Rosenwald, A., Boldrick, J.C., Sabet, H., Tran, T., Yu, X., Powell, J.I., Yang, L., Marti, G.E., Moore, T., Hudson, J., Jr., Lu, L., Lewis, D.B., Tibshirani, R., Sherlock, G., Chan, W.C., Greiner, T.C., Weisenburger, D.D., Armitage, J.O., Warnke, R., Levy, R., Wilson, W., Grever, M.R., Byrd, J.C., Botstein, D., Brown, P.O., and Staudt, L.M. (2000). Distinct types of diffuse large B-cell lymphoma identified by gene expression profiling. *Nature* 403, 503-511.
- Arlt, A. (2018). Hodgkin lymphoma secreted factors determine macrophage polarization and function. In University Medical Centre Goettingen (<http://hdl.handle.net/11858/00-1735-0000-002E-E4A8-9>; Georg-August-University Goettingen).
- Ashwell, J.D. (2006). The many paths to p38 mitogen-activated protein kinase activation in the immune system. *Nature reviews Immunology* 6, 532-540.
- Avalos, A.M., and Ploegh, H.L. (2014). Early BCR Events and Antigen Capture, Processing, and Loading on MHC Class II on B Cells. *Frontiers in immunology* 5, 1-5.
- Bain, J., Plater, L., Elliott, M., Shpiro, N., Hastie, C.J., McLauchlan, H., Klevernic, I., Arthur, J.S., Alessi, D.R., and Cohen, P. (2007). The selectivity of protein kinase inhibitors: a further update. *The Biochemical journal* 408, 297-315.
- Baracho, G.V., Miletic, A.V., Omori, S.A., Cato, M.H., and Rickert, R.C. (2011). Emergence of the PI3-kinase pathway as a central modulator of normal and aberrant B cell differentiation. *Current opinion in immunology* 23, 178-183.
- Basso, K., and Dalla-Favera, R. (2015). Germinal centres and B cell lymphomagenesis. *Nature reviews Immunology* 15, 172-184.
- Beguelin, W., Popovic, R., Teater, M., Jiang, Y., Bunting, K.L., Rosen, M., Shen, H., Yang, S.N., Wang, L., Ezponda, T., Martinez-Garcia, E., Zhang, H., Zheng, Y., Verma, S.K., McCabe, M.T., Ott, H.M., Van Aller, G.S., Kruger, R.G., Liu, Y., McHugh, C.F., Scott, D.W., Chung, Y.R., Kelleher, N., Shaknovich, R., Creasy, C.L., Gascoyne, R.D., Wong, K.K., Cerchietti, L., Levine, R.L., Abdel-Wahab, O., Licht, J.D., Elemento, O., and Melnick, A.M. (2013). EZH2 is required for germinal center formation and somatic EZH2 mutations promote lymphoid transformation. *Cancer cell* 23, 677-692.

- Bermudez, O., Marchetti, S., Pages, G., and Gimond, C. (2008). Post-translational regulation of the ERK phosphatase DUSP6/MKP3 by the mTOR pathway. *Oncogene* 27, 3685-3691.
- Bertrand, S., Berger, R., Philip, T., Bernheim, A., Bryon, P.A., Bertoglio, J., Dore, J.F., Brunat-Mentigny, M., and Lenoir, G.M. (1981). Variant translocation in a non endemic case of Burkitt's lymphoma: t (8;22) in an Epstein-Barr virus negative tumour and in a derived cell line. *Eur J Cancer* 17, 577-584.
- Bhalla, S., Evans, A.M., Dai, B., Prachand, S., Gordon, L.I., and Gartenhaus, R.B. (2011). The novel anti-MEK small molecule AZD6244 induces BIM-dependent and AKT-independent apoptosis in diffuse large B-cell lymphoma. *Blood* 118, 1052-1061.
- Birkenkamp, K.U., Tuyt, L.M., Lummen, C., Wierenga, A.T., Kruijer, W., and Vellenga, E. (2000). The p38 MAP kinase inhibitor SB203580 enhances nuclear factor-kappa B transcriptional activity by a non-specific effect upon the ERK pathway. *British journal of pharmacology* 131, 99-107.
- Blachly, J.S., and Baiocchi, R.A. (2014). Targeting PI3-kinase (PI3K), AKT and mTOR axis in lymphoma. *British journal of haematology* 167, 19-32.
- Blum, K.A., Lozanski, G., and Byrd, J.C. (2004). Adult Burkitt leukemia and lymphoma. *Blood* 104, 3009-3020.
- Bluthgen, N. (2015). Signaling output: it's all about timing and feedbacks. *Molecular systems biology* 11, 1-2.
- Boyd, S.D., Natkunam, Y., Allen, J.R., and Warnke, R.A. (2013). Selective immunophenotyping for diagnosis of B-cell neoplasms: immunohistochemistry and flow cytometry strategies and results. *Appl Immunohistochem Mol Morphol* 21, 116-131.
- Brunet, A., Bonni, A., Zigmond, M.J., Lin, M.Z., Juo, P., Hu, L.S., Anderson, M.J., Arden, K.C., Blenis, J., and Greenberg, M.E. (1999). Akt promotes cell survival by phosphorylating and inhibiting a Forkhead transcription factor. *Cell* 96, 857-868.
- Brunet, A., Pages, G., and Pouyssegur, J. (1994). Growth factor-stimulated MAP kinase induces rapid retrophosphorylation and inhibition of MAP kinase kinase (MEK1). *FEBS Lett* 346, 299-303.
- Burkitt, D. (1958). A sarcoma involving the jaws in African children. *The British journal of surgery* 46, 218-223.
- Cato, M.H., Chintalapati, S.K., Yau, I.W., Omori, S.A., and Rickert, R.C. (2011). Cyclin D3 is selectively required for proliferative expansion of germinal center B cells. *Molecular and cellular biology* 31, 127-137.
- Challa-Malladi, M., Lieu, Y.K., Califano, O., Holmes, A.B., Bhagat, G., Murty, V.V., Dominguez-Sola, D., Pasqualucci, L., and Dalla-Favera, R. (2011). Combined genetic inactivation of beta2-Microglobulin and CD58 reveals frequent escape from immune recognition in diffuse large B cell lymphoma. *Cancer cell* 20, 728-740.
- Chen, H.C. (2005). Boyden chamber assay. *Methods Mol Biol* 294, 15-22.
- Chen, R.H., Sarnecki, C., and Blenis, J. (1992). Nuclear localization and regulation of erk- and rsk-encoded protein kinases. *Molecular and cellular biology* 12, 915-927.

- Compagno, M., Lim, W.K., Grunn, A., Nandula, S.V., Brahmachary, M., Shen, Q., Bertoni, F., Ponzoni, M., Scandurra, M., Califano, A., Bhagat, G., Chadburn, A., Dalla-Favera, R., and Pasqualucci, L. (2009). Mutations of multiple genes cause deregulation of NF-kappaB in diffuse large B-cell lymphoma. *Nature* 459, 717-721.
- Corbalan-Garcia, S., Yang, S.S., Degenhardt, K.R., and Bar-Sagi, D. (1996). Identification of the mitogen-activated protein kinase phosphorylation sites on human Sos1 that regulate interaction with Grb2. *Molecular and cellular biology* 16, 5674-5682.
- Corso, J., Pan, K.T., Walter, R., Doebele, C., Mohr, S., Bohnenberger, H., Strobel, P., Lenz, C., Slabicki, M., Hullein, J., Comoglio, F., Rieger, M.A., Zenz, T., Wienands, J., Engelke, M., Serve, H., Urlaub, H., and Oellerich, T. (2016). Elucidation of tonic and activated B-cell receptor signaling in Burkitt's lymphoma provides insights into regulation of cell survival. *Proceedings of the National Academy of Sciences of the United States of America* 113, 5688-5693.
- Cox, J., and Mann, M. (2008). MaxQuant enables high peptide identification rates, individualized p.p.b.-range mass accuracies and proteome-wide protein quantification. *Nature biotechnology* 26, 1367-1372.
- Cuenda, A., and Rousseau, S. (2007). p38 MAP-kinases pathway regulation, function and role in human diseases. *Biochimica et biophysica acta* 1773, 1358-1375.
- Davis, R.E., Brown, K.D., Siebenlist, U., and Staudt, L.M. (2001). Constitutive nuclear factor kappaB activity is required for survival of activated B cell-like diffuse large B cell lymphoma cells. *The Journal of experimental medicine* 194, 1861-1874.
- Davis, R.E., Ngo, V.N., Lenz, G., Tolar, P., Young, R.M., Romesser, P.B., Kohlhammer, H., Lamy, L., Zhao, H., Yang, Y., Xu, W., Shaffer, A.L., Wright, G., Xiao, W., Powell, J., Jiang, J.K., Thomas, C.J., Rosenwald, A., Ott, G., Muller-Hermelink, H.K., Gascoyne, R.D., Connors, J.M., Johnson, N.A., Rimsza, L.M., Campo, E., Jaffe, E.S., Wilson, W.H., Delabie, J., Smeland, E.B., Fisher, R.I., Brazil, R.M., Tubbs, R.R., Cook, J.R., Weisenburger, D.D., Chan, W.C., Pierce, S.K., and Staudt, L.M. (2010). Chronic active B-cell-receptor signalling in diffuse large B-cell lymphoma. *Nature* 463, 88-92.
- Deeb, S.J., Tyanova, S., Hummel, M., Schmidt-Suprian, M., Cox, J., and Mann, M. (2015). Machine Learning-based Classification of Diffuse Large B-cell Lymphoma Patients by Their Protein Expression Profiles. *Molecular & cellular proteomics : MCP* 14, 2947-2960.
- Deshmukh, A.S., Murgia, M., Nagaraj, N., Treebak, J.T., Cox, J., and Mann, M. (2015). Deep proteomics of mouse skeletal muscle enables quantitation of protein isoforms, metabolic pathways, and transcription factors. *Molecular & cellular proteomics : MCP* 14, 841-853.
- Dhillon, A.S., Hagan, S., Rath, O., and Kolch, W. (2007). MAP kinase signalling pathways in cancer. *Oncogene* 26, 3279-3290.
- Ding, B.B., Yu, J.J., Yu, R.Y., Mendez, L.M., Shaknovich, R., Zhang, Y., Cattoretti, G., and Ye, B.H. (2008). Constitutively activated STAT3 promotes cell proliferation and survival in the activated B-cell subtype of diffuse large B-cell lymphomas. *Blood* 111, 1515-1523.
- Ding, H., Gabali, A.M., Jenson, S.D., Lim, M.S., and Elenitoba-Johnson, K.S. (2009). P38 mitogen activated protein kinase expression and regulation by interleukin-4 in human B cell non-Hodgkin lymphomas. *J Hematop* 2, 195-204.

- Ding, Q., Xia, W., Liu, J.C., Yang, J.Y., Lee, D.F., Xia, J., Bartholomeusz, G., Li, Y., Pan, Y., Li, Z., Bargou, R.C., Qin, J., Lai, C.C., Tsai, F.J., Tsai, C.H., and Hung, M.C. (2005). Erk associates with and primes GSK-3beta for its inactivation resulting in upregulation of beta-catenin. *Mol Cell* 19, 159-170.
- Dorel, M., Klinger, B., Gross, T., Sieber, A., Prahallad, A., Bosdriesz, E., Wessels, L.F.A., and Bluthgen, N. (2018). Modelling signalling networks from perturbation data. *Bioinformatics* 34, 4079-4086.
- Dougherty, M.K., Muller, J., Ritt, D.A., Zhou, M., Zhou, X.Z., Copeland, T.D., Conrads, T.P., Veenstra, T.D., Lu, K.P., and Morrison, D.K. (2005). Regulation of Raf-1 by direct feedback phosphorylation. *Mol Cell* 17, 215-224.
- Engels, N., Konig, L.M., Heemann, C., Lutz, J., Tsubata, T., Griep, S., Schrader, V., and Wienands, J. (2009). Recruitment of the cytoplasmic adaptor Grb2 to surface IgG and IgE provides antigen receptor-intrinsic costimulation to class-switched B cells. *Nature immunology* 10, 1018-1025.
- Faber, A.C., and Chiles, T.C. (2007). Inhibition of cyclin-dependent kinase-2 induces apoptosis in human diffuse large B-cell lymphomas. *Cell Cycle* 6, 2982-2989.
- Fabre-Guillevin, E., Tabrizi, R., Coulon, V., Monnereau, A., Eghbali, H., Soubeyran, I., and Soubeyran, P. (2006). Aggressive non-Hodgkin's lymphoma: concomitant evaluation of interleukin-2, soluble interleukin-2 receptor, interleukin-4, interleukin-6, interleukin-10 and correlation with outcome. *Leukemia & lymphoma* 47, 603-611.
- Feist, M. (2016). Synergism of IL10R and TLR9 signaling affects gene expression, proliferation and metabolism in B cells: A comparative study of STAT3/NF-kB and c-Myc mediated effects. In University Medical Centre Goettingen (<http://hdl.handle.net/11858/00-1735-0000-002B-7C1F-1>; Georg-August-University Goettingen).
- Feist, M., Kemper, J., Taruttis, F., Rehberg, T., Engelmann, J.C., Gronwald, W., Hummel, M., Spang, R., and Kube, D. (2017). Synergy of interleukin 10 and toll-like receptor 9 signalling in B cell proliferation: Implications for lymphoma pathogenesis. *International journal of cancer* 140, 1147-1158.
- Feist, M., Schwarzfischer, P., Heinrich, P., Sun, X., Kemper, J., von Bonin, F., Perez-Rubio, P., Taruttis, F., Rehberg, T., Dettmer, K., Gronwald, W., Reinders, J., Engelmann, J.C., Dudek, J., Klapper, W., Trumper, L., Spang, R., Oefner, P.J., and Kube, D. (2018). Cooperative STAT/NF-kappaB signaling regulates lymphoma metabolic reprogramming and aberrant GOT2 expression. *Nat Commun* 9, 1514.
- Feng, Y., Wen, J., and Chang, C.C. (2009). p38 Mitogen-activated protein kinase and hematologic malignancies. *Archives of pathology & laboratory medicine* 133, 1850-1856.
- Frank, M.J., Dawson, D.W., Bensinger, S.J., Hong, J.S., Knosp, W.M., Xu, L., Balatoni, C.E., Allen, E.L., Shen, R.R., Bar-Sagi, D., Martin, G.R., and Teitel, M.A. (2009). Expression of sprouty2 inhibits B-cell proliferation and is epigenetically silenced in mouse and human B-cell lymphomas. *Blood* 113, 2478-2487.
- Fritzsche-Guenther, R., Witzel, F., Sieber, A., Herr, R., Schmidt, N., Braun, S., Brummer, T., Sers, C., and Bluthgen, N. (2011). Strong negative feedback from Erk to Raf confers robustness to MAPK signalling. *Molecular systems biology* 7, 1-13.

- Fukunaga, R., and Hunter, T. (1997). MNK1, a new MAP kinase-activated protein kinase, isolated by a novel expression screening method for identifying protein kinase substrates. *The EMBO journal* 16, 1921-1933.
- Giardino Torchia, M.L., Dutta, D., Mittelstadt, P.R., Guha, J., Gaida, M.M., Fish, K., Barr, V.A., Akpan, I.O., Samelson, L.E., Tagad, H.D., Debnath, S., Miller Jenkins, L.M., Appella, E., and Ashwell, J.D. (2018). Intensity and duration of TCR signaling is limited by p38 phosphorylation of ZAP-70(T293) and destabilization of the signalosome. *Proceedings of the National Academy of Sciences of the United States of America* 115, 2174-2179.
- Gupta, M., Han, J.J., Stenson, M., Maurer, M., Wellik, L., Hu, G., Ziesmer, S., Dogan, A., and Witzig, T.E. (2012). Elevated serum IL-10 levels in diffuse large B-cell lymphoma: a mechanism of aberrant JAK2 activation. *Blood* 119, 2844-2853.
- Gururajan, M., Chui, R., Karuppannan, A.K., Ke, J., Jennings, C.D., and Bondada, S. (2005). c-Jun N-terminal kinase (JNK) is required for survival and proliferation of B-lymphoma cells. *Blood* 106, 1382-1391.
- Haan, C., and Behrmann, I. (2007). A cost effective non-commercial ECL-solution for Western blot detections yielding strong signals and low background. *J Immunol Methods* 318, 11-19.
- Hanafusa, H., Torii, S., Yasunaga, T., and Nishida, E. (2002). Sprouty1 and Sprouty2 provide a control mechanism for the Ras/MAPK signalling pathway. *Nat Cell Biol* 4, 850-858.
- Hand, E. (2013). Dissecting and Modeling Oncogene Dependent Molecular Mechanisms in Lymphoma Genesis and Progression. In University Medical Centre Goettingen (<http://hdl.handle.net/11858/00-1735-0000-0001-BC55-E>: Georg-August-University Goettingen).
- Hendriks, R.W., Yuvaraj, S., and Kil, L.P. (2014). Targeting Bruton's tyrosine kinase in B cell malignancies. *Nature reviews Cancer* 14, 219-232.
- Hirosawa, M., Nakahara, M., Otosaka, R., Imoto, A., Okazaki, T., and Takahashi, S. (2009). The p38 pathway inhibitor SB202190 activates MEK/MAPK to stimulate the growth of leukemia cells. *Leuk Res* 33, 693-699.
- Huang da, W., Sherman, B.T., and Lempicki, R.A. (2009). Systematic and integrative analysis of large gene lists using DAVID bioinformatics resources. *Nat Protoc* 4, 44-57.
- Hutchison, M.R. (2012). BDNF alters ERK/p38 MAPK activity ratios to promote differentiation in growth plate chondrocytes. *Mol Endocrinol* 26, 1406-1416.
- Ihle, J.N. (1995). The Janus protein tyrosine kinases in hematopoietic cytokine signaling. *Semin Immunol* 7, 247-254.
- Jeffrey, K.L., Camps, M., Rommel, C., and Mackay, C.R. (2007). Targeting dual-specificity phosphatases: manipulating MAP kinase signalling and immune responses. *Nature reviews Drug discovery* 6, 391-403.
- Jiang, A., Craxton, A., Kurosaki, T., and Clark, E.A. (1998). Different Protein Tyrosine Kinases Are Required for B Cell Antigen Receptor-mediated Activation of Extracellular Signal-Regulated kinase, c-Jun NH<sub>2</sub>-terminal Kinase 1, and p38 Mitogen-activated Protein Kinase. *The Journal of experimental medicine* 188, 1297-1306.

- Jiang, X., Guo, H., Wu, J., He, Q., Li, Y., Wang, M., Pan, H., Li, W., Wang, J., Wang, Q., Shen, J., Ke, Y., and Zhou, R. (2014). Critical role of SHP2 (PTPN11) signaling in germinal center-derived lymphoma. *Haematologica* 99, 1834-1845.
- Jin, G., Hamaguchi, Y., Matsushita, T., Hasegawa, M., Le Huu, D., Ishiura, N., Naka, K., Hirao, A., Takehara, K., and Fujimoto, M. (2013). B-cell linker protein expression contributes to controlling allergic and autoimmune diseases by mediating IL-10 production in regulatory B cells. *The Journal of allergy and clinical immunology* 131, 1674-1682.
- Jost, P.J., and Ruland, J. (2007). Aberrant NF-kappaB signaling in lymphoma: mechanisms, consequences, and therapeutic implications. *Blood* 109, 2700-2707.
- Junttila, M.R., Li, S.P., and Westermarck, J. (2008). Phosphatase-mediated crosstalk between MAPK signaling pathways in the regulation of cell survival. *FASEB journal : official publication of the Federation of American Societies for Experimental Biology* 22, 954-965.
- Kalmes, A., Deou, J., Clowes, A.W., and Daum, G. (1999). Raf-1 is activated by the p38 mitogen-activated protein kinase inhibitor, SB203580. *FEBS Letters* 444, 71-74.
- Kelemen, K., Braziel, R.M., Gatter, K., Bakke, T.C., Olson, S., and Fan, G. (2010). Immunophenotypic variations of Burkitt lymphoma. *Am J Clin Pathol* 134, 127-138.
- Klapproth, K., and Wirth, T. (2010). Advances in the understanding of MYC-induced lymphomagenesis. *British journal of haematology* 149, 484-497.
- Klein, U., and Dalla-Favera, R. (2008). Germinal centres: role in B-cell physiology and malignancy. *Nature reviews Immunology* 8, 22-33.
- Klinger, B., Sieber, A., Fritzsche-Guenther, R., Witzel, F., Berry, L., Schumacher, D., Yan, Y., Durek, P., Merchant, M., Schafer, R., Sers, C., and Bluthgen, N. (2013). Network quantification of EGFR signaling unveils potential for targeted combination therapy. *Molecular systems biology* 9, 1-14.
- Kloo, B., Nagel, D., Pfeifer, M., Grau, M., Duwel, M., Vincendeau, M., Dorken, B., Lenz, P., Lenz, G., and Krappmann, D. (2011). Critical role of PI3K signaling for NF-kappaB-dependent survival in a subset of activated B-cell-like diffuse large B-cell lymphoma cells. *Proceedings of the National Academy of Sciences of the United States of America* 108, 272-277.
- Kozakai, T., Takahashi, M., Higuchi, M., Hara, T., Saito, K., Tanaka, Y., Masuko, M., Takizawa, J., Sone, H., and Fujii, M. (2018). MAGI-1 expression is decreased in several types of human T-cell leukemia cell lines, including adult T-cell leukemia. *Int J Hematol* 107, 337-344.
- Kuppers, R. (2005). Mechanisms of B-cell lymphoma pathogenesis. *Nature reviews Cancer* 5, 251-262.
- Kurosaki, T. (1999). Genetic analysis of B cell antigen receptor signaling. *Annu Rev Immunol* 17, 555-592.
- Kurosaki, T. (2011). Regulation of BCR signaling. *Molecular immunology* 48, 1287-1291.
- Lachmann, A., and Ma'ayan, A. (2009). KEA: kinase enrichment analysis. *Bioinformatics* 25, 684-686.

- Laemmli, U.K. (1970). Cleavage of structural proteins during the assembly of the head of bacteriophage T4. *Nature* 227, 680-685.
- Lake, D., Correa, S.A., and Muller, J. (2016). Negative feedback regulation of the ERK1/2 MAPK pathway. *Cellular and molecular life sciences : CMLS* 73, 4397-4413.
- Lam, K.P., Kuhn, R., and Rajewsky, K. (1997). In vivo ablation of surface immunoglobulin on mature B cells by inducible gene targeting results in rapid cell death. *Cell* 90, 1073-1083.
- Lam, L.T., Wright, G., Davis, R.E., Lenz, G., Farinha, P., Dang, L., Chan, J.W., Rosenwald, A., Gascoyne, R.D., and Staudt, L.M. (2008). Cooperative signaling through the signal transducer and activator of transcription 3 and nuclear factor- $\kappa$ B pathways in subtypes of diffuse large B-cell lymphoma. *Blood* 111, 3701-3713.
- Laplante, M., and Sabatini, D.M. (2012). mTOR signaling in growth control and disease. *Cell* 149, 274-293.
- Lech-Maranda, E., Bienvenu, J., Michallet, A.S., Houot, R., Robak, T., Coiffier, B., and Salles, G. (2006). Elevated IL-10 plasma levels correlate with poor prognosis in diffuse large B-cell lymphoma. *Eur Cytokine Netw* 17, 60-66.
- Lenoir, G.M., Vuillaume, M., and Bonnardel, C. (1985). The use of lymphomatous and lymphoblastoid cell lines in the study of Burkitt's lymphoma. IARC scientific publications, 309-318.
- Lenz, G., Davis, R.E., Ngo, V.N., Lam, L., George, T.C., Wright, G.W., Dave, S.S., Zhao, H., Xu, W., Rosenwald, A., Ott, G., Muller-Hermelink, H.K., Gascoyne, R.D., Connors, J.M., Rimsza, L.M., Campo, E., Jaffe, E.S., Delabie, J., Smeland, E.B., Fisher, R.I., Chan, W.C., and Staudt, L.M. (2008a). Oncogenic CARD11 mutations in human diffuse large B cell lymphoma. *Science* 319, 1676-1679.
- Lenz, G., Wright, G., Dave, S.S., Xiao, W., Powell, J., Zhao, H., Xu, W., Tan, B., Goldschmidt, N., Iqbal, J., Vose, J., Bast, M., Fu, K., Weisenburger, D.D., Greiner, T.C., Armitage, J.O., Kyle, A., May, L., Gascoyne, R.D., Connors, J.M., Troen, G., Holte, H., Kvaloy, S., Dierickx, D., Verhoef, G., Delabie, J., Smeland, E.B., Jares, P., Martinez, A., Lopez-Guillermo, A., Montserrat, E., Campo, E., Braziel, R.M., Miller, T.P., Rimsza, L.M., Cook, J.R., Pohlman, B., Sweetenham, J., Tubbs, R.R., Fisher, R.I., Hartmann, E., Rosenwald, A., Ott, G., Muller-Hermelink, H.K., Wrench, D., Lister, T.A., Jaffe, E.S., Wilson, W.H., Chan, W.C., and Staudt, L.M. (2008b). Stromal gene signatures in large-B-cell lymphomas. *The New England journal of medicine* 359, 2313-2323.
- Lenz, G., Wright, G.W., Emre, N.C., Kohlhammer, H., Dave, S.S., Davis, R.E., Carty, S., Lam, L.T., Shaffer, A.L., Xiao, W., Powell, J., Rosenwald, A., Ott, G., Muller-Hermelink, H.K., Gascoyne, R.D., Connors, J.M., Campo, E., Jaffe, E.S., Delabie, J., Smeland, E.B., Rimsza, L.M., Fisher, R.I., Weisenburger, D.D., Chan, W.C., and Staudt, L.M. (2008c). Molecular subtypes of diffuse large B-cell lymphoma arise by distinct genetic pathways. *Proceedings of the National Academy of Sciences of the United States of America* 105, 13520-13525.
- Leonard, W.J., and Lin, J.X. (2000). Cytokine receptor signaling pathways. *The Journal of allergy and clinical immunology* 105, 877-888.
- Levy, D.E., and Darnell, J.E., Jr. (2002). Stats: transcriptional control and biological impact. *Nature reviews Molecular cell biology* 3, 651-662.

- Limon, J.J., and Fruman, D.A. (2012). Akt and mTOR in B Cell Activation and Differentiation. *Frontiers in immunology* 3, 1-12.
- Logue, J.S., and Morrison, D.K. (2012). Complexity in the signaling network: insights from the use of targeted inhibitors in cancer therapy. *Genes Dev* 26, 641-650.
- Love, C., Sun, Z., Jima, D., Li, G., Zhang, J., Miles, R., Richards, K.L., Dunphy, C.H., Choi, W.W., Srivastava, G., Lugar, P.L., Rizzieri, D.A., Lagoo, A.S., Bernal-Mizrachi, L., Mann, K.P., Flowers, C.R., Naresh, K.N., Evens, A.M., Chadburn, A., Gordon, L.I., Czader, M.B., Gill, J.I., Hsi, E.D., Greenough, A., Moffitt, A.B., McKinney, M., Banerjee, A., Grubor, V., Levy, S., Dunson, D.B., and Dave, S.S. (2012). The genetic landscape of mutations in Burkitt lymphoma. *Nat Genet* 44, 1321-1325.
- Low, H.B., and Zhang, Y. (2016). Regulatory Roles of MAPK Phosphatases in Cancer. *Immune network* 16, 85-98.
- MacLennan, I.C. (1994). Germinal centers. *Annu Rev Immunol* 12, 117-139.
- Magrath, I.T., Pizzo, P.A., Whang-Peng, J., Douglass, E.C., Alabaster, O., Gerber, P., Freeman, C.B., and Novikovs, L. (1980). Characterization of lymphoma-derived cell lines: comparison of cell lines positive and negative for Epstein-Barr virus nuclear antigen. I. Physical, cytogenetic, and growth characteristics. *Journal of the National Cancer Institute* 64, 465-476.
- Mandelbaum, J., Bhagat, G., Tang, H., Mo, T., Brahmachary, M., Shen, Q., Chadburn, A., Rajewsky, K., Tarakhovsky, A., Pasqualucci, L., and Dalla-Favera, R. (2010). BLIMP1 is a tumor suppressor gene frequently disrupted in activated B cell-like diffuse large B cell lymphoma. *Cancer cell* 18, 568-579.
- Mann, M. (2006). Functional and quantitative proteomics using SILAC. *Nature reviews Molecular cell biology* 7, 952-958.
- Marches, R., Scheuermann, R.H., and Uhr, J.W. (1998). Cancer dormancy: role of cyclin-dependent kinase inhibitors in induction of cell cycle arrest mediated via membrane IgM. *Cancer research* 58, 691-697.
- Mazzocetti, M., Bortolin, F., Brunelli, L., Pastorelli, R., Di Giandomenico, S., Erba, E., Ubezio, P., and Broggini, M. (2011). Combination of PI3K/mTOR inhibitors: antitumor activity and molecular correlates. *Cancer research* 71, 4573-4584.
- Molyneux, E.M., Rochford, R., Griffin, B., Newton, R., Jackson, G., Menon, G., Harrison, C.J., Israels, T., and Bailey, S. (2012). Burkitt's lymphoma. *Lancet* 379, 1234-1244.
- Muppidi, J.R., Lu, E., and Cyster, J.G. (2015). The G protein-coupled receptor P2RY8 and follicular dendritic cells promote germinal center confinement of B cells, whereas S1PR3 can contribute to their dissemination. *The Journal of experimental medicine* 212, 2213-2222.
- Muppidi, J.R., Schmitz, R., Green, J.A., Xiao, W., Larsen, A.B., Braun, S.E., An, J., Xu, Y., Rosenwald, A., Ott, G., Gascoyne, R.D., Rimsza, L.M., Campo, E., Jaffe, E.S., Delabie, J., Smeland, E.B., Braziel, R.M., Tubbs, R.R., Cook, J.R., Weisenburger, D.D., Chan, W.C., Vaidehi, N., Staudt, L.M., and Cyster, J.G. (2014). Loss of signalling via Galphai3 in germinal centre B-cell-derived lymphoma. *Nature* 516, 254-258.
- Murphy, L.O., and Blenis, J. (2006). MAPK signal specificity: the right place at the right time. *Trends Biochem Sci* 31, 268-275.

- Natkunam, Y. (2007). The biology of the germinal center. Hematology American Society of Hematology Education Program, 210-215.
- Ngo, V.N., Young, R.M., Schmitz, R., Jhavar, S., Xiao, W., Lim, K.H., Kohlhammer, H., Xu, W., Yang, Y., Zhao, H., Shaffer, A.L., Romesser, P., Wright, G., Powell, J., Rosenwald, A., Muller-Hermelink, H.K., Ott, G., Gascoyne, R.D., Connors, J.M., Rimsza, L.M., Campo, E., Jaffe, E.S., Delabie, J., Smeland, E.B., Fisher, R.I., Braziel, R.M., Tubbs, R.R., Cook, J.R., Weisenburger, D.D., Chan, W.C., and Staudt, L.M. (2011). Oncogenically active MYD88 mutations in human lymphoma. *Nature* 470, 115-119.
- Niilo, H., and Clark, E.A. (2002). Regulation of B-cell fate by antigen-receptor signals. *Nature reviews Immunology* 2, 945-956.
- Nozawa, Y., Abe, M., Wakasa, H., Ohno, H., Fukuwara, S., Kinoshita, T., and Osato, T. (1988). Establishment and characterization of an Epstein-Barr virus negative B-cell lymphoma cell line and successful heterotransplantation. *The Tohoku journal of experimental medicine* 156, 319-330.
- Ogasawara, T., Yasuyama, M., and Kawauchi, K. (2003). Constitutive activation of extracellular signal-regulated kinase and p38 mitogen-activated protein kinase in B-cell lymphoproliferative disorders. *Int J Hematol* 77, 364-370.
- Oh-hora, M., Johmura, S., Hashimoto, A., Hikida, M., and Kurosaki, T. (2003). Requirement for Ras guanine nucleotide releasing protein 3 in coupling phospholipase C-gamma2 to Ras in B cell receptor signaling. *The Journal of experimental medicine* 198, 1841-1851.
- Okada, T., Maeda, A., Iwamatsu, A., Gotoh, K., and Kurosaki, T. (2000). BCAP: the tyrosine kinase substrate that connects B cell receptor to phosphoinositide 3-kinase activation. *Immunity* 13, 817-827.
- Olsen, J.V., Blagoev, B., Gnad, F., Macek, B., Kumar, C., Mortensen, P., and Mann, M. (2006). Global, in vivo, and site-specific phosphorylation dynamics in signaling networks. *Cell* 127, 635-648.
- Ott, G., Rosenwald, A., and Campo, E. (2013). Understanding MYC-driven aggressive B-cell lymphomas: pathogenesis and classification. *Blood* 122, 3884-3891.
- Ott, G., Ziepert, M., Klapper, W., Horn, H., Szczepanowski, M., Bernd, H.W., Thorns, C., Feller, A.C., Lenze, D., Hummel, M., Stein, H., Muller-Hermelink, H.K., Frank, M., Hansmann, M.L., Barth, T.F., Moller, P., Cogliatti, S., Pfreundschuh, M., Schmitz, N., Trumper, L., Loeffler, M., and Rosenwald, A. (2010). Immunoblastic morphology but not the immunohistochemical GCB/nonGCB classifier predicts outcome in diffuse large B-cell lymphoma in the RICOVER-60 trial of the DSHNHL. *Blood* 116, 4916-4925.
- Ozaki, K., Kadomoto, R., Asato, K., Tanimura, S., Itoh, N., and Kohno, M. (2001). ERK pathway positively regulates the expression of Sprouty genes. *Biochem Biophys Res Commun* 285, 1084-1088.
- Pan, Y.R., Chen, C.C., Chan, Y.T., Wang, H.J., Chien, F.T., Chen, Y.L., Liu, J.L., and Yang, M.H. (2018). STAT3-coordinated migration facilitates the dissemination of diffuse large B-cell lymphomas. *Nat Commun* 9, 1-16.

- Pao, L.I., Famiglietti, S.J., and Cambier, J.C. (1998). Asymmetrical phosphorylation and function of immunoreceptor tyrosine-based activation motif tyrosines in B cell antigen receptor signal transduction. *Journal of immunology* 160, 3305-3314.
- Pao, L.I., Lam, K.P., Henderson, J.M., Kutok, J.L., Alimzhanov, M., Nitschke, L., Thomas, M.L., Neel, B.G., and Rajewsky, K. (2007). B cell-specific deletion of protein-tyrosine phosphatase Shp1 promotes B-1a cell development and causes systemic autoimmunity. *Immunity* 27, 35-48.
- Pasqualucci, L., Compagno, M., Houldsworth, J., Monti, S., Grunn, A., Nandula, S.V., Aster, J.C., Murty, V.V., Shipp, M.A., and Dalla-Favera, R. (2006). Inactivation of the PRDM1/BLIMP1 gene in diffuse large B cell lymphoma. *The Journal of experimental medicine* 203, 311-317.
- Paul, J., Soujon, M., Wengner, A.M., Zitzmann-Kolbe, S., Sturz, A., Haike, K., Keng Magdalene, K.H., Tan, S.H., Lange, M., Tan, S.Y., Mumberg, D., Lim, S.T., Ziegelbauer, K., and Liu, N. (2017). Simultaneous Inhibition of PI3Kdelta and PI3Kalpha Induces ABC-DLBCL Regression by Blocking BCR-Dependent and -Independent Activation of NF-kappaB and AKT. *Cancer cell* 31, 64-78.
- Pfeifer, M., Grau, M., Lenze, D., Wenzel, S.S., Wolf, A., Wollert-Wulf, B., Dietze, K., Nogai, H., Storek, B., Madle, H., Dorken, B., Janz, M., Dirnhofer, S., Lenz, P., Hummel, M., Tzankov, A., and Lenz, G. (2013). PTEN loss defines a PI3K/AKT pathway-dependent germinal center subtype of diffuse large B-cell lymphoma. *Proceedings of the National Academy of Sciences of the United States of America* 110, 12420-12425.
- Pfeifer, M., and Lenz, G. (2013). PI3K/AKT addiction in subsets of diffuse large B-cell lymphoma. *Cell Cycle* 12, 3347-3348.
- Pirkl, M., Hand, E., Kube, D., and Spang, R. (2016). Analyzing synergistic and non-synergistic interactions in signalling pathways using Boolean Nested Effect Models. *Bioinformatics* 32, 893-900.
- Polack, A., Hortnagel, K., Pajic, A., Christoph, B., Baier, B., Falk, M., Mautner, J., Geltinger, C., Bornkamm, G.W., and Kempkes, B. (1996). c-myc activation renders proliferation of Epstein-Barr virus (EBV)-transformed cells independent of EBV nuclear antigen 2 and latent membrane protein 1. *Proceedings of the National Academy of Sciences of the United States of America* 93, 10411-10416.
- Pone, E.J., Zan, H., Zhang, J., Al-Qahtani, A., Xu, Z., and Casali, P. (2010). Toll-like receptors and B-cell receptors synergize to induce immunoglobulin class-switch DNA recombination: relevance to microbial antibody responses. *Critical reviews in immunology* 30, 1-29.
- Rawlings, J.S., Rosler, K.M., and Harrison, D.A. (2004). The JAK/STAT signaling pathway. *J Cell Sci* 117, 1281-1283.
- Reth, M., and Brummer, T. (2004). Feedback regulation of lymphocyte signalling. *Nature reviews Immunology* 4, 269-277.
- Richter, J., Schlesner, M., Hoffmann, S., Kreuz, M., Leich, E., Burkhardt, B., Rosolowski, M., Ammerpohl, O., Wagener, R., Bernhart, S.H., Lenze, D., Szczepanowski, M., Paulsen, M., Lipinski, S., Russell, R.B., Adam-Klages, S., Apic, G., Claviez, A., Hasenclever, D., Hovestadt, V., Hornig, N., Korbel, J.O., Kube, D., Langenberger, D., Lawerenz, C., Lisfeld, J., Meyer, K., Picelli, S., Pischedl, J., Radlwimmer, B., Rausch, T., Rohde, M., Schilhabel, M., Scholtysik, R., Spang, R., Trautmann, H., Zenz, T., Borkhardt, A., Drexler,

- H.G., Moller, P., MacLeod, R.A., Pott, C., Schreiber, S., Trumper, L., Loeffler, M., Stadler, P.F., Lichter, P., Eils, R., Kuppers, R., Hummel, M., Klapper, W., Rosenstiel, P., Rosenwald, A., Brors, B., and Siebert, R. (2012). Recurrent mutation of the ID3 gene in Burkitt lymphoma identified by integrated genome, exome and transcriptome sequencing. *Nat Genet* 44, 1316-1320.
- Rickert, R.C. (2013). New insights into pre-BCR and BCR signalling with relevance to B cell malignancies. *Nature reviews Immunology* 13, 578-591.
- Roskoski, R., Jr. (2012). ERK1/2 MAP kinases: structure, function, and regulation. *Pharmacological research* 66, 105-143.
- Ruland, J., and Mak, T.W. (2003). Transducing signals from antigen receptors to nuclear factor kappaB. *Immunological reviews* 193, 93-100.
- Sabio, G., and Davis, R.J. (2014). TNF and MAP kinase signalling pathways. *Semin Immunol* 26, 237-245.
- Sander, S., Calado, D.P., Srinivasan, L., Kochert, K., Zhang, B., Rosolowski, M., Rodig, S.J., Holzmann, K., Stilgenbauer, S., Siebert, R., Bullinger, L., and Rajewsky, K. (2012). Synergy between PI3K signaling and MYC in Burkitt lymphomagenesis. *Cancer cell* 22, 167-179.
- Satpathy, S., Wagner, S.A., Beli, P., Gupta, R., Kristiansen, T.A., Malinova, D., Francavilla, C., Tolar, P., Bishop, G.A., Hostager, B.S., and Choudhary, C. (2015). Systems-wide analysis of BCR signalosomes and downstream phosphorylation and ubiquitylation. *Molecular systems biology* 11, 1-22.
- Schmitz, R., Ceribelli, M., Pittaluga, S., Wright, G., and Staudt, L.M. (2014). Oncogenic mechanisms in Burkitt lymphoma. *Cold Spring Harbor perspectives in medicine* 4, 1-13.
- Schmitz, R., Young, R.M., Ceribelli, M., Jhavar, S., Xiao, W., Zhang, M., Wright, G., Shaffer, A.L., Hodson, D.J., Buras, E., Liu, X., Powell, J., Yang, Y., Xu, W., Zhao, H., Kohlhammer, H., Rosenwald, A., Kluin, P., Muller-Hermelink, H.K., Ott, G., Gascoyne, R.D., Connors, J.M., Rimsza, L.M., Campo, E., Jaffe, E.S., Delabie, J., Smeland, E.B., Ogwang, M.D., Reynolds, S.J., Fisher, R.I., Braziel, R.M., Tubbs, R.R., Cook, J.R., Weisenburger, D.D., Chan, W.C., Pittaluga, S., Wilson, W., Waldmann, T.A., Rowe, M., Mbulaiteye, S.M., Rickinson, A.B., and Staudt, L.M. (2012). Burkitt lymphoma pathogenesis and therapeutic targets from structural and functional genomics. *Nature* 490, 116-120.
- Schneeberger, C., Speiser, P., Kury, F., and Zeillinger, R. (1995). Quantitative detection of reverse transcriptase-PCR products by means of a novel and sensitive DNA stain. *PCR methods and applications* 4, 234-238.
- Schreiber, E., Matthias, P., Muller, M.M., and Schaffner, W. (1989). Rapid detection of octamer binding proteins with 'mini-extracts', prepared from a small number of cells. *Nucleic acids research* 17, 6419.
- Shaul, Y.D., and Seger, R. (2007). The MEK/ERK cascade: from signaling specificity to diverse functions. *Biochimica et biophysica acta* 1773, 1213-1226.
- Shinohara, H., Yasuda, T., Aiba, Y., Sanjo, H., Hamadate, M., Watarai, H., Sakurai, H., and Kurosaki, T. (2005). PKC beta regulates BCR-mediated IKK activation by facilitating the interaction between TAK1 and CARMA1. *The Journal of experimental medicine* 202, 1423-1431.

- Smith, S.M. (2015). New drugs for the treatment of non-Hodgkin lymphomas. *Chinese clinical oncology* 4, 1-11.
- Spender, L.C., and Inman, G.J. (2012). Phosphoinositide 3-kinase/AKT/mTORC1/2 signaling determines sensitivity of Burkitt's lymphoma cells to BH3 mimetics. *Molecular cancer research : MCR* 10, 347-359.
- Spender, L.C., and Inman, G.J. (2014). Developments in Burkitt's lymphoma: novel cooperations in oncogenic MYC signaling. *Cancer management and research* 6, 27-38.
- Srinivasan, L., Sasaki, Y., Calado, D.P., Zhang, B., Paik, J.H., DePinho, R.A., Kutok, J.L., Kearney, J.F., Otipoby, K.L., and Rajewsky, K. (2009). PI3 kinase signals BCR-dependent mature B cell survival. *Cell* 139, 573-586.
- Staudt, L.M. (2010). Oncogenic activation of NF-kappaB. *Cold Spring Harbor perspectives in biology* 2, 1-30.
- Steelman, L.S., Franklin, R.A., Abrams, S.L., Chappell, W., Kempf, C.R., Basecke, J., Stivala, F., Donia, M., Fagone, P., Nicoletti, F., Libra, M., Ruvolo, P., Ruvolo, V., Evangelisti, C., Martelli, A.M., and McCubrey, J.A. (2011). Roles of the Ras/Raf/MEK/ERK pathway in leukemia therapy. *Leukemia* 25, 1080-1094.
- Stein, H., and Hummel, M. (2006). Histopathology in the light of molecular profiling. *Annals of oncology : official journal of the European Society for Medical Oncology* 17 Suppl 4, iv5-iv7.
- Sun, H., Charles, C.H., Lau, L.F., and Tonks, N.K. (1993). MKP-1 (3CH134), an immediate early gene product, is a dual specificity phosphatase that dephosphorylates MAP kinase in vivo. *Cell* 75, 487-493.
- Supek, F., Bosnjak, M., Skunca, N., and Smuc, T. (2011). REVIGO summarizes and visualizes long lists of gene ontology terms. *PloS one* 6, 1-9.
- Szklarczyk, D., Franceschini, A., Wyder, S., Forslund, K., Heller, D., Huerta-Cepas, J., Simonovic, M., Roth, A., Santos, A., Tsafou, K.P., Kuhn, M., Bork, P., Jensen, L.J., and von Mering, C. (2015). STRING v10: protein-protein interaction networks, integrated over the tree of life. *Nucleic acids research* 43, D447-452.
- Takata, M., and Kurosaki, T. (1996). A role for Bruton's tyrosine kinase in B cell antigen receptor-mediated activation of phospholipase C-gamma 2. *The Journal of experimental medicine* 184, 31-40.
- Tartaglia, M., Martinelli, S., Cazzaniga, G., Cordeddu, V., Iavarone, I., Spinelli, M., Palmi, C., Carta, C., Pession, A., Arico, M., Masera, G., Basso, G., Sorcini, M., Gelb, B.D., and Biondi, A. (2004). Genetic evidence for lineage-related and differentiation stage-related contribution of somatic PTPN11 mutations to leukemogenesis in childhood acute leukemia. *Blood* 104, 307-313.
- Thome, M., Charton, J.E., Pelzer, C., and Hailfinger, S. (2010). Antigen receptor signaling to NF-kappaB via CARMA1, BCL10, and MALT1. *Cold Spring Harbor perspectives in biology* 2, 1-16.
- Towbin, H., Staehelin, T., and Gordon, J. (1979). Electrophoretic transfer of proteins from polyacrylamide gels to nitrocellulose sheets: procedure and some applications.

Proceedings of the National Academy of Sciences of the United States of America 76, 4350-4354.

Tremblay, F., Brule, S., Hee Um, S., Li, Y., Masuda, K., Roden, M., Sun, X.J., Krebs, M., Polakiewicz, R.D., Thomas, G., and Marette, A. (2007). Identification of IRS-1 Ser-1101 as a target of S6K1 in nutrient- and obesity-induced insulin resistance. Proceedings of the National Academy of Sciences of the United States of America 104, 14056-14061.

Tremolec, N., Dave-Coll, N., and Nebreda, A.R. (2013a). SnapShot: p38 MAPK signaling. Cell 152, 656-656 e651.

Tremolec, N., Dave-Coll, N., and Nebreda, A.R. (2013b). SnapShot: p38 MAPK substrates. Cell 152, 924-924 e921.

Tweeddale, M.E., Lim, B., Jamal, N., Robinson, J., Zalcberg, J., Lockwood, G., Minden, M.D., and Messner, H.A. (1987). The presence of clonogenic cells in high-grade malignant lymphoma: a prognostic factor. Blood 69, 1307-1314.

Vainchenker, W., and Constantinescu, S.N. (2013). JAK/STAT signaling in hematological malignancies. Oncogene 32, 2601-2613.

Vardiman, J.W., Thiele, J., Arber, D.A., Brunning, R.D., Borowitz, M.J., Porwit, A., Harris, N.L., Le Beau, M.M., Hellstrom-Lindberg, E., Tefferi, A., and Bloomfield, C.D. (2009). The 2008 revision of the World Health Organization (WHO) classification of myeloid neoplasms and acute leukemia: rationale and important changes. Blood 114, 937-951.

Vega, G.G., Aviles-Salas, A., Chalapud, J.R., Martinez-Paniagua, M., Pelayo, R., Mayani, H., Hernandez-Pando, R., Martinez-Maza, O., Huerta-Yepez, S., Bonavida, B., and Vega, M.I. (2015). P38 MAPK expression and activation predicts failure of response to CHOP in patients with Diffuse Large B-Cell Lymphoma. BMC Cancer 15, 722 721-712.

Victora, G.D., Dominguez-Sola, D., Holmes, A.B., Deroubaix, S., Dalla-Favera, R., and Nussenzweig, M.C. (2012). Identification of human germinal center light and dark zone cells and their relationship to human B-cell lymphomas. Blood 120, 2240-2248.

Victora, G.D., and Nussenzweig, M.C. (2012). Germinal centers. Annu Rev Immunol 30, 429-457.

Victora, G.D., Schwickert, T.A., Fooksman, D.R., Kamphorst, A.O., Meyer-Hermann, M., Dustin, M.L., and Nussenzweig, M.C. (2010). Germinal center dynamics revealed by multiphoton microscopy with a photoactivatable fluorescent reporter. Cell 143, 592-605.

Von Knethen, A., Abts, H., Kube, D., Diehl, V., and Tesch, H. (1997). Expression of p56lck in B-cell neoplasias. Leukemia & lymphoma 26, 551-562.

Wang, Z., Yang, H., Tachado, S.D., Capo-Aponte, J.E., Bildin, V.N., Koziel, H., and Reinach, P.S. (2006). Phosphatase-mediated crosstalk control of ERK and p38 MAPK signaling in corneal epithelial cells. Investigative ophthalmology & visual science 47, 5267-5275.

Wartmann, M., Hofer, P., Turowski, P., Saltiel, A.R., and Hynes, N.E. (1997). Negative modulation of membrane localization of the Raf-1 protein kinase by hyperphosphorylation. The Journal of biological chemistry 272, 3915-3923.

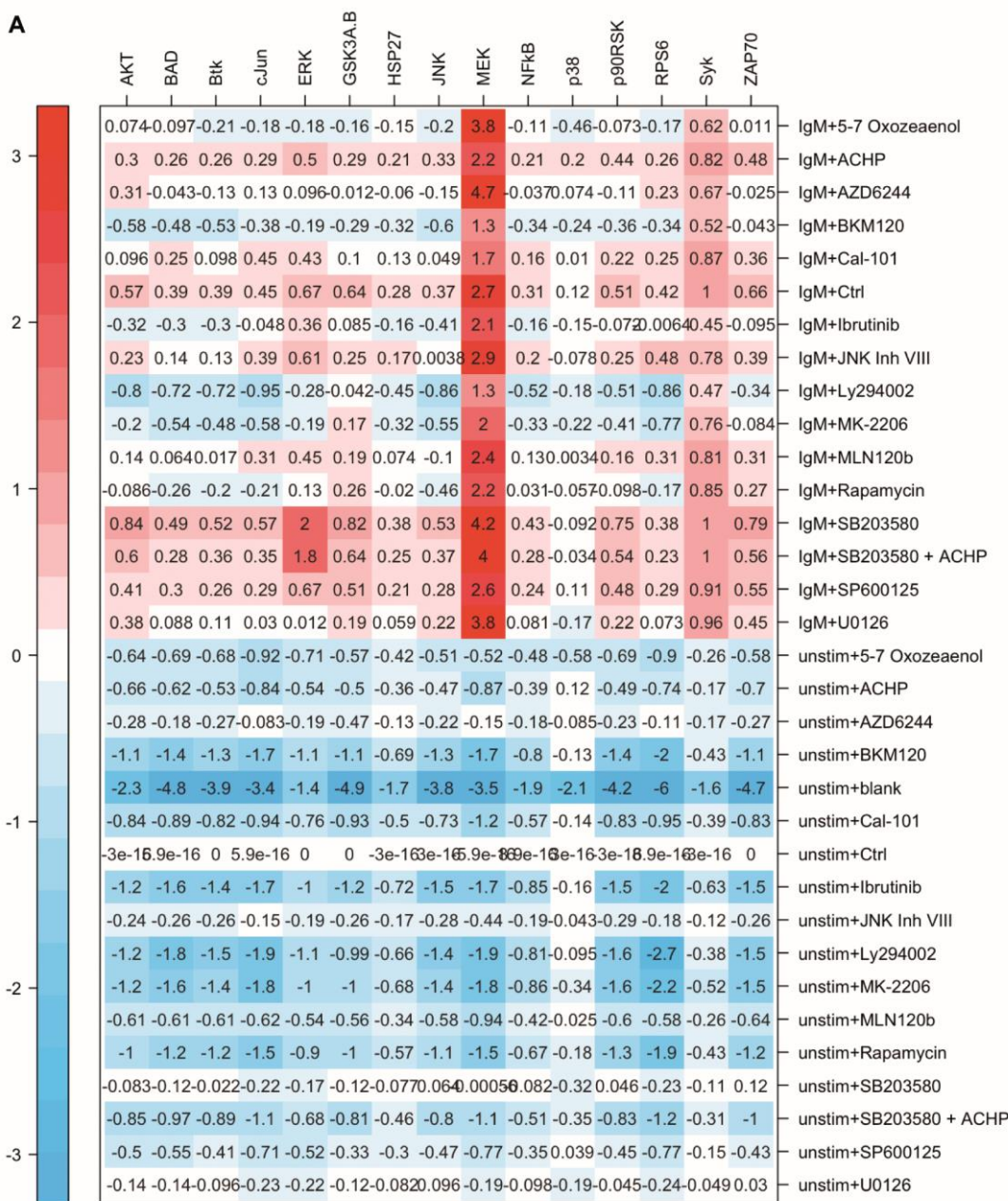
Wellbrock, C., Karasarides, M., and Marais, R. (2004). The RAF proteins take centre stage. Nature reviews Molecular cell biology 5, 875-885.

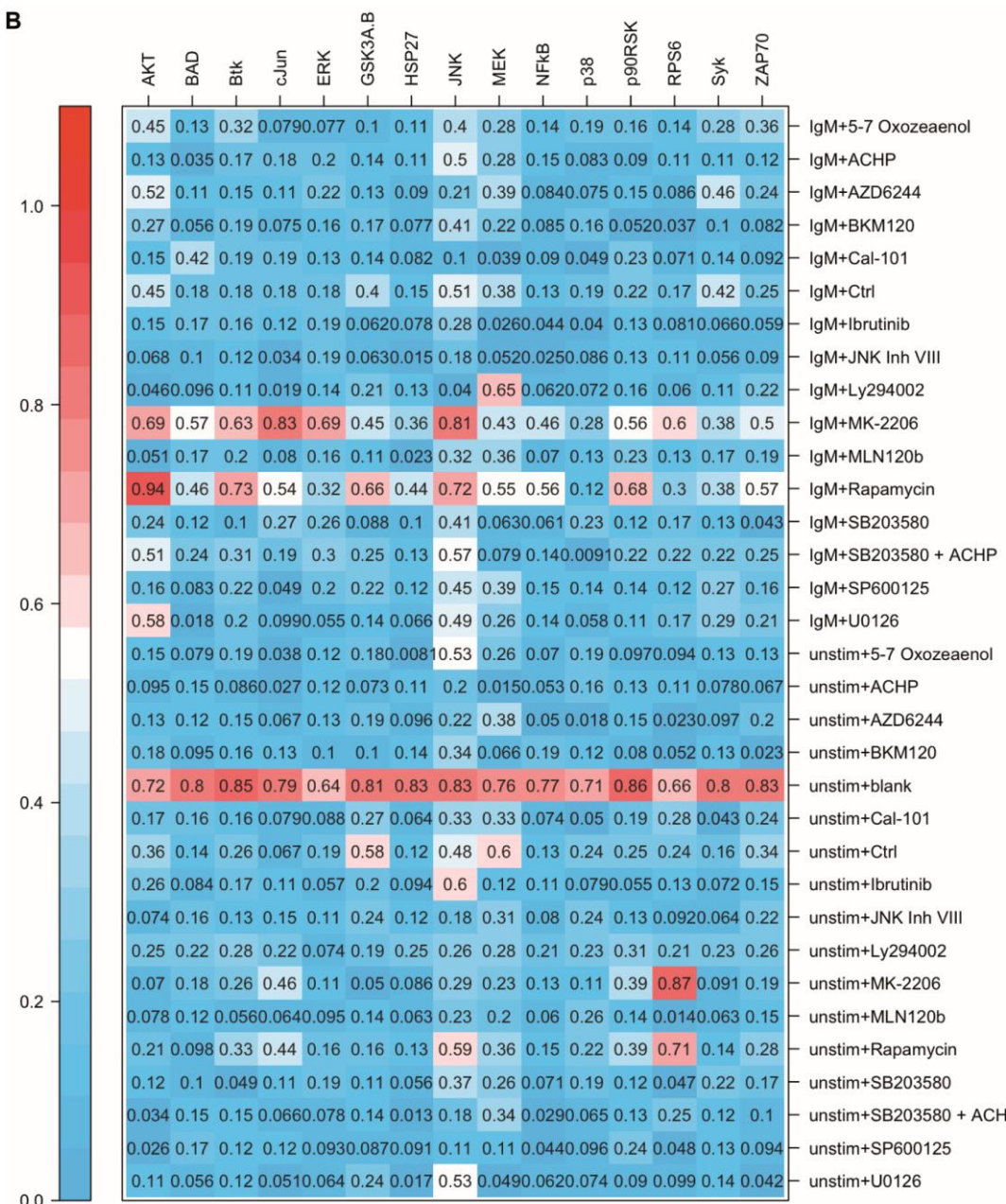
- Wienands, J., Schweikert, J., Wollscheid, B., Jumaa, H., Nielsen, P.J., and Reth, M. (1998). SLP-65: a new signaling component in B lymphocytes which requires expression of the antigen receptor for phosphorylation. *The Journal of experimental medicine* 188, 791-795.
- Wilson, W.H., Young, R.M., Schmitz, R., Yang, Y., Pittaluga, S., Wright, G., Lih, C.J., Williams, P.M., Shaffer, A.L., Gerecitano, J., de Vos, S., Goy, A., Kenkre, V.P., Barr, P.M., Blum, K.A., Shustov, A., Advani, R., Fowler, N.H., Vose, J.M., Elstrom, R.L., Habermann, T.M., Barrientos, J.C., McGreivy, J., Fardis, M., Chang, B.Y., Clow, F., Munneke, B., Moussa, D., Beaupre, D.M., and Staudt, L.M. (2015). Targeting B cell receptor signaling with ibrutinib in diffuse large B cell lymphoma. *Nature medicine* 21, 922-926.
- Winslow, M.M., Gallo, E.M., Neilson, J.R., and Crabtree, G.R. (2006). The calcineurin phosphatase complex modulates immunogenic B cell responses. *Immunity* 24, 141-152.
- Wojciechowski, W., Li, H., Marshall, S., Dell'Agnola, C., and Espinoza-Delgado, I. (2005). Enhanced expression of CD20 in human tumor B cells is controlled through ERK-dependent mechanisms. *Journal of immunology* 174, 7859-7868.
- Wolff, A., Bayerlova, M., Gaedcke, J., Kube, D., and Beissbarth, T. (2018). A comparative study of RNA-Seq and microarray data analysis on the two examples of rectal-cancer patients and Burkitt Lymphoma cells. *PloS one* 13, 1-16.
- Yasuda, T., Kometani, K., Takahashi, N., Imai, Y., Aiba, Y., and Kurosaki, T. (2011). ERKs induce expression of the transcriptional repressor Blimp-1 and subsequent plasma cell differentiation. *Science signaling* 4, ra25 21-10.
- Yasuda, T., Sanjo, H., Pages, G., Kawano, Y., Karasuyama, H., Pouyssegur, J., Ogata, M., and Kurosaki, T. (2008). Erk kinases link pre-B cell receptor signaling to transcriptional events required for early B cell expansion. *Immunity* 28, 499-508.
- Yea, S.S., and Fruman, D.A. (2011). Cell signaling. New mTOR targets Grb attention. *Science* 332, 1270-1271.
- Young, R.M., and Staudt, L.M. (2013). Targeting pathological B cell receptor signalling in lymphoid malignancies. *Nature reviews Drug discovery* 12, 229-243.
- Young, R.M., Wu, T., Schmitz, R., Dawood, M., Xiao, W., Phelan, J.D., Xu, W., Menard, L., Meffre, E., Chan, W.C., Jaffe, E.S., Gascoyne, R.D., Campo, E., Rosenwald, A., Ott, G., Delabie, J., Rimsza, L.M., and Staudt, L.M. (2015). Survival of human lymphoma cells requires B-cell receptor engagement by self-antigens. *Proceedings of the National Academy of Sciences of the United States of America* 112, 13447-13454.
- Zakaria, N., Mohd Yusoff, N., Zakaria, Z., Widera, D., and Yahaya, B.H. (2018). Inhibition of NF-kappaB Signaling Reduces the Stemness Characteristics of Lung Cancer Stem Cells. *Front Oncol* 8, 166 161-112.
- Zarubin, T., and Han, J. (2005). Activation and signaling of the p38 MAP kinase pathway. *Cell research* 15, 11-18.
- Zhang, J.X., Zhuang, W.J., Poon, K.H., Yang, M., and Fong, W.F. (2003). Induction of HL-60 cell differentiation by the p38 mitogen-activated protein kinase inhibitor SB203580 is mediated through the extracellular signal-regulated kinase signaling pathway. *Anti-Cancer Drugs* 14, 31-38.

- Zhou, J., Zhang, Q., Henriquez, J.E., Crawford, R.B., and Kaminski, N.E. (2018). Lymphocyte-Specific Protein Tyrosine Kinase (LCK) is Involved in the Aryl Hydrocarbon Receptor-Mediated Impairment of Immunoglobulin Secretion in Human Primary B Cells. *Toxicological sciences : an official journal of the Society of Toxicology* 165, 322-334.
- Zimmermann, S., and Moelling, K. (1999). Phosphorylation and regulation of Raf by Akt (protein kinase B). *Science* 286, 1741-1744.
- Zmajkovicova, K., Jesenberger, V., Catalanotti, F., Baumgartner, C., Reyes, G., and Baccarini, M. (2013). MEK1 is required for PTEN membrane recruitment, AKT regulation, and the maintenance of peripheral tolerance. *Mol Cell* 50, 43-55.

## Appendix

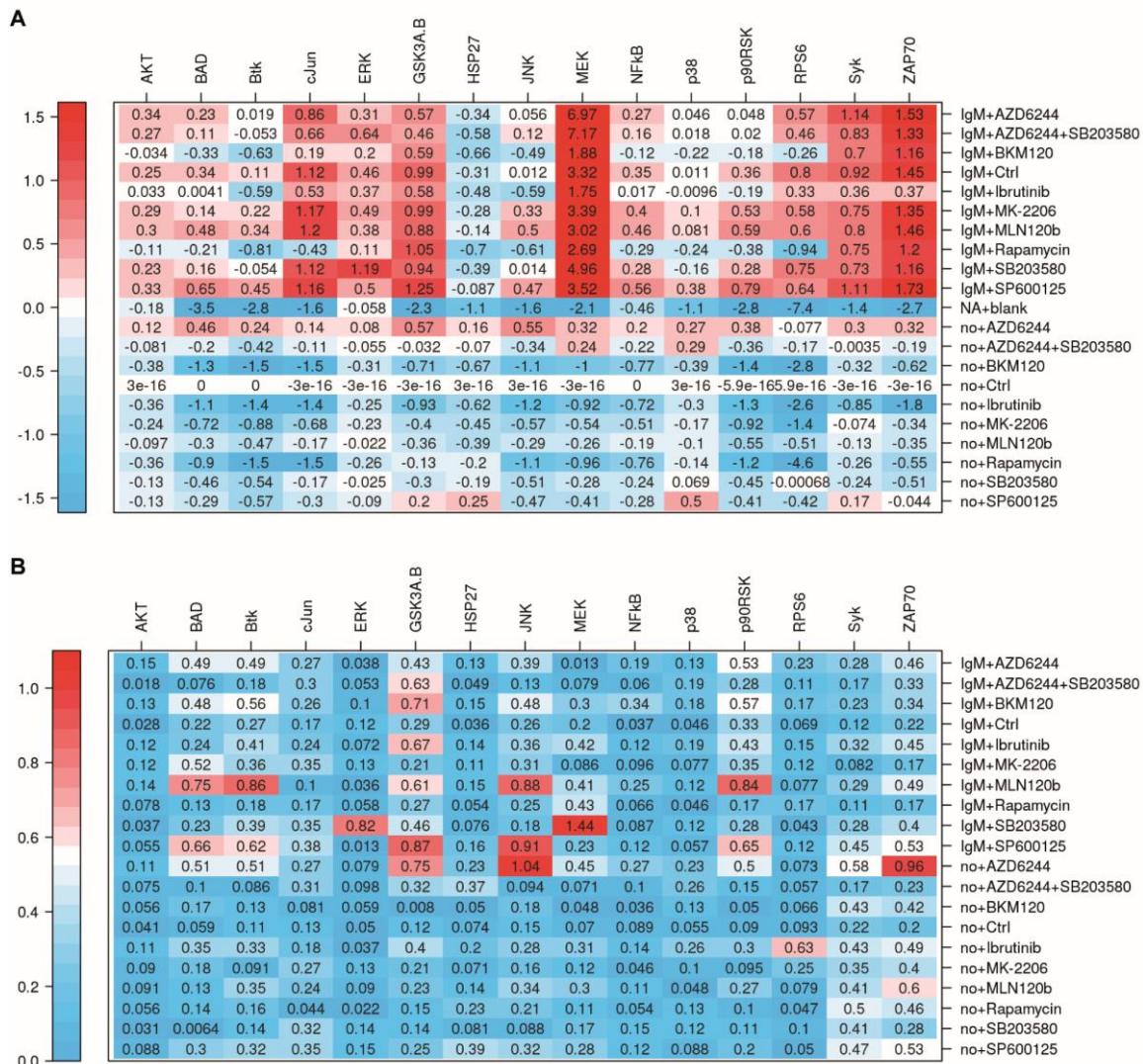
Figure A-1 displays the mean  $\log_2$  fold changes and the standard deviation of the measured protein phosphorylations after distinct pathway perturbation in BL-2 cells. The analysis was done with the multiplex immunoassay, the means were calculated with three independent experiments and the values were normalized to the untreated control. These results were evaluated by Bertram Klinger (Institute of Pathology, Charité – University Medicine Berlin) and are part of Figure 4 and Figure 6.





**Figure A-1: Multiplex immunoassay values and standard deviation of the BL-2 cell analysis**  
BL-2 cells were analyzed with the multiplex immunoassay after 3 hours inhibitor treatment and additionally BCR activation for 30 minutes. **(A)** Mean log<sub>2</sub> fold changes of measured protein phosphorylations were presented for each pathway perturbation normalized to the untreated control (n=3). **(B)** Standard deviation of A was calculated. This evaluation was done by Bertram Klinger (Institute of Pathology, Charité – University Medicine Berlin).

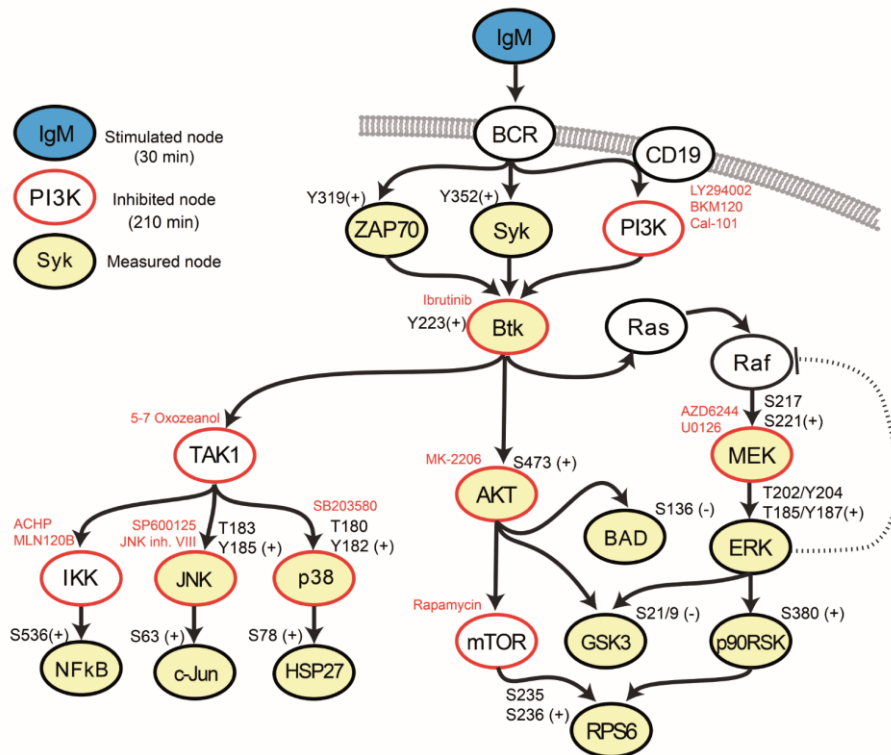
Figure A-2 displays the mean  $\log_2$  fold changes and the standard deviation of the measured protein phosphorylations after distinct pathway perturbation in BL-41 cells. The analysis was done with the multiplex immunoassay, the means were calculated with three independent experiments and the values were normalized to the untreated control. These results were evaluated by Bertram Klinger (Institute of Pathology, Charité – University Medicine Berlin) and are part of Figure 4 and Figure 6



**Figure A-2: Multiplex immunoassay values and standard deviation of the BL-41 cell analysis**

BL-41 cells were analyzed with the multiplex immunoassay after 3 hours inhibitor treatment and additionally BCR activation for 30 minutes. **(A)** Mean  $\log_2$  fold changes of measured protein phosphorylations were presented for each pathway perturbation normalized to the untreated control (n=3). **(B)** Standard deviation of A was calculated. This evaluation was done by Bertram Klinger (Institute of Pathology, Charité – University Medicine Berlin).

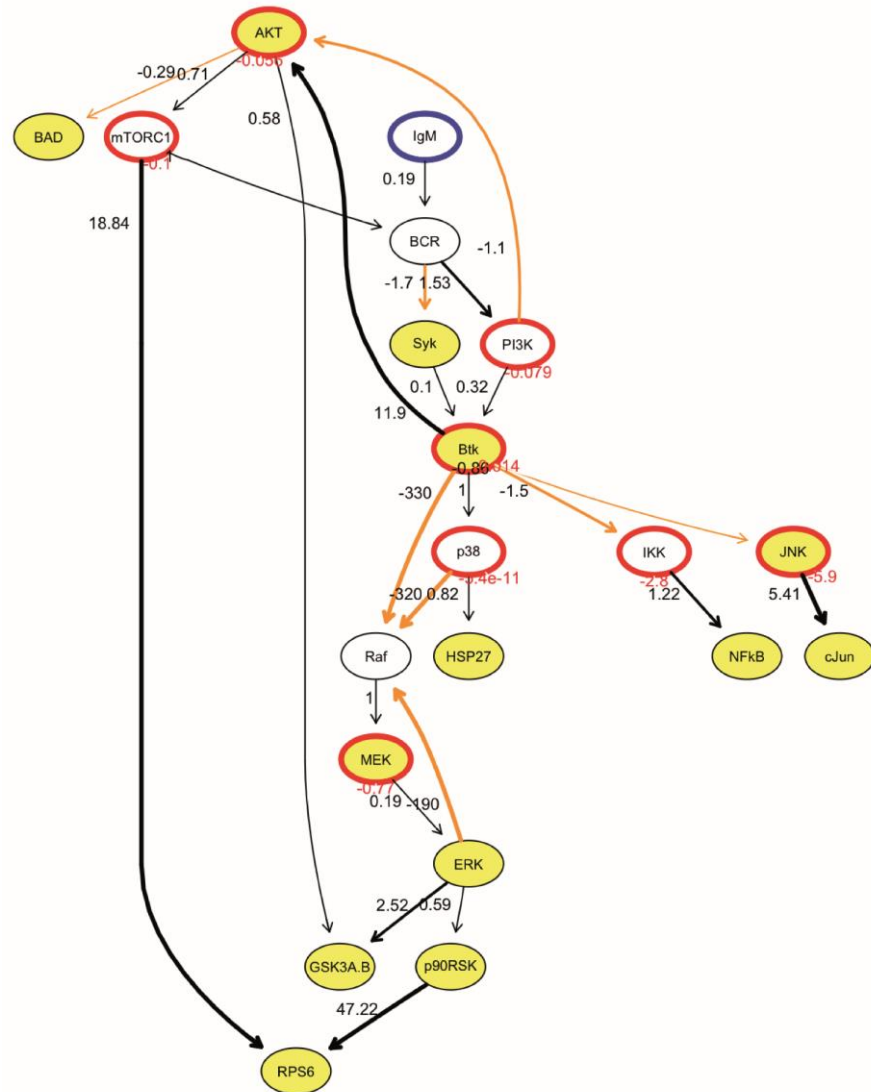
Figure A-3 presents the starting network of the BCR signaling which was complemented with the results of the multiplex immunoassay to generate a refined network model. This scheme was created by Bertram Klinger (Institute of Pathology, Charité – University Medicine Berlin).



**Figure A-3: Literature-derived network model with the experimental setup**

Network model scheme based on the review of Hendriks *et al.* was created by Bertram Klinger (Institute of Pathology, Charité – University Medicine Berlin) (Hendriks *et al.*, 2014). Stimulated (blue), inhibited (red) and measured (yellow) nodes are displayed. The corresponding details present the used inhibitors (red) and the measured protein phosphorylations (black).

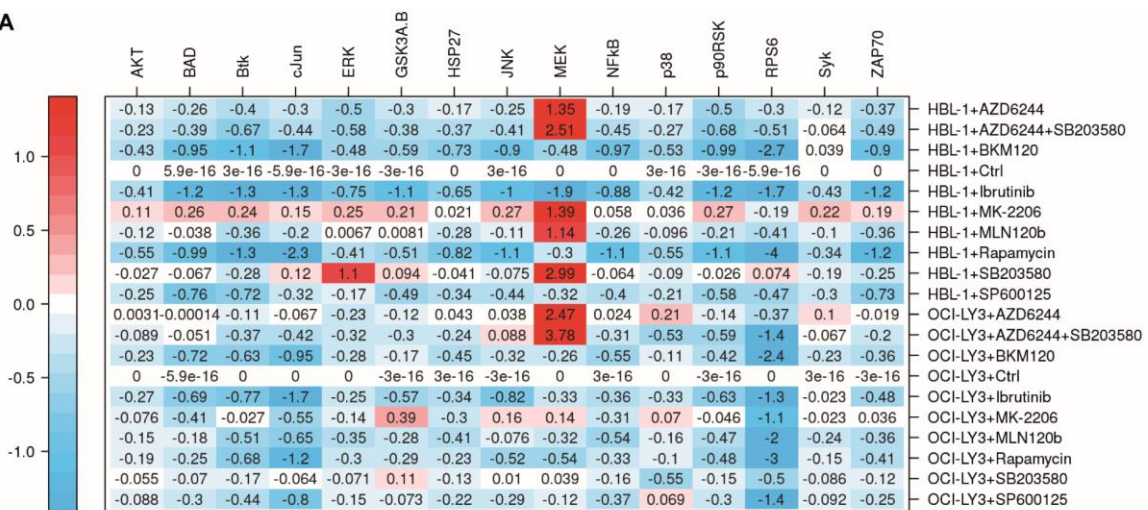
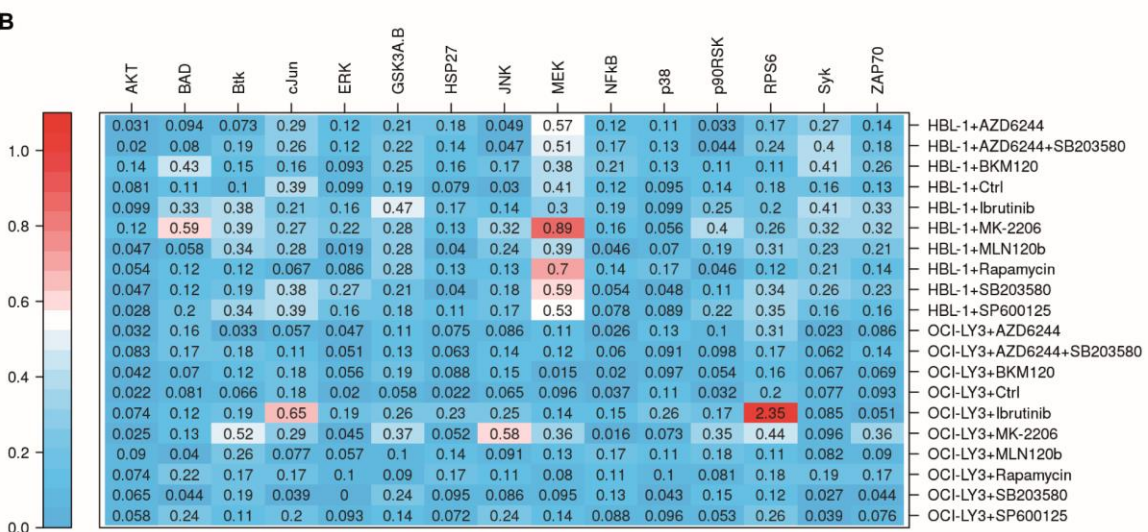
Figure A-4 displays the generated network model of BL-41 cells which was done by Bertram Klinger (Institute of Pathology, Charité – University Medicine Berlin) and belongs to Figure 7.



**Figure A-4: Network model of BCR signaling interactions and feedbacks of BL-41 cells**

Network model of BL-41 cells based on Modular Response Analysis by STASTNet was calculated by Bertram Klinger (Institute of Pathology, Charité – University Medicine Berlin). Stimulated (blue), inhibited (red) and measured (yellow) nodes are displayed. The corresponding numbers indicate the inhibition strength (red) and the value of the local response coefficients (black). Arrows present interaction with positive (black) or negative (orange) local response coefficients.

Figure A-5 displays the mean  $\log_2$  fold changes and the standard deviation of the measured protein phosphorylations after distinct pathway perturbation in HBL-1 and OCI-LY3 cells. The analysis was done with the multiplex immunoassay, the means were calculated with three independent experiments and the values were normalized to the untreated control. These results were evaluated by Bertram Klinger (Institute of Pathology, Charité – University Medicine Berlin) and are part of Figure 15.

**A****B**

**Figure A-5: Multiplex immunoassay values and standard deviation of ABC DLBCLs analyses**  
HBL-1 and OCI-LY3 cells were analyzed with the multiplex immunoassay after 3 hours inhibitor treatment. (A) Mean  $\log_2$  fold changes of measured protein phosphorylations were presented for each pathway perturbation normalized to the untreated control (n=3). (B) Standard deviation of A was calculated. This evaluation was done by Bertram Klinger (Institute of Pathology, Charité – University Medicine Berlin).

A list of all quantified protein phosphorylations in P493-6 cells, which are shown in Figure 19, is attached. This includes the name of protein, phosphorylation site, mean  $\log_2$  values of the light/heavy ratio, p-values and the measured intensities. The calculation of the  $\log_2$  values were done by Jasmin Corso from the Bioanalytical Mass Spectrometry Group of Henning Urlaub (Max-Planck-Institute for Biophysical Chemistry, Goettingen).

The significantly changed phosphosites after IL10+CpG stimulation displayed in Figure 19 are listed in Table A-1. This includes the name of protein, phosphorylation site, mean  $\log_2$  values of the light/heavy ratio, p-values and the measured intensities.

**Table A-1: The changed phosphosites after IL10+CpG stimulation**

T: Gene names	C: Amino acid	N: Position	light Myc low /heavy Myc high IL10+CpG	light Myc low /heavy Myc high IL10+CpG	Difference IL10+ CpG - Ctrl	Individual p-value	N: Intensity
ABL2	S	936	-0,90	-0,07	0,83	0,0011	103040000
ACIN1;DKFZp667N107	S	652	-0,81	-0,18	0,62	0,0142	399670000
ADD1	T	11	0,09	1,13	1,05	0,0001	1904600000
ADRBK1	S	652	-1,07	-0,11	0,96	0,0002	574690000
AHNAK	S	3426	-1,56	1,35	2,91	0,0001	461270000
AHNAK	S	5110	0,32	1,26	0,94	0,0002	642210000
AHNAK	S	135	1,19	2,07	0,88	0,0005	3396400000
AHNAK	S	210	0,63	1,27	0,64	0,0118	962530000
AHNAK	S	5830	0,87	1,30	-0,73	0,0187	50311000
AKAP1	S	150	-2,06	-1,32	0,74	0,0035	101850000
AKAP13	S	2709	-1,77	0,74	2,34	0,0001	78983000
AMFR;hCG_1811773	S	191	-0,91	0,03	0,94	0,0002	61806000
ANKRD28	S	1011	-1,27	-0,29	0,70	0,0241	30248000
APOB48R;APOBR	T	563	1,29	1,96	0,67	0,0313	67005000
APPL1	S	401	1,22	0,62	-0,64	0,0147	185830000
ARHGAP30	S	240	-0,54	0,15	0,69	0,0067	67400000
ARHGAP4	S	340	-0,75	0,22	0,96	0,0001	291210000
ARHGEF6	S	684	1,26	0,86	-0,69	0,0089	103420000
ASAP1	S	660	0,79	-0,15	-1,06	0,0001	54716000
BET1;DKFZp781C0425	S	50	-0,13	0,44	0,75	0,0157	131550000
BIN1	S	267	0,86	0,22	-0,64	0,0031	650660000
C2orf49	S	151	-0,93	0,24	1,17	0,0001	187440000
CAMSAP1	S	945	-1,00	-0,06	0,94	0,0002	212820000
CARHSP1	S	30	0,28	-0,46	-0,74	0,0001	1537300000
CCDC55;NSRP1	T	221	-0,19	-0,82	-0,80	0,0025	117450000
CD2AP	S	458	2,01	1,14	-0,87	0,0001	597740000
CD72	Y	7	3,44	2,74	-0,70	0,0011	44524000
CDC42EP3	S	144	1,59	2,33	0,74	0,0178	95180000

T: Gene names	C: Amino acid	N: Position	light Myc low /heavy Myc high IL10+CpG	light Myc low /heavy Myc high IL10+CpG	Differ- ence IL10+ CpG - Ctrl	Individual p-value	N: Intensity
CDV3	Y	190	-0,11	0,85	0,81	0,0094	530910000
CENPF	S	3119	-1,62	-2,35	-0,72	0,0201	26095000
CHAMP1	S	427	-0,69	0,10	0,78	0,0020	824110000
CIC;CIC/DUX4 fusion	S	1405	-0,17	0,59	0,77	0,0138	34471000
CLASP2;DKFZp686D11262	S	934	-1,53	-0,44	1,10	0,0004	44827000
CLTA	S	105	-0,80	0,15	0,95	0,0002	1956200000
DIDO1	S	1456	-0,96	0,10	1,05	0,0001	1413300000
DKC1	S	485	-1,35	-0,59	0,76	0,0026	121250000
DKFZp781H1925;EIF2AK3	S	564	-2,12	-0,54	1,32	0,0001	44186000
DNMBP	S	684	-1,40	0,16	1,12	0,0003	17740000
DNMT1	S	130	-2,47	-0,63	1,89	0,0001	136570000
DOCK2	S	1685	-0,63	0,36	0,99	0,0001	4787800000
DTL	S	236	-2,57	-1,26	1,31	0,0001	31988000
DYNC1LI1	S	516	-1,26	0,10	1,37	0,0001	3187700000
EIF4B	S	382	-1,23	-0,69	0,62	0,0471	973860000
ELMSAN1;C14orf43	S	996	-2,32	-0,72	1,61	0,0001	10157000
ELMSAN1;C14orf43	S	461	-1,05	0,02	1,07	0,0001	1275800000
EPB41L1	T	378	-0,51	0,78	1,29	0,0001	140210000
EPS15	S	796	-0,98	0,65	1,63	0,0001	227790000
EPS15L1	S	376	-2,70	-1,32	1,28	0,0001	180320000
ESCO2	S	512	-1,32	0,12	1,45	0,0001	97003000
FAM195A	S	82	-1,83	-0,86	0,97	0,0001	249730000
FAM21C;FAM21A	S	728	-0,35	0,48	0,78	0,0123	141120000
FAM21C;FAM21A	S	288	-0,43	0,33	0,75	0,0152	144640000
FBRSL1	S	937	-2,05	-2,69	-0,64	0,0031	146610000
FCHO1	S	520	0,23	0,84	0,61	0,0171	153990000
FHOD1	S	549	-1,44	-0,02	1,43	0,0001	107880000
GABPA	S	303	-2,99	0,10	3,08	0,0001	100250000
GATAD2B	S	470	-1,51	-0,30	1,26	0,0001	212070000
GBF1	S	1784	-1,67	0,44	2,16	0,0001	103570000
GCC2	S	554	-1,96	-0,09	1,87	0,0001	491240000
GCC2	S	409	-1,02	-0,03	1,13	0,0003	47754000
GPATCH8	S	1107	-0,63	0,13	0,76	0,0027	609850000
GPS1	S	454	0,48	-0,21	-0,69	0,0013	284620000
GTF3C1;DKFZp686A111;DKFZp686O0870	S	1068	-0,26	-1,07	-0,90	0,0007	124150000
HAUS6	T	448	-3,07	-0,61	2,46	0,0001	324730000
hCG_1989366;NUP50	S	221	-2,36	-1,58	0,79	0,0019	107330000
HEL-S-102;HSPB1	S	15	-2,62	0,42	3,04	0,0001	60325000
HEL-S-102;HSPB1	S	82	-0,75	0,29	1,03	0,0001	2,0624E+10
HEL-S-270;ANXA2;ANXA2P2	S	26	0,69	-0,34	-1,03	0,0001	114390000
HEL-S-37;LCP1	S	5	1,38	2,31	0,94	0,0002	1,2519E+10
HNRPD;HNRNPD	S	87	-0,55	0,57	1,12	0,0003	347070000
HSH2D	S	210	0,61	1,41	0,80	0,0017	302560000

T: Gene names	C: Amino acid	N: Position	light Myc low /heavy Myc high IL10+CpG	light Myc low /heavy Myc high IL10+CpG	Differ- ence IL10+ CpG - Ctrl	Individual p-value	N: Intensity
INPP5D	S	971	0,64	1,34	0,75	0,0155	2998000000
INPP5D	T	963	0,64	1,33	0,75	0,0166	154000000
IQGAP2	S	16	0,56	1,39	0,83	0,0012	348440000
IRF2BP2	S	240	-0,70	0,04	0,74	0,0036	201260000
IRF2BP2	S	457	0,38	-0,58	-0,72	0,0063	172360000
JUN;JUND	S	100	-1,13	0,88	2,01	0,0001	112020000
KCNAB2	S	9	-0,64	-1,25	-0,68	0,0100	88158000
KDM3B;JMJD1B	S	798	-2,79	0,22	3,05	0,0001	179340000
KDM4B;JMJD2B	S	324	-1,55	-0,09	1,35	0,0001	291910000
KIAA1267;KANSL1	S	1081	-1,33	-0,52	0,80	0,0099	78048000
KIAA1737;CIPC	S	113	-1,73	-1,02	1,11	0,0004	78929000
KIF18B	S	94	-1,86	-1,04	0,82	0,0084	39783000
KIF4A	S	804	-1,30	0,50	1,81	0,0001	52333000
KIFC1	S	6	0,99	-0,17	-1,16	0,0001	534050000
KLC2	S	610	-0,70	-0,04	0,66	0,0336	21362000
KMT2D	S	2274	-0,95	-0,05	0,90	0,0004	346090000
LCK;YES1;FYN;SRC	Y	419	-0,07	0,69	1,09	0,0005	282310000
LRMP	S	28	-1,47	-0,36	0,71	0,0228	33192000
LSM14A	S	183	0,21	-0,51	-0,72	0,0008	1415700000
LSP1	S	177	-1,04	-1,94	-0,90	0,0038	252620000
MAP1B;DKFZp686F1345	S	1852	-0,78	0,45	1,32	0,0001	55692000
MAP2K2;DKFZp686L02273	S	295	-0,13	0,51	0,63	0,0416	243570000
MAP3K1	S	1018	1,03	0,23	-1,10	0,0001	77596000
MAPK14	Y	182	-1,99	0,02	2,02	0,0001	2425900000
MAPRE1	S	155	0,11	1,24	0,91	0,0034	143320000
MARCKS	S	118	-0,77	1,11	1,71	0,0001	216990000
MAVS	S	222	-1,54	0,05	1,60	0,0001	143590000
MCM3AP	S	153	-0,47	0,30	0,77	0,0132	111300000
MCM4	S	80	-1,51	-2,34	-0,65	0,0135	32890000
MED24	S	38	-1,53	0,14	1,40	0,0001	74733000
MEF2C	S	226	-1,57	0,68	2,15	0,0001	173660000
MEF2C	S	220	-0,42	0,44	0,86	0,0001	298990000
MEF2C	S	238	-0,18	0,60	0,80	0,0099	36709000
MEF2D variant protein;MEF2D	S	126	-2,14	0,04	2,30	0,0001	98449000
MEF2D variant protein;MEF2D	S	185	-1,05	0,08	1,13	0,0001	187660000
MEPCE	S	152	-1,84	0,01	1,86	0,0001	59393000
MICAL3	S	1310	-2,19	-0,85	1,34	0,0001	66870000
MKI67	S	1130	-0,52	0,15	0,67	0,0321	59047000
MKL1;mkl1	S	454	0,09	0,79	0,70	0,0060	172650000
MLLT4	S	1234	0,62	-0,19	-0,91	0,0006	80188000
MPZL1	Y	237	0,02	0,67	0,65	0,0025	84308000
MS4A1	S	36	-1,32	0,84	2,15	0,0001	5718200000
MS4A1	S	35	0,47	1,65	1,27	0,0001	711490000

T: Gene names	C: Amino acid	N: Position	light Myc low /heavy Myc high IL10+CpG	light Myc low /heavy Myc high IL10+CpG	Differ- ence IL10+ CpG - Ctrl	Individual p-value	N: Intensity
MS4A1	S	36	0,47	1,65	1,27	0,0001	5718200000
MS4A1	S	218	0,37	1,60	1,09	0,0005	275800000
MS4A1	S	35	1,46	0,74	-0,72	0,0001	711490000
MST065;TOMM22	S	15	-0,18	0,41	0,60	0,0189	2241200000
MTSS1L	S	455	-2,05	-1,44	0,83	0,0076	91922000
MYO9B variant protein;MYO9B	T	1352	-2,21	0,03	2,24	0,0001	145300000
MYO9B variant protein;MYO9B	S	1411	-2,48	-0,41	2,07	0,0001	352100000
MYO9B variant protein;MYO9B	S	1273	-1,05	0,26	1,32	0,0001	371830000
MYO9B variant protein;MYO9B	S	1296	-1,21	-0,01	1,21	0,0001	1558700000
NAP1L1	S	69	-0,28	-0,71	-0,66	0,0347	77631000
NELFE;RDBP;NELF-E	S	51	-2,56	-0,18	2,23	0,0001	309490000
NELFE;RDBP;NELF-E	S	115	-1,94	-0,49	1,45	0,0001	2085800000
NELFE;RDBP;NELF-E	S	251	-1,23	-0,62	0,61	0,0166	376780000
NOC2L	S	49	-0,79	-0,39	0,63	0,0434	148950000
NOL8	S	1031	-0,75	-0,12	0,63	0,0429	67523000
NOLC1	T	610	-1,63	-2,22	-0,70	0,0079	284210000
NOLC1	S	397	-2,16	-3,07	-0,76	0,0041	123650000
NOP2	S	58	-2,34	0,35	2,68	0,0001	288400000
NUCKS1	T	179	-0,84	-1,46	-0,62	0,0038	862350000
NUCKS1	S	181	-0,81	-1,47	-0,66	0,0023	2,325E+10
NUMA1;NUMA1 variant protein	S	1741	-1,10	-0,17	0,92	0,0003	376830000
NUP188	S	1709	-1,75	-0,95	0,82	0,0086	134880000
OSBPL11	S	181	0,49	-0,25	-0,74	0,0006	59062000
OSBPL3	S	437	-0,93	0,25	1,18	0,0001	137170000
OXR1	S	113	0,63	1,35	0,79	0,0110	185140000
OXSR1	S	359	-0,69	0,35	1,04	0,0008	16074000
PAK1	T	114	-2,27	-0,17	2,05	0,0001	52953000
PAK2	S	58	-1,96	0,21	1,83	0,0001	15526000
PAPOLG	S	525	-2,70	-0,56	2,14	0,0001	73832000
PARN	S	557	-1,47	-0,59	0,88	0,0005	150810000
PDS5A	T	1208	-0,55	-1,21	-0,67	0,0020	178640000
PFKL	S	775	-1,09	0,22	1,31	0,0001	227750000
PI4K2A	S	462	0,54	1,13	0,77	0,0130	44624000
PLEKHM1	S	346	0,40	1,26	0,77	0,0130	30251000
PML	S	518	1,33	0,68	-0,65	0,0027	596350000
PML	S	527	1,33	0,68	-0,65	0,0027	1175000000
PML	S	527	1,64	0,92	-0,71	0,0010	1175000000
PPFIBP2;DKFZp781K06126	S	252	-0,60	0,63	1,37	0,0001	66492000
PPP1R10	S	313	-0,35	0,34	0,68	0,0071	1795000000
PRKD2	S	198	1,24	1,73	0,86	0,0057	33320000
PROSER1	S	552	-1,61	-0,84	0,77	0,0023	163150000
PROSER2;C10orf47	S	212	-2,61	-1,70	0,92	0,0003	67830000

T: Gene names	C: Amino acid	N: Position	light Myc low /heavy Myc high IL10+CpG	light Myc low /heavy Myc high IL10+CpG	Differ- ence IL10+ CpG - Ctrl	Individual p-value	N: Intensity
PSM8;PSMB8	S	39	1,35	1,97	0,62	0,0143	35825000
PSMA5	S	56	-0,33	0,58	0,91	0,0004	372170000
PSMA5	S	16	-0,65	-0,02	0,63	0,0124	367770000
PSMF1	S	153	-1,11	-0,41	0,71	0,0054	601910000
RAF1;SRGAP3:RAF1	S	609	0,36	1,36	0,81	0,0093	80432000
RALGPS2	S	308	1,94	0,98	-1,28	0,0001	330400000
RALGPS2	S	296	1,94	0,31	-1,95	0,0001	407060000
RANBP3	S	126	-0,25	0,42	0,66	0,0089	115560000
RBM34	S	17	-1,03	0,16	1,19	0,0001	497240000
RBM7	S	136	-2,48	0,10	2,58	0,0001	106880000
RCSD1	S	82	-2,76	0,19	2,96	0,0001	808720000
RCSD1	S	83	-2,63	-0,23	2,40	0,0001	5518600000
RCSD1	S	68	-0,99	0,47	1,46	0,0001	863810000
RCSD1	S	284	-0,41	0,58	0,99	0,0001	1637100000
RCSD1	S	179	-0,17	0,67	0,84	0,0010	3197800000
RCSD1	S	120	0,97	0,20	-0,77	0,0003	394830000
RHBDL2	S	61	-0,79	-0,14	0,65	0,0107	143330000
RIC1	S	909	-1,14	0,97	2,11	0,0001	151090000
RNF214;DKFZp547C195	S	15	0,02	-0,62	-0,64	0,0398	13980000
RPRD2	S	1099	-1,32	0,24	1,56	0,0001	289780000
RPS6	S	240	-0,85	0,01	0,74	0,0175	58425000
SACS	S	1779	-2,52	-0,67	1,85	0,0001	31816000
SACS	S	4264	-1,71	-0,35	1,35	0,0001	112540000
SART1	S	448	-0,73	0,19	0,92	0,0003	518090000
SCRIB	S	1448	-0,98	-0,20	0,78	0,0021	583260000
SCRIB	S	1486	-1,67	-0,92	0,74	0,0034	141830000
SCRIB	S	1475	-1,44	-0,72	0,72	0,0045	973960000
SCRIB	S	504	-1,03	-0,36	0,67	0,0088	1100700000
SEC16A	S	1964	-0,73	0,15	0,76	0,0151	139820000
SETX	S	1366	-0,71	0,69	1,40	0,0001	762420000
SLC29A2	S	252	-2,17	-1,11	0,92	0,0031	34200000
SLC9A1	S	364	0,29	1,07	0,77	0,0023	272210000
SLC9A3R1	S	290	0,20	1,17	0,97	0,0018	338940000
SNAPIN	T	14	-1,16	-0,47	0,87	0,0054	90821000
SOS1	S	752	2,08	0,74	-1,02	0,0001	39536000
SPTBN1	S	2254	-0,16	-0,77	-0,61	0,0050	482260000
SRPK1	S	311	-0,33	-0,94	-0,73	0,0056	128830000
SRRM2;KIAA0324	S	2272	-1,60	-0,90	0,71	0,0054	313600000
SRRM2;KIAA0324	T	2104	0,33	-0,53	-0,87	0,0001	2267000000
STAT1	S	727	1,33	2,12	0,78	0,0020	415540000
STAT3	Y	607	-4,26	1,52	5,84	0,0001	515900000
STAT3	Y	704	-1,33	1,51	2,85	0,0001	73240000
STAU2;STAU2 variant protein	S	105	-1,81	-0,13	1,69	0,0001	75642000

T: Gene names	C: Amino acid	N: Position	light Myc low /heavy Myc high IL10+CpG	light Myc low /heavy Myc high IL10+CpG	Differ- ence IL10+ CpG - Ctrl	Individual p-value	N: Intensity
STK10	T	952	0,04	0,73	0,69	0,0062	650860000
STK24;HEL-S-95	S	4	-0,54	0,09	0,63	0,0131	699270000
STMN1	S	25	-1,13	0,83	1,95	0,0001	5048800000
STX6	S	2	-1,16	-1,07	0,63	0,0414	17434000
TAOK3	S	442	0,68	0,12	-0,62	0,0181	75975000
TBC1D4	S	591	-0,83	-1,58	-0,75	0,0005	1062200000
TBC1D5	S	43	1,53	0,83	-0,70	0,0012	153940000
TFAP4	S	63	-3,17	-3,81	-0,63	0,0418	47441000
THRAP3	S	184	-0,03	-0,89	-0,85	0,0012	57521000
TMEM201	S	364	-1,16	-2,79	-1,63	0,0001	17847000
TMF1	S	333	-1,44	-0,19	1,25	0,0001	30240000
TMPO	S	424	-1,25	-1,85	-0,60	0,0056	69924000
TMPO	T	160	1,23	0,59	-0,64	0,0028	110670000
TNKS1BP1	S	836	-2,05	-0,74	1,15	0,0002	70829000
TRIM24	S	953	-2,13	-0,18	2,12	0,0001	242790000
TRIM28	S	473	-0,89	-0,14	0,75	0,0034	1906700000
TRRAP	S	1772	-2,25	-0,53	2,02	0,0001	130780000
TSC22D4	S	165	0,90	0,29	-0,64	0,0150	22224000
UBAP1	S	172	-0,32	1,06	1,19	0,0001	58307000
UBE2O	S	839	-1,38	-0,21	1,10	0,0004	767920000
UBE4B	S	105	-1,11	-0,23	0,81	0,0092	179120000
UBR5	S	1543	-0,97	-0,10	0,87	0,0006	577750000
ULK1	S	450	-0,73	-0,05	0,68	0,0287	23276000
ULK1	S	623	-0,70	-0,03	0,66	0,0089	48393000
USP1	S	313	-1,29	-0,82	0,94	0,0025	109970000
USP10	S	365	-0,27	-0,65	-0,62	0,0182	33173000
VGLL4	S	149	-2,10	-1,38	0,72	0,0008	58534000
WAC	T	293	-2,11	-0,43	1,61	0,0001	40383000
WDR62;DKFZp434J046	S	1123	-1,56	-0,83	0,68	0,0279	63753000
ZC3H12D;FLJ00361	S	428	-1,55	1,20	2,64	0,0001	81621000
ZC3H13	S	993	-0,84	-1,55	-0,71	0,0010	143120000
ZCCHC8	S	420	-1,53	-0,06	1,56	0,0001	37632000
ZDHHC5	S	398	0,21	-0,43	-0,64	0,0148	34041000
ZFC3H1	S	352	-2,11	-0,28	1,83	0,0001	387690000
ZFC3H1	T	766	-1,33	-0,19	1,16	0,0002	67428000
ZFP91-CNTF;hCG_2042749;ZFP91	S	83	0,97	-0,08	-1,04	0,0001	241060000
ZNF609	S	413	-0,86	0,35	1,40	0,0001	268850000
ZYX	S	238	0,31	1,19	0,88	0,0005	262250000
ZZE1	S	1518	-0,78	0,52	1,30	0,0001	186700000
	S	18	-1,41	0,78	2,10	0,0001	61626000

Table A-2 presents the GO annotation of the phosphorylated proteins which were significantly changed by IL10+CpG stimulation. Only terms with more than 10 counts and p-values below 0.05 were included.

**Table A-2: GO annotation of phosphoproteins changed by IL10+CpG stimulation**

Category	Term	Count	%	P value	-log <sub>10</sub> P value
<i>Annotation Cluster 1</i>					
GOTERM_BP_FAT	Enrichment Score: 3,7335796159192123 GO:0010608 posttranscriptional regulation of gene expression	15	7,81	0,0003327	3,48
<i>Annotation Cluster 2</i>					
GOTERM_BP_FAT	Enrichment Score: 3,3521003094311026 GO:0043933 macromolecular complex subunit organization	48	25,00	0,0000083	5,08
GOTERM_BP_FAT	GO:0065003 macromolecular complex assembly	35	18,23	0,0000946	4,02
GOTERM_BP_FAT	GO:0006461 protein complex assembly	31	16,15	0,0001234	3,91
GOTERM_BP_FAT	GO:0070271 protein complex biogenesis	31	16,15	0,0001250	3,90
GOTERM_BP_FAT	GO:0044085 cellular component biogenesis	49	25,52	0,0002912	3,54
GOTERM_BP_FAT	GO:0071822 protein complex subunit organization	33	17,19	0,0003225	3,49
GOTERM_BP_FAT	GO:0022607 cellular component assembly	45	23,44	0,0003687	3,43
GOTERM_BP_FAT	GO:0043623 cellular protein complex assembly	12	6,25	0,0328116	1,48
GOTERM_BP_FAT	GO:0034622 cellular macromolecular complex assembly	17	8,85	0,0491809	1,31
<i>Annotation Cluster 3</i>					
GOTERM_BP_FAT	Enrichment Score: 3,1526962069914504 GO:0007049 cell cycle	41	21,35	0,0000002	6,73
GOTERM_BP_FAT	GO:0000278 mitotic cell cycle	29	15,10	0,0000005	6,32
GOTERM_BP_FAT	GO:0022402 cell cycle process	33	17,19	0,0000056	5,25
GOTERM_BP_FAT	GO:1903047 mitotic cell cycle process	25	13,02	0,0000114	4,94
GOTERM_BP_FAT	GO:0007067 mitotic nuclear division	14	7,29	0,0004644	3,33
GOTERM_BP_FAT	GO:0000280 nuclear division	16	8,33	0,0008974	3,05
GOTERM_BP_FAT	GO:0048285 organelle fission	16	8,33	0,0017042	2,77
GOTERM_BP_FAT	GO:0044772 mitotic cell cycle phase transition	14	7,29	0,0022892	2,64
GOTERM_BP_FAT	GO:0044770 cell cycle phase transition	14	7,29	0,0038923	2,41
GOTERM_BP_FAT	GO:0007017 microtubule-based process	15	7,81	0,0042328	2,37
GOTERM_BP_FAT	GO:0007059 chromosome segregation	10	5,21	0,0071646	2,14
GOTERM_BP_FAT	GO:0000226 microtubule cytoskeleton organization	10	5,21	0,0308129	1,51
GOTERM_BP_FAT	GO:0051301 cell division	12	6,25	0,0328116	1,48
<i>Annotation Cluster 4</i>					
GOTERM_BP_FAT	Enrichment Score: 2,9792557107087028 GO:0044093 positive regulation of molecular function	40	20,83	0,0000057	5,24
GOTERM_BP_FAT	GO:0035556 intracellular signal transduction	49	25,52	0,0000287	4,54
GOTERM_BP_FAT	GO:0051336 regulation of hydrolase activity	31	16,15	0,0000298	4,53
GOTERM_BP_FAT	GO:0043085 positive regulation of catalytic activity	34	17,71	0,0000362	4,44
GOTERM_BP_FAT	GO:0065009 regulation of molecular function	51	26,56	0,0000455	4,34
GOTERM_BP_FAT	GO:0051345 positive regulation of hydrolase activity	24	12,50	0,0000545	4,26
GOTERM_BP_FAT	GO:0043087 regulation of GTPase activity	19	9,90	0,0002358	3,63
GOTERM_BP_FAT	GO:0009966 regulation of signal transduction	47	24,48	0,0002390	3,62
GOTERM_BP_FAT	GO:0010646 regulation of cell communication	50	26,04	0,0003530	3,45
GOTERM_BP_FAT	GO:0023051 regulation of signalling	50	26,04	0,0005208	3,28
GOTERM_BP_FAT	GO:0023014 signal transduction by protein phosphorylation	21	10,94	0,0005913	3,23
GOTERM_BP_FAT	GO:0043547 positive regulation of GTPase activity	17	8,85	0,0007437	3,13
GOTERM_BP_FAT	GO:0006468 protein phosphorylation	34	17,71	0,0008926	3,05
GOTERM_BP_FAT	GO:0007264 small GTPase mediated signal transduction	15	7,81	0,0009821	3,01

Category	Term		Count	%	P value	$-\log_{10}$ P value
GOTERM_BP_FAT	GO:0050790	regulation of catalytic activity	40	20,83	0,0011813	2,93
GOTERM_BP_FAT	GO:0016310	phosphorylation	37	19,27	0,0028837	2,54
GOTERM_BP_FAT	GO:1902531	regulation of intracellular signal transduction	30	15,63	0,0040778	2,39
GOTERM_BP_FAT	GO:0009967	positive regulation of signal transduction	26	13,54	0,0050427	2,30
GOTERM_BP_FAT	GO:0023056	positive regulation of signalling	27	14,06	0,0081512	2,09
GOTERM_BP_FAT	GO:0000165	MAPK cascade	17	8,85	0,0116933	1,93
GOTERM_BP_FAT	GO:0010647	positive regulation of cell communication	26	13,54	0,0141272	1,85
GOTERM_BP_FAT	GO:0048584	positive regulation of response to stimulus	30	15,63	0,0355079	1,45
<i>Annotation Cluster 5</i>						
	Enrichment Score: 2,859204278988926					
GOTERM_BP_FAT	GO:0051641	cellular localization	52	27,08	0,0000006	6,20
GOTERM_BP_FAT	GO:0051649	establishment of localization in cell	40	20,83	0,0000410	4,39
GOTERM_BP_FAT	GO:0046907	intracellular transport	34	17,71	0,0000561	4,25
GOTERM_BP_FAT	GO:0034504	protein localization to nucleus	14	7,29	0,0000872	4,06
GOTERM_BP_FAT	GO:0017038	protein import	13	6,77	0,0001381	3,86
GOTERM_BP_FAT	GO:0044744	protein targeting to nucleus	12	6,25	0,0001383	3,86
GOTERM_BP_FAT	GO:0006606	protein import into nucleus	12	6,25	0,0001383	3,86
GOTERM_BP_FAT	GO:1902593	single-organism nuclear import	12	6,25	0,0001425	3,85
GOTERM_BP_FAT	GO:0051170	nuclear import	12	6,25	0,0002440	3,61
GOTERM_BP_FAT	GO:1902582	single-organism intracellular transport	19	9,90	0,0002529	3,60
GOTERM_BP_FAT	GO:0034613	cellular protein localization	32	16,67	0,0003219	3,49
GOTERM_BP_FAT	GO:0070727	cellular macromolecule localization	32	16,67	0,0003704	3,43
GOTERM_BP_FAT	GO:0008104	protein localization	42	21,88	0,0006682	3,18
GOTERM_BP_FAT	GO:1902580	single-organism cellular localization	24	12,50	0,0007753	3,11
GOTERM_BP_FAT	GO:0033365	protein localization to organelle	21	10,94	0,0008381	3,08
GOTERM_BP_FAT	GO:0033036	macromolecule localization	46	23,96	0,0009425	3,03
GOTERM_BP_FAT	GO:0051169	nuclear transport	14	7,29	0,0010960	2,96
GOTERM_BP_FAT	GO:0006886	intracellular protein transport	22	11,46	0,0015721	2,80
GOTERM_BP_FAT	GO:1903827	regulation of cellular protein localization	15	7,81	0,0017988	2,75
GOTERM_BP_FAT	GO:0015031	protein transport	33	17,19	0,0019200	2,72
GOTERM_BP_FAT	GO:0045184	establishment of protein localization	35	18,23	0,0019784	2,70
GOTERM_BP_FAT	GO:0006913	nucleocytoplasmic transport	13	6,77	0,0028511	2,54
GOTERM_BP_FAT	GO:0060341	regulation of cellular localization	18	9,38	0,0048767	2,31
GOTERM_BP_FAT	GO:0051049	regulation of transport	30	15,63	0,0077832	2,11
GOTERM_BP_FAT	GO:0072594	establishment of protein localization to organelle	15	7,81	0,0080232	2,10
GOTERM_BP_FAT	GO:0032880	regulation of protein localization	19	9,90	0,0089895	2,05
GOTERM_BP_FAT	GO:1903829	positive regulation of cellular protein localization	10	5,21	0,0119474	1,92
GOTERM_BP_FAT	GO:0006605	protein targeting	15	7,81	0,0122015	1,91
<i>Annotation Cluster 6</i>						
	Enrichment Score: 2,6955951501894386					
GOTERM_BP_FAT	GO:0007265	Ras protein signal transduction	13	6,77	0,0001064	3,97
GOTERM_BP_FAT	GO:0043087	regulation of GTPase activity	19	9,90	0,0002358	3,63
GOTERM_BP_FAT	GO:0043547	positive regulation of GTPase activity	17	8,85	0,0007437	3,13
GOTERM_BP_FAT	GO:0007264	small GTPase mediated signal transduction	15	7,81	0,0009821	3,01
<i>Annotation Cluster 7</i>						
	Enrichment Score: 2,628977224705781					
GOTERM_BP_FAT	GO:0051276	chromosome organization	31	16,15	0,0000028	5,56
GOTERM_BP_FAT	GO:0051129	negative regulation of cellular component organization	19	9,90	0,0000661	4,18
GOTERM_BP_FAT	GO:0010639	negative regulation of organelle organization	12	6,25	0,0003605	3,44
GOTERM_BP_FAT	GO:0033044	regulation of chromosome organization	10	5,21	0,0027466	2,56

Category	Term		Count	%	P value	$-\log_{10}$ P value
GOTERM_BP_FAT	GO:0006325	chromatin organization	17	8,85	0,0051095	2,29
GOTERM_BP_FAT	GO:0016570	histone modification	12	6,25	0,0053534	2,27
GOTERM_BP_FAT	GO:0016569	covalent chromatin modification	13	6,77	0,0104628	1,98
<i>Annotation Cluster 8</i>						
GOTERM_BP_FAT	Enrichment Score: 2,450069107726637					
GOTERM_BP_FAT	GO:0006259	DNA metabolic process	24	12,50	0,0001842	3,73
GOTERM_BP_FAT	GO:0006281	DNA repair	13	6,77	0,0079391	2,10
GOTERM_BP_FAT	GO:0006974	cellular response to DNA damage stimulus	17	8,85	0,0080847	2,09
GOTERM_BP_FAT	GO:0051052	regulation of DNA metabolic process	10	5,21	0,0133948	1,87
<i>Annotation Cluster 10</i>						
GOTERM_BP_FAT	Enrichment Score: 2,2644571324985088					
GOTERM_BP_FAT	GO:0035556	intracellular signal transduction	49	25,52	0,0000287	4,54
GOTERM_BP_FAT	GO:0033554	cellular response to stress	36	18,75	0,0000843	4,07
GOTERM_BP_FAT	GO:0023014	signal transduction by protein phosphorylation	21	10,94	0,0005913	3,23
GOTERM_BP_FAT	GO:0006468	protein phosphorylation	34	17,71	0,0008926	3,05
GOTERM_BP_FAT	GO:0016310	phosphorylation	37	19,27	0,0028837	2,54
GOTERM_BP_FAT	GO:0000165	MAPK cascade	17	8,85	0,0116933	1,93
GOTERM_BP_FAT	GO:0036211	protein modification process	52	27,08	0,0174549	1,76
GOTERM_BP_FAT	GO:0006464	cellular protein modification process	52	27,08	0,0174549	1,76
GOTERM_BP_FAT	GO:0071900	regulation of protein serine/threonine kinase activity	11	5,73	0,0236050	1,63
<i>Annotation Cluster 11</i>						
GOTERM_BP_FAT	Enrichment Score: 2,262335128933962					
GOTERM_BP_FAT	GO:0018193	peptidyl-amino acid modification	22	11,46	0,0088483	2,05
<i>Annotation Cluster 12</i>						
GOTERM_BP_FAT	Enrichment Score: 2,20248095655825					
GOTERM_BP_FAT	GO:1902589	single-organism organelle organization	39	20,31	0,0000006	6,22
GOTERM_BP_FAT	GO:0007010	cytoskeleton organization	28	14,58	0,0000333	4,48
GOTERM_BP_FAT	GO:0030036	actin cytoskeleton organization	16	8,33	0,0005232	3,28
GOTERM_BP_FAT	GO:0032956	regulation of actin cytoskeleton organization	11	5,73	0,0008570	3,07
GOTERM_BP_FAT	GO:0030029	actin filament-based process	17	8,85	0,0013675	2,86
GOTERM_BP_FAT	GO:0032970	regulation of actin filament-based process	11	5,73	0,0022626	2,65
GOTERM_BP_FAT	GO:0051493	regulation of cytoskeleton organization	12	6,25	0,0039288	2,41
GOTERM_BP_FAT	GO:0043254	regulation of protein complex assembly	11	5,73	0,0056071	2,25
GOTERM_BP_FAT	GO:0007015	actin filament organization	10	5,21	0,0073000	2,14
GOTERM_BP_FAT	GO:0044087	regulation of cellular component biogenesis	16	8,33	0,0174964	1,76
GOTERM_BP_FAT	GO:0043623	cellular protein complex assembly	12	6,25	0,0328116	1,48
<i>Annotation Cluster 13</i>						
GOTERM_BP_FAT	Enrichment Score: 2,165151910246645					
GOTERM_BP_FAT	GO:0006915	apoptotic process	33	17,19	0,0006793	3,17
GOTERM_BP_FAT	GO:0012501	programmed cell death	34	17,71	0,0008926	3,05
GOTERM_BP_FAT	GO:0008219	cell death	35	18,23	0,0011554	2,94
GOTERM_BP_FAT	GO:0043065	positive regulation of apoptotic process	14	7,29	0,0056338	2,25
GOTERM_BP_FAT	GO:0043068	positive regulation of programmed cell death	14	7,29	0,0060475	2,22
GOTERM_BP_FAT	GO:0042981	regulation of apoptotic process	25	13,02	0,0077278	2,11
GOTERM_BP_FAT	GO:0043067	regulation of programmed cell death	25	13,02	0,0086204	2,06
GOTERM_BP_FAT	GO:0010942	positive regulation of cell death	14	7,29	0,0090671	2,04
GOTERM_BP_FAT	GO:0010941	regulation of cell death	25	13,02	0,0181630	1,74
<i>Annotation Cluster 14</i>						
GOTERM_BP_FAT	Enrichment Score: 2,0883071313015815					
GOTERM_BP_FAT	GO:0016032	viral process	24	12,50	0,0001193	3,92

Category	Term		Count	%	P value	$-\log_{10} P$ value
GOTERM_BP_FAT	GO:0044764	multi-organism cellular process	24	12,50	0,0001328	3,88
GOTERM_BP_FAT	GO:0044403	symbiosis; encompassing mutualism through parasitism	24	12,50	0,0001925	3,72
GOTERM_BP_FAT	GO:0044419	interspecies interaction between organisms	24	12,50	0,0001925	3,72
GOTERM_BP_FAT	GO:0050792	regulation of viral process	10	5,21	0,0014392	2,84
GOTERM_BP_FAT	GO:0043903	regulation of symbiosis; encompassing mutualism through parasitism	10	5,21	0,0025537	2,59
GOTERM_BP_FAT	GO:0043900	regulation of multi-organism process	10	5,21	0,0149688	1,82
GOTERM_BP_FAT	GO:0019058	viral life cycle	11	5,73	0,0179019	1,75
<i>Annotation Cluster 15</i> Enrichment Score: 1,9941548315648696						
GOTERM_BP_FAT	GO:0010608	posttranscriptional regulation of gene expression	15	7,81	0,0003327	3,48
<i>Annotation Cluster 16</i> Enrichment Score: 1,9755340900925409						
GOTERM_BP_FAT	GO:0098609	cell-cell adhesion	22	11,46	0,0072871	2,14
GOTERM_BP_FAT	GO:0007155	cell adhesion	28	14,58	0,0124756	1,90
GOTERM_BP_FAT	GO:0022610	biological adhesion	28	14,58	0,0130251	1,89
<i>Annotation Cluster 17</i> Enrichment Score: 1,959411589145368						
GOTERM_BP_FAT	GO:0051248	negative regulation of protein metabolic process	24	12,50	0,0003924	3,41
GOTERM_BP_FAT	GO:0032269	negative regulation of cellular protein metabolic process	23	11,98	0,0004541	3,34
GOTERM_BP_FAT	GO:0010605	negative regulation of macromolecule metabolic process	40	20,83	0,0009171	3,04
GOTERM_BP_FAT	GO:0031324	negative regulation of cellular metabolic process	39	20,31	0,0020281	2,69
GOTERM_BP_FAT	GO:0009892	negative regulation of metabolic process	41	21,35	0,0022467	2,65
GOTERM_BP_FAT	GO:0031400	negative regulation of protein modification process	14	7,29	0,0061331	2,21
<i>Annotation Cluster 18</i> Enrichment Score: 1,936584758141524						
GOTERM_BP_FAT	GO:0016050	vesicle organization	11	5,73	0,0008793	3,06
GOTERM_BP_FAT	GO:0051656	establishment of organelle localization	12	6,25	0,0037914	2,42
GOTERM_BP_FAT	GO:0051640	organelle localization	13	6,77	0,0042647	2,37
GOTERM_BP_FAT	GO:0061024	membrane organization	19	9,90	0,0166639	1,78
<i>Annotation Cluster 19</i> Enrichment Score: 1,8795156753917819						
GOTERM_BP_FAT	GO:0044772	mitotic cell cycle phase transition	14	7,29	0,0022892	2,64
GOTERM_BP_FAT	GO:0044770	cell cycle phase transition	14	7,29	0,0038923	2,41
GOTERM_BP_FAT	GO:0007346	regulation of mitotic cell cycle	13	6,77	0,0044042	2,36
GOTERM_BP_FAT	GO:0051726	regulation of cell cycle	19	9,90	0,0103361	1,99
GOTERM_BP_FAT	GO:0010564	regulation of cell cycle process	13	6,77	0,0183945	1,74
<i>Annotation Cluster 20</i> Enrichment Score: 1,8009512240557284						
GOTERM_BP_FAT	GO:0006928	movement of cell or subcellular component	36	18,75	0,0001080	3,97
GOTERM_BP_FAT	GO:0001667	ameboidal-type cell migration	11	5,73	0,0016181	2,79
GOTERM_BP_FAT	GO:0016477	cell migration	23	11,98	0,0042877	2,37
GOTERM_BP_FAT	GO:0040011	locomotion	27	14,06	0,0062275	2,21
GOTERM_BP_FAT	GO:0051674	localization of cell	24	12,50	0,0082302	2,08
GOTERM_BP_FAT	GO:0048870	cell motility	24	12,50	0,0082302	2,08
<i>Annotation Cluster 22</i> Enrichment Score: 1,6759945901312603						
GOTERM_BP_FAT	GO:0051098	regulation of binding	10	5,21	0,0035997	2,44
<i>Annotation Cluster 23</i> Enrichment Score: 1,6693802181144233						

Category	Term		Count	%	P value	$-\log_{10}$ P value
GOTERM_BP_FAT	GO:0016050	vesicle organization	11	5,73	0,0008793	3,06
<i>Annotation Cluster 24</i> Enrichment Score: 1,6676421778588604						
GOTERM_BP_FAT	GO:0010605	negative regulation of macromolecule metabolic process	40	20,83	0,0009171	3,04
GOTERM_BP_FAT	GO:0016070	RNA metabolic process	66	34,38	0,0018345	2,74
GOTERM_BP_FAT	GO:0031324	negative regulation of cellular metabolic process	39	20,31	0,0020281	2,69
GOTERM_BP_FAT	GO:0009892	negative regulation of metabolic process	41	21,35	0,0022467	2,65
GOTERM_BP_FAT	GO:0010467	gene expression	72	37,50	0,0033792	2,47
GOTERM_BP_FAT	GO:1903508	positive regulation of nucleic acid-templated transcription	25	13,02	0,0049290	2,31
GOTERM_BP_FAT	GO:0045893	positive regulation of transcription; DNA-templated	25	13,02	0,0049290	2,31
GOTERM_BP_FAT	GO:1902680	positive regulation of RNA biosynthetic process	25	13,02	0,0059035	2,23
GOTERM_BP_FAT	GO:0071310	cellular response to organic substance	35	18,23	0,0068966	2,16
GOTERM_BP_FAT	GO:0051254	positive regulation of RNA metabolic process	25	13,02	0,0087650	2,06
GOTERM_BP_FAT	GO:0070887	cellular response to chemical stimulus	40	20,83	0,0091588	2,04
GOTERM_BP_FAT	GO:0045944	positive regulation of transcription from RNA polymerase II promoter	20	10,42	0,0094253	2,03
GOTERM_BP_FAT	GO:2000113	negative regulation of cellular macromolecule biosynthetic process	23	11,98	0,0149422	1,83
GOTERM_BP_FAT	GO:0010629	negative regulation of gene expression	25	13,02	0,0152244	1,82
GOTERM_BP_FAT	GO:0006366	transcription from RNA polymerase II promoter	29	15,10	0,0164142	1,78
GOTERM_BP_FAT	GO:0010558	negative regulation of macromolecule biosynthetic process	24	12,50	0,0167612	1,78
GOTERM_BP_FAT	GO:0051172	negative regulation of nitrogen compound metabolic process	25	13,02	0,0177728	1,75
GOTERM_BP_FAT	GO:0010557	positive regulation of macromolecule biosynthetic process	26	13,54	0,0191004	1,72
GOTERM_BP_FAT	GO:0051171	regulation of nitrogen compound metabolic process	58	30,21	0,0211689	1,67
GOTERM_BP_FAT	GO:0010033	response to organic substance	40	20,83	0,0242937	1,61
GOTERM_BP_FAT	GO:0031327	negative regulation of cellular biosynthetic process	24	12,50	0,0261876	1,58
GOTERM_BP_FAT	GO:0045935	positive regulation of nucleobase-containing compound metabolic process	26	13,54	0,0286900	1,54
GOTERM_BP_FAT	GO:0006357	regulation of transcription from RNA polymerase II promoter	28	14,58	0,0305811	1,51
GOTERM_BP_FAT	GO:0009890	negative regulation of biosynthetic process	24	12,50	0,0307789	1,51
GOTERM_BP_FAT	GO:0071495	cellular response to endogenous stimulus	20	10,42	0,0318812	1,50
GOTERM_BP_FAT	GO:0010628	positive regulation of gene expression	26	13,54	0,0354523	1,45
GOTERM_BP_FAT	GO:0010468	regulation of gene expression	56	29,17	0,0357412	1,45
GOTERM_BP_FAT	GO:0034645	cellular macromolecule biosynthetic process	63	32,81	0,0383441	1,42
GOTERM_BP_FAT	GO:0031328	positive regulation of cellular biosynthetic process	26	13,54	0,0441184	1,36
<i>Annotation Cluster 26</i> Enrichment Score: 1,6267402762137324						
GOTERM_BP_FAT	GO:0007015	actin filament organization	10	5,21	0,0073000	2,14
<i>Annotation Cluster 27</i> Enrichment Score: 1,573279514658293						
GOTERM_BP_FAT	GO:0044265	cellular macromolecule catabolic process	20	10,42	0,0048455	2,31
GOTERM_BP_FAT	GO:0009057	macromolecule catabolic process	22	11,46	0,0102123	1,99
GOTERM_BP_FAT	GO:0044257	cellular protein catabolic process	14	7,29	0,0234922	1,63
GOTERM_BP_FAT	GO:0006511	ubiquitin-dependent protein catabolic process	12	6,25	0,0335224	1,47
GOTERM_BP_FAT	GO:0051603	proteolysis involved in cellular protein catabolic process	13	6,77	0,0358169	1,45
GOTERM_BP_FAT	GO:0019941	modification-dependent protein catabolic process	12	6,25	0,0364752	1,44

Category	Term		Count	%	P value	$-\log_{10}$ P value
GOTERM_BP_FAT	GO:0030163	protein catabolic process	15	7,81	0,0367867	1,43
GOTERM_BP_FAT	GO:0043632	modification-dependent macromolecule catabolic process	12	6,25	0,0396070	1,40
Annotation Cluster 28		Enrichment Score: 1,556576769515713				
GOTERM_BP_FAT	GO:0048534	hematopoietic or lymphoid organ development	16	8,33	0,0129480	1,89
GOTERM_BP_FAT	GO:0002520	immune system development	16	8,33	0,0200911	1,70
GOTERM_BP_FAT	GO:0030097	haemopoiesis	14	7,29	0,0382189	1,42
Annotation Cluster 29		Enrichment Score: 1,5536345503696056				
GOTERM_BP_FAT	GO:0016071	mRNA metabolic process	14	7,29	0,0196111	1,71
GOTERM_BP_FAT	GO:0008380	RNA splicing	10	5,21	0,0211074	1,68
GOTERM_BP_FAT	GO:0006396	RNA processing	17	8,85	0,0228503	1,64
Annotation Cluster 31		Enrichment Score: 1,433959843797708				
GOTERM_BP_FAT	GO:0071407	cellular response to organic cyclic compound	13	6,77	0,0068716	2,16
GOTERM_BP_FAT	GO:1901699	cellular response to nitrogen compound	13	6,77	0,0116311	1,93
GOTERM_BP_FAT	GO:1901701	cellular response to oxygen-containing compound	17	8,85	0,0232646	1,63
GOTERM_BP_FAT	GO:0032870	cellular response to hormone stimulus	13	6,77	0,0233614	1,63
GOTERM_BP_FAT	GO:0071495	cellular response to endogenous stimulus	20	10,42	0,0318812	1,50
GOTERM_BP_FAT	GO:1901698	response to nitrogen compound	16	8,33	0,0389384	1,41
Annotation Cluster 32		Enrichment Score: 1,4086294256407783				
GOTERM_BP_FAT	GO:0031175	neuron projection development	18	9,38	0,0039748	2,40
GOTERM_BP_FAT	GO:0030030	cell projection organization	23	11,98	0,0124018	1,91
GOTERM_BP_FAT	GO:0048666	neuron development	18	9,38	0,0189116	1,72
GOTERM_BP_FAT	GO:2000026	regulation of multicellular organismal development	27	14,06	0,0252845	1,60
Annotation Cluster 36		Enrichment Score: 1,3372413426913092				
GOTERM_BP_FAT	GO:0002768	immune response-regulating cell surface receptor signalling pathway	11	5,73	0,0076645	2,12
GOTERM_BP_FAT	GO:0002764	immune response-regulating signalling pathway	13	6,77	0,0080526	2,09
GOTERM_BP_FAT	GO:0002757	immune response-activating signal transduction	11	5,73	0,0308856	1,51
GOTERM_BP_FAT	GO:0002682	regulation of immune system process	22	11,46	0,0395641	1,40
GOTERM_BP_FAT	GO:0006955	immune response	24	12,50	0,0415212	1,38
GOTERM_BP_FAT	GO:0031347	regulation of defence response	13	6,77	0,0429616	1,37
Annotation Cluster 37		Enrichment Score: 1,3324823788934246				
GOTERM_BP_FAT	GO:0097190	apoptotic signalling pathway	14	7,29	0,0065757	2,18

Figure A-6 shows the graphic representation of Table A-2 with terms including a p-value below 0.001.

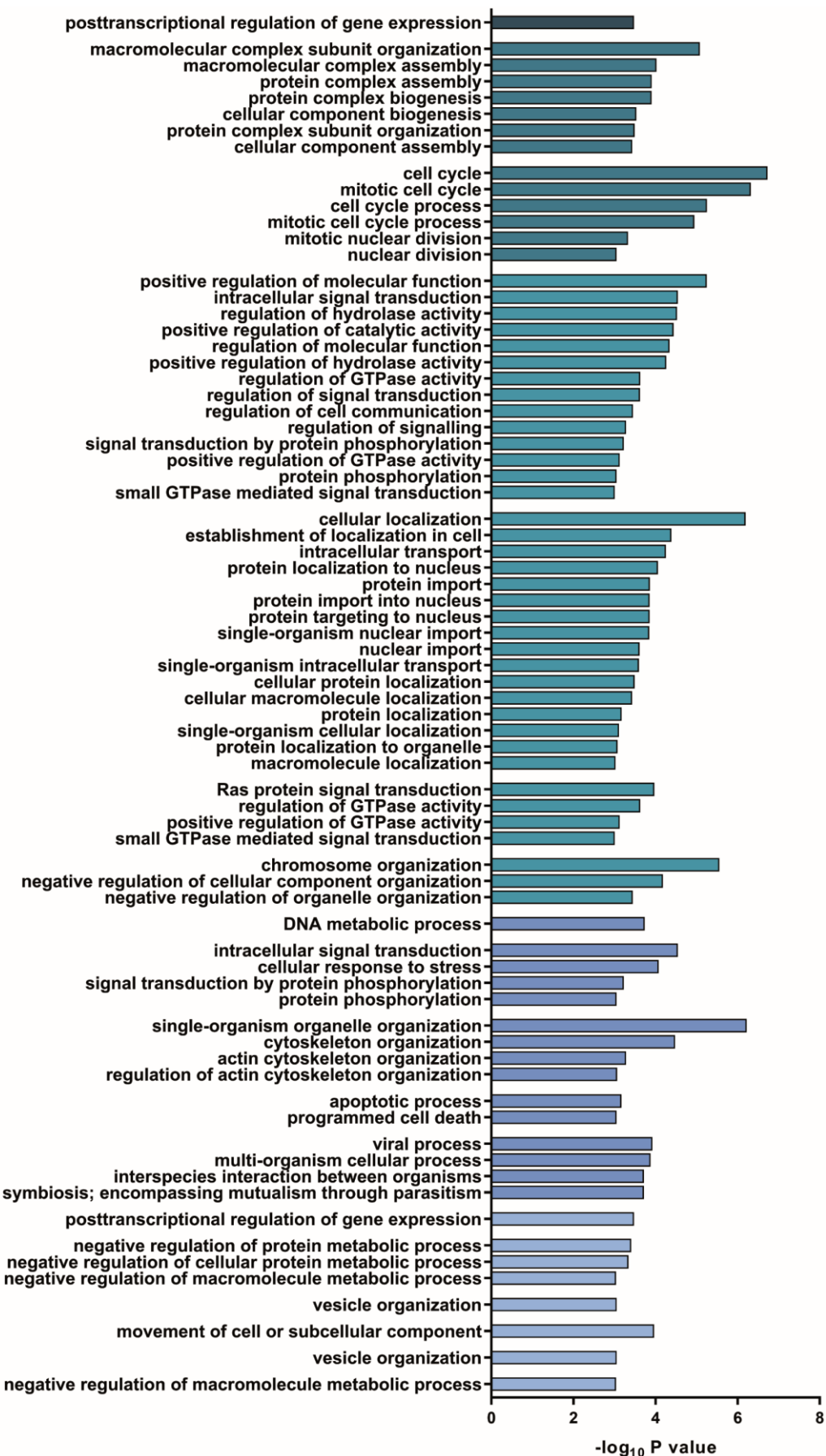


**Figure A-6: GO annotation of phosphoproteins changed by IL10+CpG stimulation**  
Terms of Table A-2 with a p-value below 0.001 are displayed.